ACKNOWLEDGEMENTS

The author wishes to express his gratitude and sincere thanks to Dr. R. S. Mann, under whose supervision this investigation was carried out, for his guidance and interest in the work, and to Dr. B. C.-Y. Lu, Chairman of the Chemical Engineering Department, for providing the facilities of the department.

Indebtedness is acknowledged with pleasure to the teaching staff of the department for valuable discussions, and to Dr. K. J. Laidler for his interesting course in chemical kinetics.

The project was carried out with the financial aid of a University teaching assistantship, a fellowship from the Ontario Government, and a research grant from the National Research Council of Canada.

TABLE OF CONTENTS

Page

LIST OF TABLES

LIST OF FIGURES

ABSTRACT

The kinetics of the vapor phase air oxidation of methanol to formaldehyde over a manganese dioxide-molybdenum trioxide catalyst, at atmospheric pressure, in the temperature range 250° - 460°C, has been studied using a fixed-bed integral reactor heated in fluidised sand.

The effect of various process variables, namely, the feed ratio of methanol to oxygen (in the air), ratio of catalyst to feed flow rate, and process temperature, on the conversion and yield were determined.

The reactor effluent was analyzed by a departmental gas chromatograph and a Fisher Gas Partitioner. Fifteen weight percent sucrose octa-acetate on Columpak T was used in the gas chromatograph assembled in the department for analyzing the liquid products, and hexamethylphosphoramide (HMPA) and molecular sieve 13X columns were used in the gas partitioner for analyzing the gaseous products.

The rates of formation of formaldehyde and water at the optimal temperature were found to depend on the partial pressure of methanol. The effects of diffusion and catalyst surface temperature were negligible. The highest selectivity, nearly one hundred

percent, was obtained at 365°C for a conversion of 84%, W/F ratio of 22.0 gm-hr/moles, and methanol in air content of 8 moles %

It was found that of the several models proposed, only one correlated the data satisfactorily. This model was derived from a two-stage irreversible oxidation-reduction process:

$$CH_3OH(g) + s_{ox} \xrightarrow{k_1} HCHO(g) + s_{red}$$

$$O_2(g) + s_{red} \xrightarrow{k_2} s_{ox}$$

where s_{ox} was an active site of lattice or adsorbed oxygen, and s_{red}, the reduced site of lattice oxygen or the empty site. The rate of reaction was expressed by:

$$r = \frac{k_1 p_M}{1 + k_1 p_M / 2k_2 p_{O_2}^{\frac{1}{2}}}$$

where k_1 and k_2 are temperature-dependent constants.

I. INTRODUCTION

A. The Importance of Chemical Kinetics

Chemical kinetics is a study of the factors that influence the rate of a chemical reaction. In chemistry, it is a tool for gaining insight into the nature of reacting systems, for understanding how chemical bonds are formed and broken, for estimating their energies and stability, and for identifying the molecular structure of compounds.

In chemical engineering, it permits considerable freedom of choice in reactor design, in the adoption of a batch or continuous process, in the initial concentration of reagents, operating temperatures and pressures, and in making controlled alterations in these variables during the course of the reaction.

Since the purpose of a kinetic study is not the same in chemical engineering as in chemistry, there are some differences in the requirements and approach. The chemist, in general, prefers to choose a case in which all complexities not related to the kinetic mechanism have been eliminated; as for example, a homogeneous reaction, in order to gain an insight into the true nature of the reaction. The reaction itself may or may not be of any practical or industrial significance. The chemical engineer, on the other hand,

must keep a high yield and selectivity in mind. In most instances a heterogeneous catalytic reaction is the only alternative. Generally, the use of an empirical rate expression is sufficient in designing the equipment for such reactions. However, it is desirable to ascertain the true equation if it can be obtained, since then it may be safe to extrapolate outside the range of experimental data.

B. Heterogeneous Catalytic Reactions

The term catalysis is used to describe all processes in which the rate of the reaction is influenced by a substance which remains theoretically unaffected. An early definition by Ostwald (81) was that a catalyst is "any substance that alters the velocity of a chemical reaction without modification of the energy factors of the reaction." Later he proposed an alternate definition (82) which has been widely quoted: "a catalyst is any substance that alters the velocity of a chemical reaction without appearing in the end product of the reaction."

It is to be noted (65) that in the definitions of catalysis no reference is made to the fact that a small amount of catalyst will have a large effect on the rate. This is frequently the case, but it is not an essential characteristic of a catalyst. Although by definition the amount of catalyst should be unchanged at the end of the reaction, it does not follow that the

catalyst has not entered into the chemical reaction as the reaction proceeded.

It is convenient to classify catalyzed reactions according to whether they occur homogeneously (in a single phase) or heterogeneously (at an interface between two phases). An important group of heterogeneous reactions, the oxidation of oxygenated hydrocarbons catalyzed by a solid surface, is the subject of the present investigation.

C. Method of Study

Although several methods (62) are available for measuring the reaction rates using a differential or an integral reactor, yet there is no entirely satisfactory method by which the reaction rates can be measured directly.

The differential method consists in operating the reactor with a small conversion so that the reaction rate may be assumed constant. Rate determinations in a differential reactor can be made in a straightforward manner.

The integral method is not restricted by a small conversion and the experimental accuracy is greater. However, it is much more difficult to integrate the rate equations since there are several hidden parameters which may diminish the value of the experimental data (63).

In the present studies, the vapor phase oxidation of methanol to formaldehyde over a solid catalyst, it was easier to investigate the rate mechanism using the differential approach, because formaldehyde readily polymerized at high concentrations. Since a chemical engineer is more interested in yield and selectivity, and since the present industrial process uses a mixture of methanol and air over a heated stationary catalyst at approximately atmospheric pressure, a fixed-bed integral reactor operating at atmospheric pressure was used in this research. The drawbacks inherent in this choice have been minimized as much as possible by the means at our disposal and within the limits of available time.

D. <u>The Importance of Formaldehyde Production</u>

Since the discovery of formaldehyde in the latter half of the nineteenth century, it has become a chemical of great industrial importance. Production in the United States alone reached an estimated level of 2600 million pounds in 1963, with a world production of at least six billion pounds (107). The marked increase in demand can be partly attributed to the rapid increase in the variety of formaldehyde applications.

Though formaldehyde is mainly produced today by partial oxidation of methanol, increasing quantities

are being manufactured from the direct oxidation of hydrocarbon gases. For its successful use and a cheaper method of production, the unique character of formaldehyde chemistry and kinetics must be fully understood.

B. The Objective of the Present Work

The purpose of the present investigation was to study the kinetics and a possible mechanism for the oxidation of methanol to formaldehyde over an oxide catalyst and to develop a suitable rate expression, which might satisfactorily represent the data.

For this study, an integral-flow reactor was used, and the effect of temperature on conversion and yield, as well as the effect of various variables on the reaction kinetics is discussed.

II. LITERATURE SURVEY

Although the oxidation of methanol to formaldehyde has been of great industrial importance, very little scientific literature is available on the kinetics and mechanism of the reaction. Several patents have appeared in the last decade.

The number of publications relating to formaldehyde per se are very large. A comprehensive bibliography on formaldehyde research was published in 1964 by J. F. Walker, as part of the American Chemical Society's Chemical Monograph Series (105).

The present review is limited to studies on the heterogeneous oxidation of methanol to formaldehyde, and includes a general discussion of metal and oxide catalysts, and a summary of the published literature on ferric trioxide-molybdenum trioxide and manganese dioxide-molybdenum trioxide catalysts.

A. Metal and Oxide Catalysts

Formaldehyde is produced principally from methanol oxidation over metal catalysts. The original or classical approach, as it may be called, employed high temperatures, in the approximate range of 500-600°C, and a rich methanol-air mixture, 30-50% methanol

by volume. Effluent gases from this process contained 18-20% hydrogen, less than 1% oxygen, and minor amounts of carbon oxides and methane. Unreacted methanol in the product solution was separated from the formaldehyde by fractional distillation and could be returned to the evaporating chamber for further use.

As early as 1868, Hofmann (40) produced formaldehyde by drawing a mixture of air and methanol vapors over a hot platinum spiral. Once initiated the reaction was self-sustaining, as manifested by the glowing spiral. Twenty years later (16), the firm of Mereklin and Lösekann was founded, near Hanover, Germany, and commercial manufacture of formaldehyde was begun in 1889. The subsequent developments in the oxidation of methanol over metallic catalysts (copper, gold, and silver) have been reviewed by Marek and Hahn (73) in 1938, and by Walker (103) in 1964. Although the kinetics of the reaction over copper and gold was similar to silver, these metals were found to be much less active and to cause more decomposition of formaldehyde. Hence, only the development of the silver process is traced in greater detail.

In 1910, O. Blank (11) in Germany patented the use of a silver catalyst. A year later, LeBlanc and Plaschke (69) reported that formaldehyde yields obtained with silver catalysts were higher than those with copper. In 1913, use of the silver catalyst was introduced into United States operations with the

patent of Kuznesow (60); and in 1920, Thomas (99), an American, in a comparative study on the value of copper, gold, and silver in the catalytic oxidation of methanol reported laboratory-scale results for the preparation of formaldehyde. The net yield of formaldehyde obtained by Thomas with silver, 83 to 92% of theoretical, was in general agreement with that reported by Homer (41) in England in 1941, for commercial production, namely 89.3% of theoretical.

Thomas (99) studied the oxidation of methanol over a silver gauze approximately 13 mm in diameter by 100 mm long. Weight ratios of oxygen to methanol were varied from about 0.15 to 0.60 and air rates were varied from about 90 to 200 l/hr. Whereas the inlet gas temperatures were in the range of 350° to 565°C, temperatures in the center of the gauze varied from 530° to above 900°C. Data from these experiments were compared at constant air flow rates.

Homer describes the operation of a British plant which used silver gauze of the type patented by Blank (11), with high methanol-air ratios in order to keep the catalyst active over an extensive period, the excess methanol being subsequently distilled from the formaldehyde and returned to the vaporizer.

More recently, Pumderson (86), in 1960, discovered a selective dehydrogenation catalyst for methanol consisting of 97.8% silver, 2% copper, and

0.2% silicon. He claims to have obtained good yields over this catalyst when pure, preheated methanol vapors in the range of 600° to 700°C were passed over it. The catalyst can be reactivated easily when necessary by heating with air at the same temperatures.

Aries (4), describes a pressure dehydrogenation process in which methanol and hydrogen are passed over a finely divided silver catalyst at 700° to 800°C and 5 to 8 atmospheres pressure.

Kushnarenko and Atroshenko (59), in 1965, outline a pressure oxidation, in which 0 - 0.4 molar ratios of oxygen to methanol are passed over a silver catalyst at 450° to 650°C and 1 to 3.5 atmospheres pressure. They found that at gas velocities above the critical level, conversion of methanol to formaldehyde increased with temperature and pressure. Below the critical level, formation of carbon monoxide was accelerated.

Stadnik et al (97) observed that cathodic polarization of silver catalysts increased the yield of formaldehyde by 6 - 7% as compared to experiments without an electric field, whereas anodic polarization decreased the yield.

The reaction mechanism for the formation of formaldehyde from methanol and air using a metal catalyst may be either a dehydrogenation, followed by

oxidation of hydrogen, to the extent that oxygen is present in the gaseous mixture:

$$CH_3OH \rightleftharpoons HCHO + H_2 \quad - 20 \text{ kcal}$$

$$H_2 + \tfrac{1}{2}O_2 \longrightarrow H_2O \quad + 58 \text{ kcal}$$

or, a combination of these reactions.

Sator's study (103), in Germany in 1938, indicates the reaction to be exclusively a dehydrogenation, the combustion of hydrogen merely offsetting the endothermic nature of the first reaction to make the process self-sustaining. LeBlanc and Plaschke (69) and Thomas (99), conclude the reaction mechanism to be a combination of the two reactions. The function of oxygen, aside from maintaining the necessary temperature, was to keep the catalyst active by oxidizing and removing any "poisons" or to keep the surface of the metal in the proper physical and chemical state.

The proper control of reaction temperature is very important in the oxidation of methanol to formaldehyde, since pyrolytic decomposition of formaldehyde to carbon monoxide and hydrogen

$$HCHO(g) \rightleftharpoons CO + H_2$$

though slow, is measurable at 300°C, and increases rapidly at temperatures above 400°C (14).

In recent years, the oxide catalyst process for formaldehyde production has assumed increasing importance. This process differs from the classical procedure in that it employs lower temperatures (300 - 400°C), a lean methanol-air mixture (5 - 10% methanol by volume), and produces formaldehyde that is substantially free of methanol (0 - 1%). The off-gases from this process contain unreacted oxygen and insignificant amounts of hydrogen. Manufacturing yields are said to be higher with the metallic oxides than with the pure metals.

Catalysts patented for this type of process prior to 1945 include vanadium oxide (7), mixtures involving salts or oxides of vanadium with other metal oxides (22, 50), iron-molybdenum oxide mixtures (76) and tungsten-molybdenum oxide mixtures (5). The patent literature since 1955 has been devoted chiefly to improvements in the methods of preparation, use and recovery of catalysts based on iron-molybdenum oxide mixtures (2, 8, 35, 38, 39, 80).

The oxide catalyst process converts methanol to formaldehyde by an oxidation process, as indicated in the following equation:

$$CH_3OH + \tfrac{1}{2}O_2 \longrightarrow HCHO + H_2O + 38 \text{ kcal.}$$

B. Ferric trioxide-molybdenum trioxide as a Catalyst

Adkins and Peterson (1) studied the effect of

the composition of oxide catalysts on their activity in the oxidation of methanol using as the basis for their investigation ferric trioxide and molybdenum trioxide and mixtures of the two oxides. Most of the studies were made using a catalyst bed 15 cm in length, with a cross-sectional area of 3 sq cm and feed rates of 10 gm of methanol in 93 l of air/hr.

With pure molybdenum trioxide, approximately 100% formaldehyde yields based on the methanol oxidised were obtained. However, the percentage conversion decreased from about 60% to a steady value of about 32% after 12 to 24 hours of operation at 400°C. Raising the catalyst bath temperature from 360° to 400°C raised the steady state conversion level from 24 to 32%. With pure ferric trioxide under similar conditions, almost all of the methanol was oxidised to carbon dioxide with the formation of little or no formaldehyde.

The most satisfactory catalyst was found to be an equimolar mixture of ferric trioxide and molybdenum trioxide. The percentage conversion of methanol to formaldehyde increased from an initial value of about 82%, to an equilibrium value of about 91%, when feeding 10 grams of methanol in 93 liters of air at 373°C through the catalyst bed. Decreasing the length of the bed from 15 to 5 cm gave the same conversion of methanol to formaldehyde but a somewhat higher yield of formaldehyde. Decreasing the feed rate (at constant methanol to air ratio) resulted in a loss in formaldehyde

yield due to further oxidation. Similarly, at temperatures of 353°, 373° and 400°C, conversions of methanol to formaldehyde of 85.2, 91.8 and 91.9% were obtained. However, at 400°C some loss in yield due to continued oxidation of formaldehyde was observed.

Jiru et al (52) taking into consideration the work of Adkins and Peterson together with a number of patents (2, 8, 35, 38, 39, 80) carried out an extensive study on the oxidation of methanol to formaldehyde over a catalyst composed of 17.5% ferric trioxide and 82.5% molybdenum trioxide.

The rate of catalytic oxidation of methanol to formaldehyde was measured in a throughflow integral reactor at atmospheric pressure using the microcatalytic pulse method. Methanol and air were introduced into the reactor separately. Traces of oxygen (less than 0.01% by weight) in the carrier gas, nitrogen, were removed by passing it over heated copper wire at 300°C, and traces of water by passing it through a dry ice trap at -76°C. The required amount of methanol vapor in nitrogen, obtained by passage of the nitrogen through a methanol saturator, was introduced into the carrier gas by means of a dosing cock, equipped with two constant volume loops of 5.2 and 8.4 ml respectively. The volume of the mixture was displaced from the dosing cock into the reactor containing the ferric trioxide-molybdenum trioxide at the velocity of the carrier gas. The time for the passage of 5.2 ml of reactant was 5.43×10^{-3}

hours and for 8.4 ml was 8.83×10^{-3} hours. They claimed that with this arrangement and successive dosing it was possible to ascertain the composition of the product as a function of the overall-time of passage of the reactants (methanol or oxygen) through the catalyst bed. Methanol was introduced first in each of the experiments and oxygen later. The interaction between methanol or oxygen and the catalyst was studied in a static sorption apparatus with a McLeod manometer.

The rate of oxidation of methanol was determined in the integral reactor at 270°C, for a feed containing methanol and oxygen at 1.5 - 7.5% and 5 - 40 % by volume respectively. During the oxidation it was observed that the catalyst changed in color from yellowish green to greyish blue. Based on this and the fact that both constituents of the catalyst may exist in a state of lower valency, Jiru et al have postulated a two-stage oxidation reduction mechanism:

$$CH_3OH(g) + K_{ox} \xrightarrow{k_1} HCHO(g) + H_2O(g) + K_{red}$$

$$O_2(g) + K_{red} \xrightarrow{k_2} K_{ox}$$

and derived the rate equation:

$$r = \frac{k_1 p_M^m}{1 + k_1 p_M^m / k_2 p_{O_2}^n}$$

where m = 1, and n = 1, or 0.5.

Later Jiru et al (51), using a differential reactor in the temperature range 210 - 290°C, obtained the same kinetic mechanism.

Bente et al (26 - 28) studied the oxidation of methanol in an integral reactor between 220° and 300°C, and obtained a rate expression similar to the one obtained by Jiru et al. Friedlander and Bennett (31) and Cotter (21) also studied the methanol oxidation and obtained the rate expression:

$$r = k\, p_M^n$$

Friedlander and Bennett employed a flow-recycling differential reactor between 402° and 452°C and a methanol-air mixture containing 0.4 to 3% methanol. Cotter used a fixed-bed integral reactor between 260° and 330°C, methanol concentrations of 1 - 3 mole%, and a gas flow rate of 0.3 to 0.9 cu ft/ min.

C. <u>Manganese dioxide-molybdenum trioxide as a catalyst</u>

Field (30) patented a new method for the preparation of a manganese dioxide-molybdenum trioxide catalyst with operating temperatures preferably held between 250° and 450°C at atmospheric pressure. Conversion of methanol was found to be practically complete at the optimum temperature. The product was primarily formaldehyde with small amounts of carbon monoxide as the principal by-product. At lower temperatures some

Later Jiru et al (51), using a differential reactor in the temperature range 210 - 290°C, obtained the same kinetic mechanism.

Bonte et al (26 - 28) studied the oxidation of methanol in an integral reactor between 220° and 300°C, and obtained a rate expression similar to the one obtained by Jiru et al. Friedlander and Bennett (31) and Cotter (21) also studied the methanol oxidation and obtained the rate expression:

$$r = k\, p_M^n$$

Friedlander and Bennett employed a flow-recycling differential reactor between 402° and 452°C and a methanol-air mixture containing 0.4 to 3% methanol. Cotter used a fixed-bed integral reactor between 260° and 330°C, methanol concentrations of 1 - 3 mole%, and a gas flow rate of 0.3 to 0.9 cu ft/ min.

C. Manganese dioxide-molybdenum trioxide as a catalyst

Field (30) patented a new method for the preparation of a manganese dioxide-molybdenum trioxide catalyst with operating temperatures preferably held between 250° and 450°C at atmospheric pressure. Conversion of methanol was found to be practically complete at the optimum temperature. The product was primarily formaldehyde with small amounts of carbon monoxide as the principal by-product. At lower temperatures some

methanol might have passed over the catalyst unchanged. This catalyst was found to give excellent results when used under optimum conditions of time, temperature, and concentration of vaporised methanol in the mixture undergoing reaction at any suitable ratio of methanol to oxygen. However, no details of the optimum conditions or physical characteristics of the catalyst were given.

Klissouraki and Klisnakov (59), basing their work in part on Field's patent (30), studied the effect of the manganese dioxide:molybdenum trioxide ratio on conversion. They found that a catalyst containing twenty weight percent of manganese dioxide to eighty weight percent of molybdenum trioxide gave the best results, possessing both high catalytic activity and selectivity. However, the kinetics of the reaction and other physical aspects of the system were not examined.

Klisnakov et al (12) have recently published a note regarding the rate mechanism of the oxidation of methanol to formaldehyde over a manganese dioxide-molybdenum trioxide catalyst. Based on seventeen runs at 370°C, and using a differential reactor, they derived a rate expression similar to the one obtained earlier by Jiru et al for ferric trioxide-molybdenum trioxide:

$$r = \frac{k_1 p_M^n}{1 + 0.5\, k_1 p_M^n / k_2\, p_{O_2}^n}$$

where m = either 0.5 or 1 and n = 1. No effort appears to have been made to study the effect of process variables, such as temperature and concentration of methanol in the feed, on the yield and conversion.

The kinetics of the oxidation of methanol to formaldehyde have been studied over manganese dioxide-molybdenum trioxide with a view to reconciling the apparent differences which exist in the published literature, and to postulate a possible reaction mechanism.

III. EXPERIMENTAL

A. Reactants and Chemicals

Certified butanol (Lot no. 31307, Catalog no. A-400) and spectroscopic grade methanol (Lot no. 762008, Catalog no. A-936) supplied by Fisher Scientific Company were used in this investigation.

Air, argon, helium and nitrogen cylinders were obtained from LindeCo. The gas chromatographic analysis of the air gave the composition as: 20.95% oxygen, 0.05% carbon dioxide, and 79% nitrogen. The argon, helium, and nitrogen possessed minimum purities of 99.99%. Gas chromatographic analyses of these gases showed no significant impurity. Moisture was removed by passing each gas through a tube containing drierite.

The chemicals used in the preparation of the catalysts were: ammonium molybdate, $(NH_4)_6Mo_7O_{24}.4H_2O$, M.W. 1235.954 (Baker Analar grade, molybdenum trioxide assay weight percent 81.6, Lot no. 20116); manganese (ous) 50% nitrate solution, $Mn(NO_3)_2$, M.W. 179.04, (Fisher certified, Lot no. 762191); ammonium vanadate, NH_4VO_3, (Fisher purified grade, Lot no. 79262); oxalic acid, $(COOH)_2.2H_2O$ (Fisher certified, Lot no. 700897); and manganese dioxide, MnO_2, (Fisher certified, Lot no. 770514).

The substrates tested were sucrose octa-acetate, $C_{28}H_{38}O_{19}$, M. W. 678.59, (Eastman Kodak grade, Lot no. P4024, Canlab Catalog no. V-134); and Ethofat 60/25 (Lot no. 8174, Armour Industrial Chemical Co.), a polyethylene monostearate, containing an average of 15 ethylene oxide units, M.W. 938. The solid supports used were Columpak T (Lot no. 724875, Fisher Scientific Co., Catalog no. C-587); Porapak N, 800-100 mesh (Batch no. 500, Waters Associates Inc.); and Porapak Q, 80-100 mesh (Waters Associates Inc.). Methylene chloride (reagent grade, Fisher Scientific Co.) was used as a solvent for all substrates.

The chemicals used in the qualitative tests for the products were: basic fuchsin, total dye content 99%, (Fisher certified, Lot no. 760154, Catalog no. F-98); sodium bisulfite, $NaHSO_3$ and $Na_2S_2O_5$, Fisher certified, Lot no. 710148, Catalog no. S-654); hydrochloric acid, 37-38% HCl, (Shawinigan Chemicals, Montreal, Lot no. 6066); sulfuric acid, 95.5 - 98.0% H_2SO_4, (Shawinigan Chemicals, Lot no. 9175); potassium hydroxide, KOH, (analytical reagent, British Drug Houses, Lot no. 201333, Catalog no. 280-p); phenolphthalein, $C_{20}H_{14}O_4$, (Fisher, Lot no. 710971, Catalog no. P-79); and thymolphthalein, $C_{28}H_{30}O_4$, (Fisher certified, Catalog no. T-119).

B. Preparation and Properties of the Catalysts

1. Manganese dioxide-Molybdenum trioxide

A paste (59) made from ammonium molybdate and manganese nitrate, in the required amounts to yield a final product containing manganese dioxide:molybdenum trioxide in a ratio of 20:80 percent by weight, was dried for 6 hours at room temperature, 12 hours at 40°C and 6 hours at 150°C. The catalyst was activated by successive one hour heatings at 200°, 250°, 300°, and 350°C, and a 6 hour calcination at 420°C. Samples of manganese dioxide and molybdenum trioxide were obtained by thermal decomposition of manganese nitrate and ammonium molybdate at similar temperatures.

The physical characteristics of the catalyst are given in Table 3-1

Table 3-1

Physical Properties of MnO_2-MoO_3 Catalyst

Particle Diameter (D_p)	=	0.525	mm
Particle Density (ρ_B)	=	4.6	gm/ml
Surface Area (A_m)	=	7.8	m^2/gm

The particle diameter (D_p) was determined by measurement with a micrometer. A random sample of 25

granules was taken and the diameter of each measured with a micrometer. An arithmetic average of these measurements gave the value of the particle diameter as 0.525 mm, with a deviation of ± 5%

The particle density (ρ_B) was determined by measuring the weight and volume occupied by 100 granules of the catalyst. Since the granules were relatively small, the sphericity was taken as 0.9 (111).

The surface area of the catalyst per unit mass (A_m), as determined by the Division of Mineral Processing, Department of Mines and Technical Surveys, Ottawa, Ontario, was 7.8 m^2/gm.

The color of the catalyst was yellow prior to use but turned black on calcination and subsequent activation. There was also some shrinkage of the surface of the catalyst on heating. It is believed that this was caused by the loss of ammonia and water which had been trapped in the particles when they were formed.

Catalytic activity was verified periodically by passing a specified mixture of methanol and air over the catalyst and determining the percentage conversion of methanol to formaldehyde. The change in catalytic activity was negligible (Table-8-B-1).

The manganese dioxide-molybdenum trioxide catalyst appeared to be highly selective, much more stable, and hence

more suitable for the kinetic study of the oxidation of methanol to formaldehyde. In view, therefore, of the stability and selectivity of the catalyst, it was used throughout in the kinetic investigation of the reaction, except where stated otherwise.

2. Manganese dioxide, Molybdenum trioxide, and Vanadium pentoxide

The other catalysts tested were manganese dioxide, molybdenum trioxide, and vanadium pentoxide. The first two were obtained by heating manganese dioxide and ammonium molybdate respectively. Vanadium pentoxide was prepared by precipitating ammonium vanadate solution with oxalic acid, and drying the precipitate at room temperature. All three catalysts were calcined and activated in a manner identical to the one used for activation of the manganese dioxide-molybdenum trioxide catalyst.

C. Experimental Apparatus

A schematic diagram of the experimental apparatus used in this study is given in Figure 3-1.

All tubing, unless otherwise specified, was 1/4" standard copper, except for the following which was 1/8" high pressure stainless steel from Autoclave Engineers Inc., of Erie, Pa.: the portion of gas line 3 from the duplicate methanol containers to the sight glass and from the sight glass to the evaporating chamber; all of gas line 4, that is, from the air cylinder to the evaporating

Fig. 3-1. Diagram of Experimental Apparatus

Symbol	Item
C	Water condenser
D_1, D_2, D_3, D_4, D_5	Drying tubes
E	Evaporating chamber
F_1, F_2	Funnels for methanol input
GC	Gas chromatograph
GP	Gas partitioner
I	Insulation material--vermiculite
LT	Liquid trap
MC_1, MC_2	Liquid methanol containers
NV	Needle valve for adjusting methanol flow rate
P	Pressure regulator, Edwards
PR	Porous plate
PM	Air pump for fluidized sand bed
R	Reactor and fluidized sand bed
R_1, R_2, R_3, R_4, R_5	Rotameters
SG	Sight glass
SV	Sample valve
T_1, T_2	Thermocouples
TC_1, TC_2, TC_3	Temperature controllers

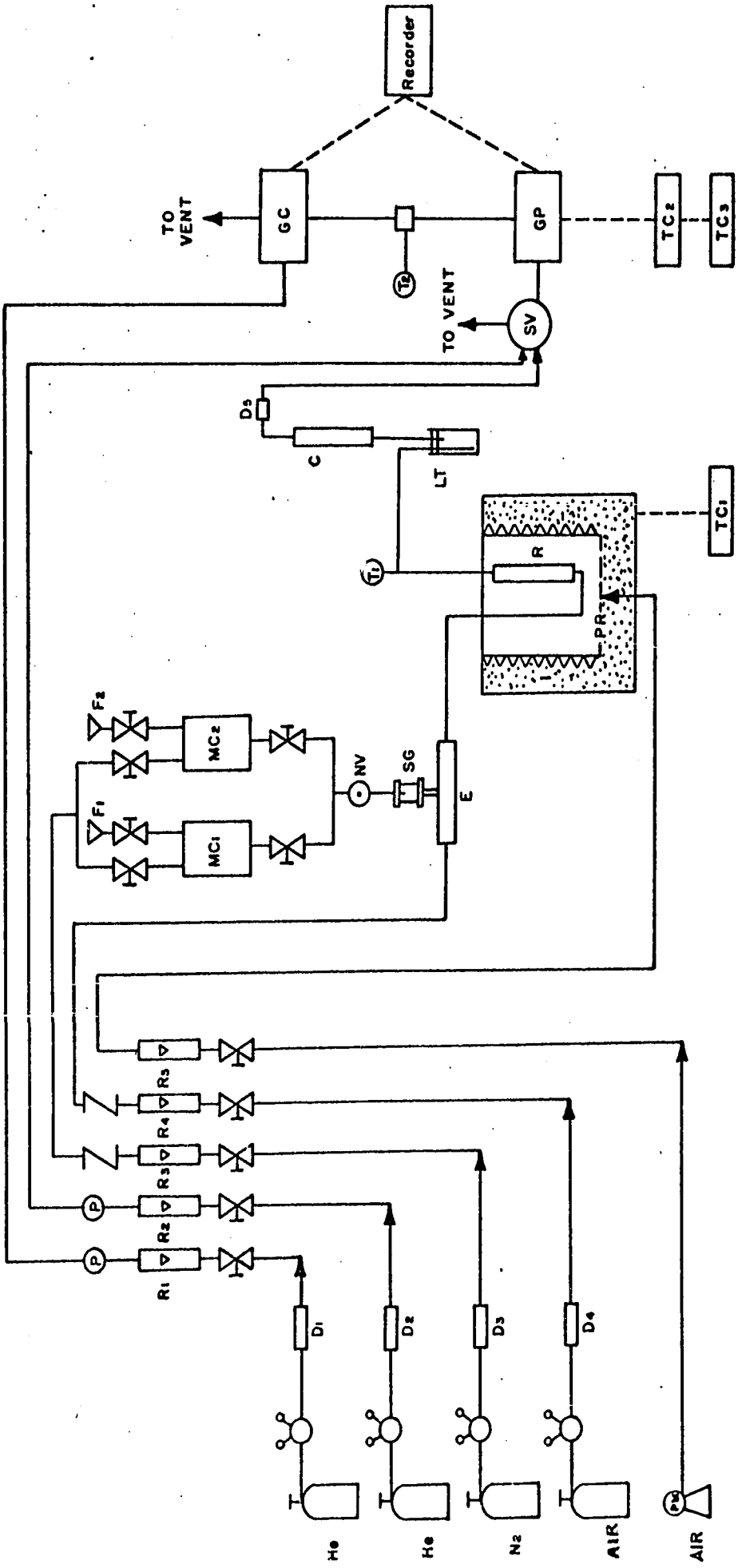

Fig. 3-1. Diagram of Experimental Apparatus

chamber; the feed line from the evaporating chamber to the reactor; the product transport line from the reactor to the liquid trap; the condensing tube in the water condenser; the tubing to and from the drying tube to the gas sample valve and the gas partitioner; and all interconnections within the gas chromatographs.

Swagelok standard stainless steel fittings were used throughout. Check, fine metering and bellow stainless steel valves were made by Nupro Company, Cleveland, Ohio. All valves used unless specified were bellow valves. Both valves and fittings were obtained from Laurentian Valves and Fittings Limited, Ottawa.

Heating cords (supplied by the Chemical Rubber Company of Cleveland, Ohio, Catalog no. 37-278) covered the last two feet of line 4 immediately preceding the evaporating chamber, the line from the methanol sight glass to the evaporating chamber, the evaporating chamber itself, the air-methanol feed line from the evaporator to just above the fluidized bed, the product transport line from the reactor to the upper part of the liquid trap, and all the interconnections of the departmental gas chromatograph. The cords were 3/16" in diameter and made of a glass fabric capable of withstanding 400°C. They could easily be applied to and removed from the tubing without damage and had no unsafe loose terminals at the ends. Asbestos cloth tape, 1/32" thick, woven of plain, purified asbestos (Fisher Catalog no. 1-473) was wrapped around the heating cords for insulation. The temperature of all the heating cords was controlled by

temperature controller 3. Details of this controller and the arrangement of the sensing probe are given in the product analysis section.

The experimental apparatus itself may be divided into three main sections: (1) feed, (2) reactor assembly and (3) product analysis.

1. Feed Section

The feed section consisted of five gas streams, the first and second of which transported helium, carrier gas for the gas chromatograph. The third line carried nitrogen used in compressing methanol in order to keep the pressure in the methanol container just a little higher than the pressure below the needle valve. Two lines carried air: one to the methanol evaporator, and the other to the fluidizing sand which was used for heating the reactor.

Two-stage pressure regulators (Model 8, Matheson of Canada, Ltd., Whitby, Ontario) were used to control the pressure and volume flow rate of the five gas streams. In addition to the two-stage pressure regulators, two Edwards pressure controllers (Model VPC1, Code no. D8301, Edwards High Vacuum Ltd., Sussex, England) maintained a constant pressure in the helium lines.

A Matheson Company flowmeter with needle valve (body series 620, flowmeter tubes and float series 600-605) was used for measuring the flow rate of each of the gas

streams. The flowmeters were panel mounted with chromed-brass end fittings. All tubes were interchangeable.

Methanol was kept in a container and fed to the reactor through a sight glass and evaporating chamber as shown in Figure 3-2. Two identical feed vessels were employed to permit continuous operation. While one supplied methanol to the evaporating chamber, the other was being recharged. Methanol entered the feed vessel through valve V-2, while the nitrogen pressure regulator and valve V-3 were closed. During operation, while valve V-2 was closed, valves V-1 and V-3 were opened, and the methanol flow rate regulated by the needle valve, NV, between the feed vessel and the sight glass. The volume of methanol flowing to the reactor was estimated by observing the number of drops per unit time passing through the sight glass into the evaporating chamber, E. Reproducibility by this method was within ± 2%. In the evaporating chamber methanol was vaporized and mixed with air before entering the reactor.

The sight glass, SG, for determining the methanol drop rate was constructed from two circular plates of chromium-nickel stainless steel (see Figure 3-2), with three holes in the top of each plate; one for methanol passage through a pointed dropper, and the other two for screws. Between the two plates, a plexiglass viewing cylinder was inserted (1" in diameter by 0.5" high by 0.2" thick) and Epoxi-Patch glue from Hysol Corp., Orlean,

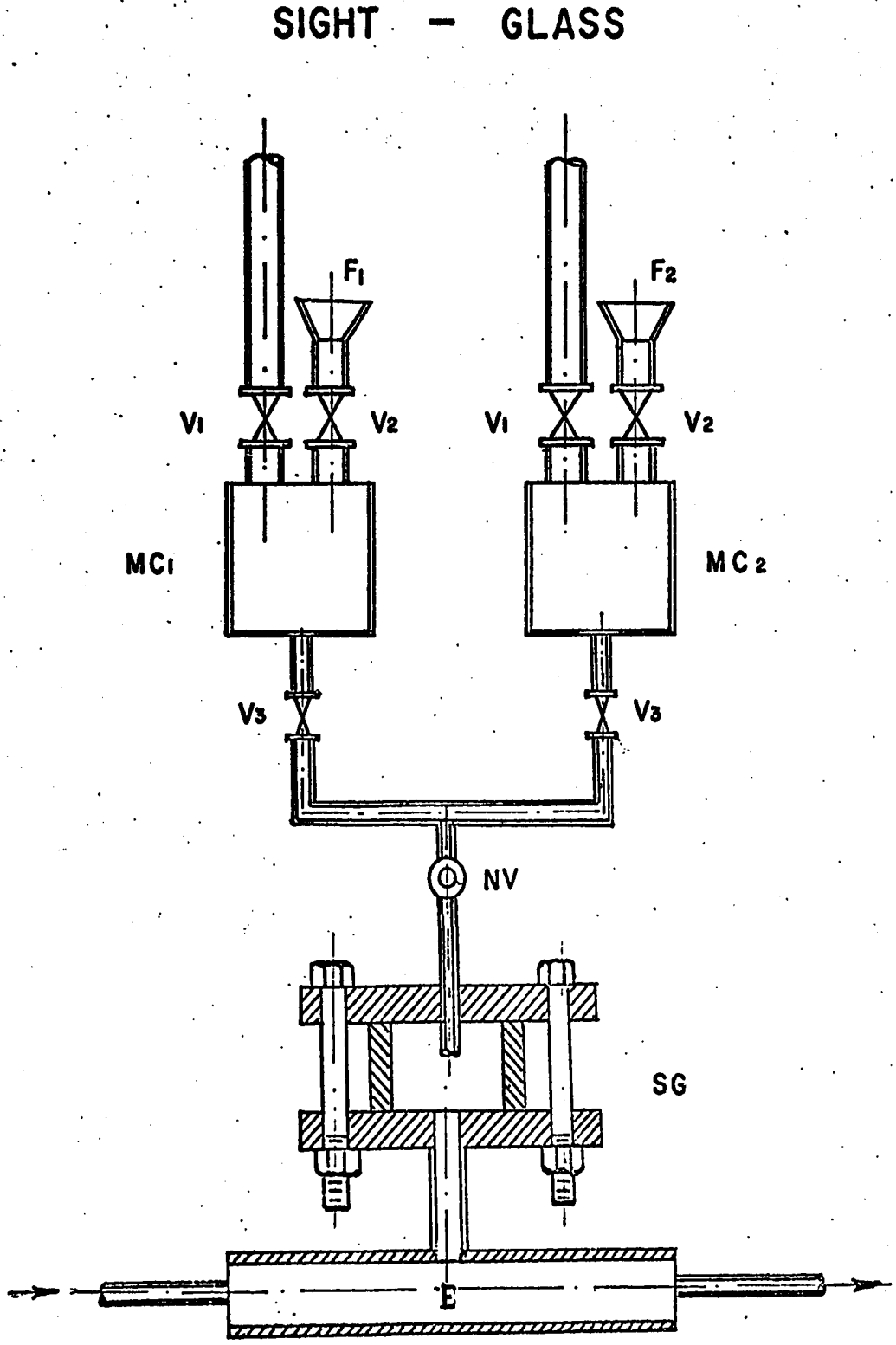

Fig. 3-2. Symbols: E, evaporating chamber; F_1 and F_2, methanol input funnels; MC_1 and MC_2, duplicate methanol containers; NV, needle valve for adjusting methanol flow rate; SG, sight glass with dropper; V_1, V_2, and V_3, valves for inflow of N_2 and CH_3OH, and outflow of CH_3OH respectively.

N.Y., was spread between the top and bottom of the cylinder and the stainless steel plates before tightening the screws.

The evaporating chamber was made from two 1/2" O.D. stainless steel tubes, arc welded together in the form of an inverted "T", and was packed with small pieces of broken ceramicware and glass (see Figure 3-2). A 1/4" O.D. stainless steel tube was then welded in place between the vertical portion of the inverted "T" and the methanol sight glass, and 1/8" O.D. stainless steel tubing was used to connect the horizontal portion of the "T" with air line number 4, on the left and with the reactor on the right.

2. Reactor Assembly

The reactor was made from a 6 x 1/2 inch piece of stainless steel tubing (see Figure 3-3). A porous stainless steel plate, supplied by Pall Trinity Micro Corporation, Cortland, New York, was installed at the bottom of the tube. The grade D plate had a mean pore size of 65 microns, a normal thickness of 1/16", and produced a pressure drop of approximately 0.1 p.s.i.g. per 180 cfm/sq ft of air. A Swagelok reducer was used below the porous plate and attached to the air-methanol feed line from the evaporating chamber.

The top of the reactor was fitted with a Swagelok "T" connection (810-3-2-316). A 1/16" protection tube

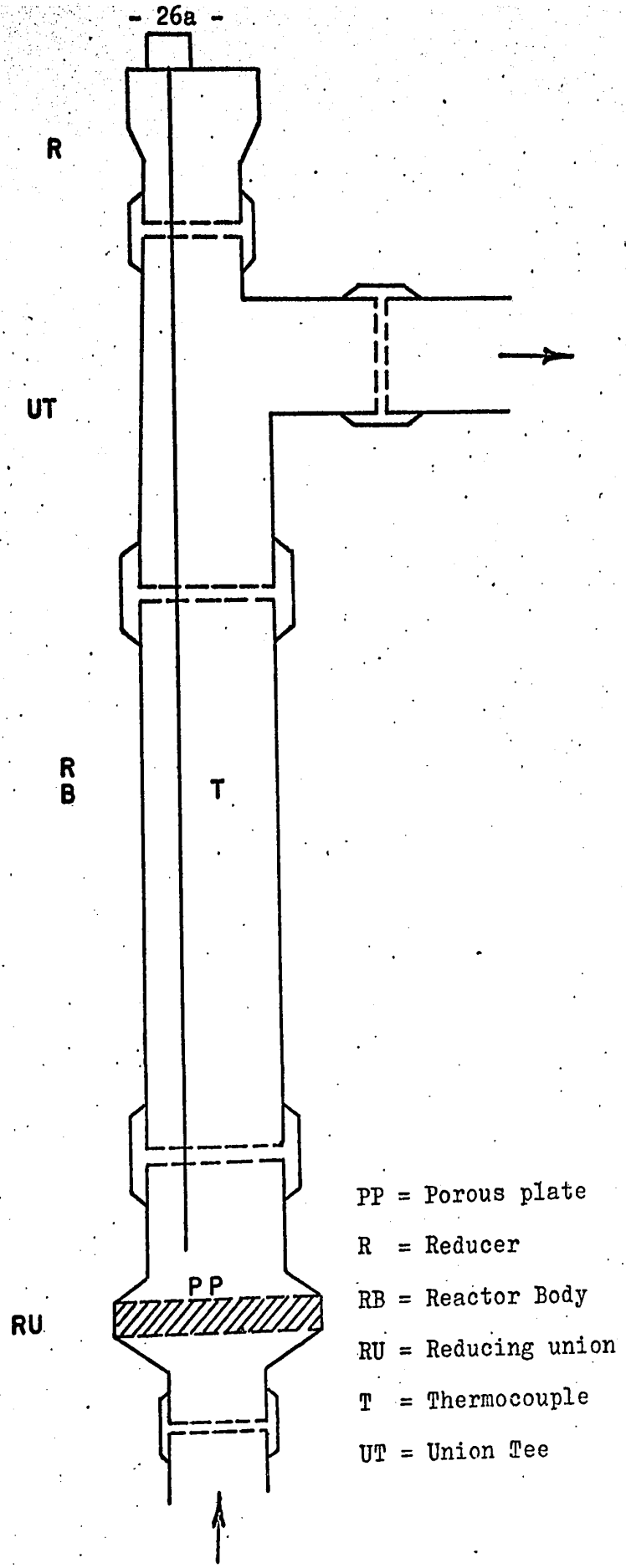

Fig. 3-3. Reactor

containing two thermocouples, was inserted through this connection to a level just above the top of the porous plate. The ends of the thermocouples inside the protection tube were one inch apart; the first being connected with Temperature Controller number 1, for controlling the temperature inside the reactor; the second going to a potentiometer (Honeywell, Model 2745) for recording the temperature during the reaction. The temperature at both levels in the reactor was checked periodically. The differences between the temperatures at the two ends was found to be negligible and the axial temperature gradient could be neglected (Appendix D, 21). The thermocouples were supplied by Thermo Electric Canada Ltd., Brampton, Ontario.

Thermo Electric Potentiometer Circuit Controller (Model no. 80025) was used to control the temperature of the reactor. It was used with transducers such as thermocouples that generated a millivolt signal. The controller measured the output of a thermocouple positioned in the reactor and provided relay contact closure to maintain the reactor temperature. A constant voltage supply circuit provided a standard voltage for the measuring circuit eliminating the need for a standard cell, battery and standardization of the battery circuit. The accuracy was within 5 microvolts (around 0.08°C); and the sensitivity was 1 microvolt, which in terms of temperature, would be approximately equivalent to a change of 0.0167°C for Iron-Constantan thermocouples. The response speed had a maximum of 1/4 second and an ambient temperature of 15° to 40°C was used.

The container for the fluidized sand bed (Figure 3-1) was made from an 8" O.D. steel cylinder, with a porous stainless steel plate (Pall Trinity Micro Corporation, Cortland, New York) inserted at the bottom, and a steel funnel, eight inches wide at the top, tapering to 1/4" O.D. at the bottom, welded to the base of the cylinder below the porous plate, and attached to compressed air line.

A layer of clean Ottawa sand, mesh numbers 40 to 60, was placed in the container on top of the porous plate, and the reactor was held upright in the center of the bed, while the vessel was completely filled with sand. During operation, only enough air was passed through the fluidized bed to make the sand bubble a little.

Two layers of Ceram-A-Flex beaded heating wire (Chemical Rubber Co., Cleveland, Ohio, Catalog no. 39-207) were wrapped around the steel cylinder. One was connected to a 10 ampere powerstat (Fisher Catalog no. 9-521) and was left on all the time. The powerstat was set in such a way as to produce sufficient heat to maintain the reactor temperature just a little below the required set temperature of Temperature Controller number 1. The other heating wire was connected to a 7.5 ampere powerstat (Fisher Catalog no. 9-521-120V2), then to Temperature Controller number 1. Asbestos powder (Asbestos Corporation, Ltd., Montreal, Quebec) was mixed with a small amount of water and applied in a 3/4" thick layer to the heating wires for insulation and also to fix the wires in position.

The reactor and fluidized bed were then placed in an outer aluminum cylinder, one foot in diameter, resting on a piece of asbestos board (Fisher Catalog no. 1-435), in the center of which a hole had been drilled for the compressed air line. The space between the aluminum cylinder and the "bed" was packed with vermiculite. The surface of the outer cylinder was coated with a layer of asbestos powder 2" thick for further insulation.

3. Product Analysis Section

The liquid trap consisted of a 4" x 7/8" O.D. glass tube fitted with a two-hole rubber stopper, for insertion of the product transport line and the tube from the condenser. The heavier reaction products, formaldehyde, methanol, and water were condensed in the trap from which samples could be withdrawn when required.

The copper water condenser was two feet long and fitted with a central condensing tube of 1/8" stainless steel.

The drying tube, made of pyrex and steel separated by rubber seals and held together by screws, was packed with drierite. Pieces of glass wool were placed at either end to stop the small drierite particles from escaping into the gas stream.

All traces of moisture from the gaseous reaction

products were removed prior to their analysis in the Fisher Gas Partitioner by the condenser and drierite tube.

The product stream after the removal of formaldehyde, methanol and water passed through a sample valve and coil, and was then vented. A stream of the carrier gas--helium--passed through the other leg of the sample valve on its way to the separating column in the gas partitioner. When the sample valve was turned on, the sample coil was taken out of series with the product stream and was simultaneously connected with the carrier gas. Using this scheme, it was possible to flush reproducible sample volumes into the separating column of the gas partitioner.

The Fisher Gas Partitioner (Model 25V) could separate and analyse oxygen, nitrogen, methane, carbon monoxide and carbon dioxide in approximately five minutes, using a 30-inch hexamethyl-phosphoramide (HMPA) column, a 6.5-foot molecular sieve 13X column, and a carrier gas flow rate of 80 ml/min. A constant temperature of 35°C was maintained by a Fisher Thermal Stabiliser (Model 27). The order of elution: composite peak, carbon dioxide, oxygen, nitrogen, methane, and carbon monoxide, is shown in Figure 3-4.

When the formaldehyde concentration in the liquid sample was high, it was somewhat difficult to accumulate

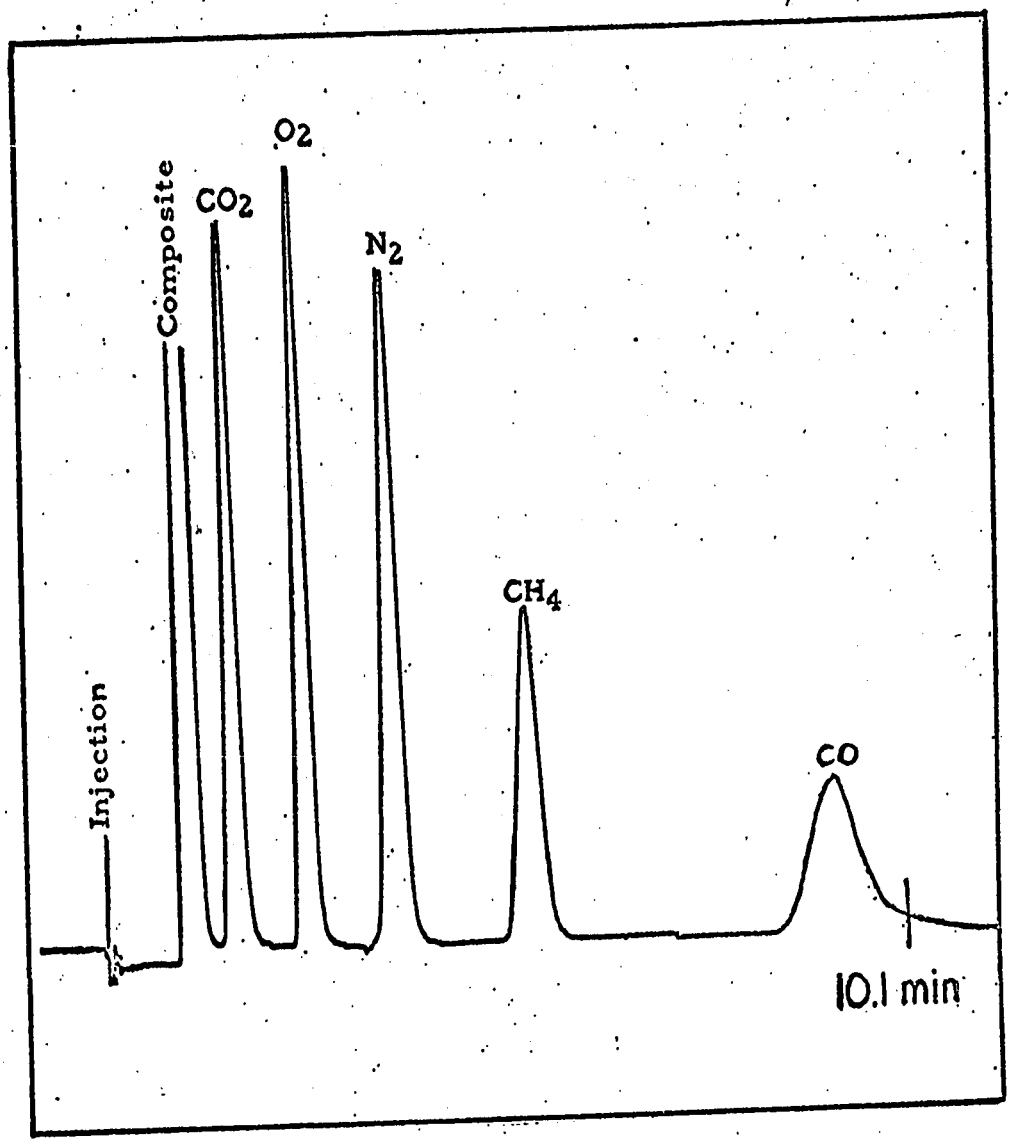

Fig. 3-4 Typical Analysis of the Gaseous Products

and analyze. Various methods of detection had therefore to be tried.

The gas chromatograph and columns used in analysing the products were assembled in the department.

All interconnections were made of 1/8" stainless steel tubing and were wrapped with heating tapes controlled by Temperature Controller number 2 (a Yellow Springs thermistor temperature controller, Model 63), having a temperature deviation of ± 0.05°C. The sensing probe was placed between the connection of the column and the detector through a Swagelok union tee.

The column was immersed in a liquid bath (Fisher bath oil no. 2) for better temperature control. The liquid was heated with an immersion heater (Fisher Catalog no. 11-463-5W4) and a "Variac." A constant bath temperature was maintained by Temperature Controller number 3 (a Yellow Springs thermistor temperature controller, Model 71), having a controlled deviation within ± 0.01°C. A 1-1/2" thick layer of glass wool around and below the liquid bath (Pyrex-Corning Glass Works, Corning, N.Y.), and an asbestos board (Fisher Catalog no. 1-435) placed on top of the bath reduced the heat loss to the surroundings.

Two-hundred-inch 15 weight percent sucrose octa-acetate on Columpak T, 400-inch 10 weight percent Ethofat 60/25 on Columpak T, 80-inch Porapak N and 80-inch Porapak Q, 80-100 mesh, columns were used to separate and analyze the reaction products. The sucrose octa-acetate and

Ethofat columns were dried at 195°C for one hour prior to use, while the Porapak N and Q columns were dried at 200°C overnight. All columns were made from 1/4" copper tube.

Three detectors were tested for product analysis in the gas chromatograph: a thermistor, gas density and thermal conductivity cell. The thermistor was not selected for further use due to the low operating temperatures recommended by the instrument manufacturer. Both the gas density detector and thermal conductivity cell were assembled in the department and had the same type of filament (a Gow-Mac W-2X hotwire, 333 mount, made of rhenium-tungsten, in a four-element macro cell). The filament possessed a cold resistance in air at 25°C of 60 ohms, and after passage of 160 ma direct current, of 80 ohms. The Gow-Mac filament gas density detector (36, 66, 71, 75, 83, 84, 92), when in use, was immersed in the same oil bath as the gas chromatograph column, but proved less sensitive to formaldehyde and methanol than the thermal conductivity cell. Thus, of the three, only the thermal conductivity detector, a Gow-Mac Model TRIIIA, 4W2 temperature-regulated cell, recommended for temperatures between 30° and 150°C, was found satisfactory, and was used throughout the rest of the investigation. Since water, one of the products of the reaction, could condense at temperatures less than 100°C, the cell temperature was maintained constantly at 100°C $\pm$ 0.1%. The detection temperature was controlled by a Fenwal Thermo Switch with an adjustable range from ambient to 205°C.

Two 120-watt cartridge heaters were connected in series with the Therme Switch. The temperature range of the unit could be varied by turning the adjusting screw at the bottom of the case, one revolution clockwise for every 32°C rise in temperature, or vice versa.

Direct current for the detectors was supplied by a Gow-Mac Model 405-Sil solid state DC Power Supply. Input power was 115 volts A.C. at 60 cycles per second; output power was from 0 to 40 volts direct current. Ripple was less than 1 mv. Regulated output ranged from 0 to 500 ma with a four-step voltage control starting at 6 - 10 volts.

The evaporating block for the liquid sample, supplied by Wilkens Instrument and Research Inc., of California, was maintained at 200°C. The liquid sample itself was injected with a two microliter syringe, Pressure-Lok, Series "A" (Precision Sampling Corporation, Baton Rouge, Louisiana.)

Liquid separations were also checked on an Aerograph Model 90-P3 gas chromatograph equipped with a thermal conductivity filament detector, and on a Perkin-Elmer Model 1540 with thermistor.

A Philips recorder PR2210U, with various multirange units connected to the appropriate gas chromatograph, recorded the peak composition of the effluent stream. A printing integrator computed the areas under the curves.

At times these areas were used in calculating the concentration of the various materials in the product stream.

D. Calibration of Equipment

Flow rates of the gas streams were measured in calibrated rotameters, and the measurements corrected for temperature and pressure variations. The flow rates were checked by both the soap bubble method and "Fisher Wet Test" gas meter. Flow rate calibration curves for air are given in the Appendix (Figure A-1).

The liquid feed rate of methanol was controlled by a needle valve, and estimated by counting the number of drops per unit time flowing from the pointed dropper in the sight glass chamber. The average volume per drop was 0.016 ml.

A sample calculation showing the calibration of the thermocouples is given in Appendix A-1.

Synthetic mixtures, similar to the actual samples, were used to calibrate the gas chromatographs, with the time and order of elution of the components based on previous injections of the pure compounds.

Since gas samples were separated on the Fisher Gas Partitioner and liquid samples in the other chromatographs, synthetic mixtures of both gases and liquids had

to be prepared. Mixtures of oxygen, carbon monoxide, carbon dioxide and nitrogen in varying proportions were accordingly made for separation on the gas partitioner. Mixtures of methanol, formaldehyde and water of known composition were prepared for injection into the other chromatographic columns.

The widths of each of the component peaks in the samples tested were found to be nearly equal (Figure 3-5). A quantitative analysis could therefore be based on either peak height or the relative peak height ratio versus percentage composition. The peak height ratio method was chosen due to its simplicity and greater accuracy over the method of measuring the areas under the peaks with an integrator which had an accuracy of only $\pm$ 0.1% at full scale deflection. It also eliminated the variations due to differences in the volumes of injected liquids, especially when the sample quantities were very small.

E. Analysis of the Products

The success of a kinetic study depends on the ability to measure accurately the rate of change in the chemical constituents of the system. An accurate quantitative analysis of the reaction products must be known if the reaction rate or conversion is to be described by a mathematical equation. Attempts were therefore made to modify the existing analytical methods to obtain a quicker and more accurate analysis of the reaction products (72).

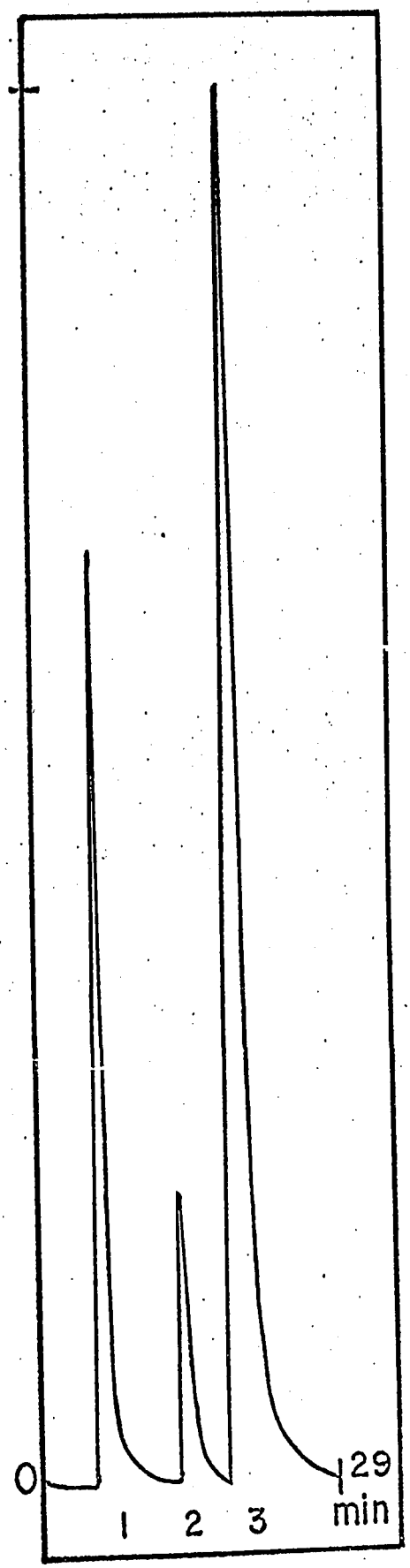

Fig. 3-5 Typical Analysis of the Liquid Products.

Chromatographic separation on 15 wt% sucrose octa-acetate-Columpak T at 93°C.
Column: Length 200 in, inlet pressure 872 (20 psig) mm Hg (at room temperature), outlet pressure 769 mm Hg.
Sample size: 1 μl of solution containing 37.2% formaldehyde, 13.1% methanol, and 49.7% water.
Bridge current: 250 ma.
Sensitivity setting: 32.
Carrier gas flow rate: 54 ml/minute.
Room temperature: 24.5°C.
Detector: thermal conductivity-filaments.
Carrier gas: Helium.

1. Formaldehyde
2. Methanol
3. Water

Recently several workers have reported the separation of formaldehyde from methanol by gas chromatography (13, 78, 79, 90, 91, 95, 102); the more interesting separations being those of McReynolds (78), Bombaugh and Bull (13) and Smolkova et al (95).

McReynolds (78) reported the separations on columns using sucrose octa-acetate supported on Celite, which had been previously washed with acetic acid. However, he reported that methanol interfered with the elution of formaldehyde. Bombaugh and Bull (13) described a quantitative procedure for determining formaldehyde in solution and as a high purity gas. They tested eight substrates and five solid supports using four different gas chromatographs, one equipped with a thermistor detector and the others with hot wire filaments, and recommended a five meter, 1/4" copper column with 10 wt% Ethofat 60/25 on Columpak T. Smolkova et al (95) tried seven different substrates on two solid supports. They found that formaldehyde, water and methanol could be determined both qualitatively and quantitatively using 30wt% Reoplex on Celite, 28 wt% PEGA on Rysorb and 28 wt% PEGA on Celite, the last gave the best results and methanol eluted much before formaldehyde.

Porapak N may also be used to separate formaldehyde from methanol and water. However, it usually produces a greater pressure drop across the column than Columpak T, and therefore is not suitable in cases where long columns are required. In studying the kinetics of

the oxidation of methanol to formaldehyde, the latter is the more important product. A sharp symmetrical peak with a short retention time is desirable, and no advantage is to be gained by having the formaldehyde elute after methanol and water.

The present work describes the use of 15 wt% sucrose octa-acetate on Columpak T in a 200 by 1/4 inch copper tube and compares the results with 10 wt% Ethofat 60/25 on Columpak T, with 28 wt% PEGA on Celite, and with Porapak N. Separations were checked on an Aerograph Model 90-P3 gas chromatograph with filament detector, a Perkin-Elmer Model 1540 with thermistor and the departmental Gow-Mac 4W2 gas chromatographs. Similar curves were obtained with all three instruments. Procedures like those described by Bombaugh and Bull (13) were followed.

The presence of formaldehyde was confirmed by absorption of part of the effluent stream in water, followed by volumetric analysis using Schiff's reagent (106).

The quantitative analysis of formaldehyde proved to be difficult due to its rapid polymerization. This polymerization was probably caused by the presence of a trace of water in the formaldehyde at room temperature. The temperature was therefore maintained at 100°C to prevent polymerization of formaldehyde in the air stream, and the presence of methanol in the mixture of water and

formaldehyde in the liquid trap effectively prevented the polymerisation from occurring there. Since polymerisation can occur at low methanol concentrations, methanol (or butanol) may be added to the products in the trap if necessary.

The total acid content was obtained by titration of the condensate from the trap with 0.055N potassium hydroxide solution. Phenolphthalein was used as the indicator for the titration. The total acid was found to be too low to affect the material balance.

A Porapak Q column six feet long, 3/16 inch in diameter, with helium, the carrier gas, flowing at a rate of 50 ml/min, was used in Aerograph Model 90-P3 with filament detector to test for the presence of formic, acetic and propionic acids in the product stream. The retention time for water, methanol and formaldehyde (a composite peak), formic, acetic and propionic acids were 0.65, 1.10, 2.05, 4.30, and 10.50 minutes respectively at 157°C. No significant amount of the acids was found.

After removal of the low-boiling-point compounds --formaldehyde, methanol, and water--from the product stream by the liquid trap, the remaining gases were passed through the condenser, drying tube, sampling valve and coil, and were either vented or analysed in the Fisher Gas Partitioner.

F. Experimental Procedure

Details of the experimental procedure for making an initial run with a specific weight of catalyst are described in this section.

The following procedure was adopted 18 to 24 hours prior to the actual taking of data so that the system might reach a steady state:

1. Purge the feed and product transport lines and the reactor by the passage of air under high pressure.

2. Remove the top of the reactor, place a specific weight of catalyst in the reactor chamber, and cover it with a layer of glass wool. Replace the top and the thermocouples, and wrap asbestos thread around any portion of the Swagelok "T" visible above the reactor chamber, to prevent sand from adhering to the connection during operation of the fluidized bed.

3. Switch on the various heating tapes for preheating the air and methanol entering the evaporating chamber, vaporizing the methanol, warming the feed line leading to the reactor, and maintaining the transport line at or above 100°C.

4. Set the two "Variac" transformers for heating the fluidized bed and adjust them periodically until the desired temperature is attained. Approximately 48 hours were required for this system to reach equilibrium.

5. Check the oil bath temperature for the gas chromatography column.

6. Turn on the helium gas for the gas chromatograph (streams 1 and 2), air for the activation of the catalyst and later the oxidation of methanol (stream 4), and compressed air for heat fluidisation of the reactor bed (stream 5). Adjust to obtain the required flow rates.

7. Switch on the recorder for the gas partitioner and gas chromatographs, in order to allow the base line to become straight and stable.

The procedures which can be carried out immediately prior to or during the experimental runs are:

1. Turn on the water for the condenser above the liquid trap.

2. Switch on the detector for the gas chromatograph.

3. Turn on the nitrogen gas stream, line 3. When the catalyst has reached the required temperature add methanol to the feed, and adjust the rates of methanol and air so as to give the desired total flow rate and correct molar ratio of oxygen to methanol.

4. Maintain these gases at their specified rates over a period of 30 minutes in which steady state conditions at the required temperature are reached.

5. Place the liquid trap in position and continue the run for at least an hour, while maintaining the required methanol and air flow rates constant.

6. Introduce the effluent gases from the reactor into the Fisher Gas Partitioner via the sample valve and coil. Inject liquid samples from the trap into the gas chromatograph, until both the liquid and gas samples show no change in composition thereby indicating that a steady state has been attained.

7. Continue the steady state run for another hour during which time at least two gas and liquid samples should be analysed.

8. After each analysis, check rotameter temperature and pressure settings and record the readings.

9. Shut off the methanol feed and keep air flowing through the catalyst bed for another hour, before the start of a second run.

At the end of each day's operation, the preceding steps were reversed. In general, any change in the reactor temperature was made at this time, by adjustment of the "Variacs" controlling the fluidized bed. Periodically, the gas chromatograph calibrations were checked to assure the stability of the columns.

IV. RESULTS

In order to compare the efficiency of the product separation in gas chromatography with different columns, comparisons are generally made on the basis of theoretical plate or minimum detectable quantity of sample.

The theoretical plate (n) requirement is defined according to Kaiser (54) as:

$$n = 5.54\left(\frac{t_{dr}}{b_{\frac{1}{2}}}\right)^2$$

where t_{dr} = retention time (uncorrected) measured in mm or min., and $b_{\frac{1}{2}}$ = peak width at half height, measured in mm or min.

The minimum detectable quantity of sample (MDQ) is defined as the quantity required to produce 0.1 mv signal on a 1 mv recorder, when the sensitivity setting of the gas chromatograph is one, or

$$MDQ = \frac{(\text{mg sample})\ (\text{wt\% sample})\ (0.1\ \text{mv})}{(\text{Sensitivity of gas chromatograph})\ (\text{ht of peak in mv})}$$

The results of the gas chromatographic analysis of formaldehyde, $b_{\frac{1}{2}}$ (min.), $t_{dr}/b_{\frac{1}{2}}$, n, and MDQ (mg), are given in Table S-A-2.

The retention time of formaldehyde on 15 wt% sucrose octa-acetate supported on Columpak T was 4 minutes at 97°C (Figure 4-1). The injected sample contained a mixture of 26.9% formaldehyde, 9.5% methanol, 35.9% water, and 27.8% butanol by weight. The column inlet pressure was 872 (20 psig) mm Hg at room temperature (24.5°C); outlet pressure, 769 mm Hg; bridge current, 250 ma; sensitivity setting 32; and carrier gas flow rate 54 ml/min. With Ethofat 60/25 on Columpak T, formaldehyde eluted after methanol and water, and the formaldehyde peaks were broader in comparison to those obtained with sucrose octa-acetate. On Porapak N, the retention time of formaldehyde was much greater than on sucrose octa-acetate and higher inlet pressures (17.5 psig) were required.

Sucrose octa-acetate on Columpak T gave the lowest $t_{dr}/b_{\frac{1}{2}}$ values (4.1 at 97°), the smallest number of theoretical plates (92), and the greatest sensitivity (MDQ-formaldehyde = 0.0009 mg) of all the columns tested. The substrate for this column could be easily loaded on its support up to 20% by weight, and still pack without difficulty. It was also stable over a wide range of temperature.

As compared to sucrose octa-acetate on Columpak T, the $t_{dr}/b_{\frac{1}{2}}$ values for formaldehyde with 10 wt% Ethofat 60/25 on Columpak T at 115°C, with 20 wt% PEGA on Celite at 110°C (95), and with Porapak N at 110°C

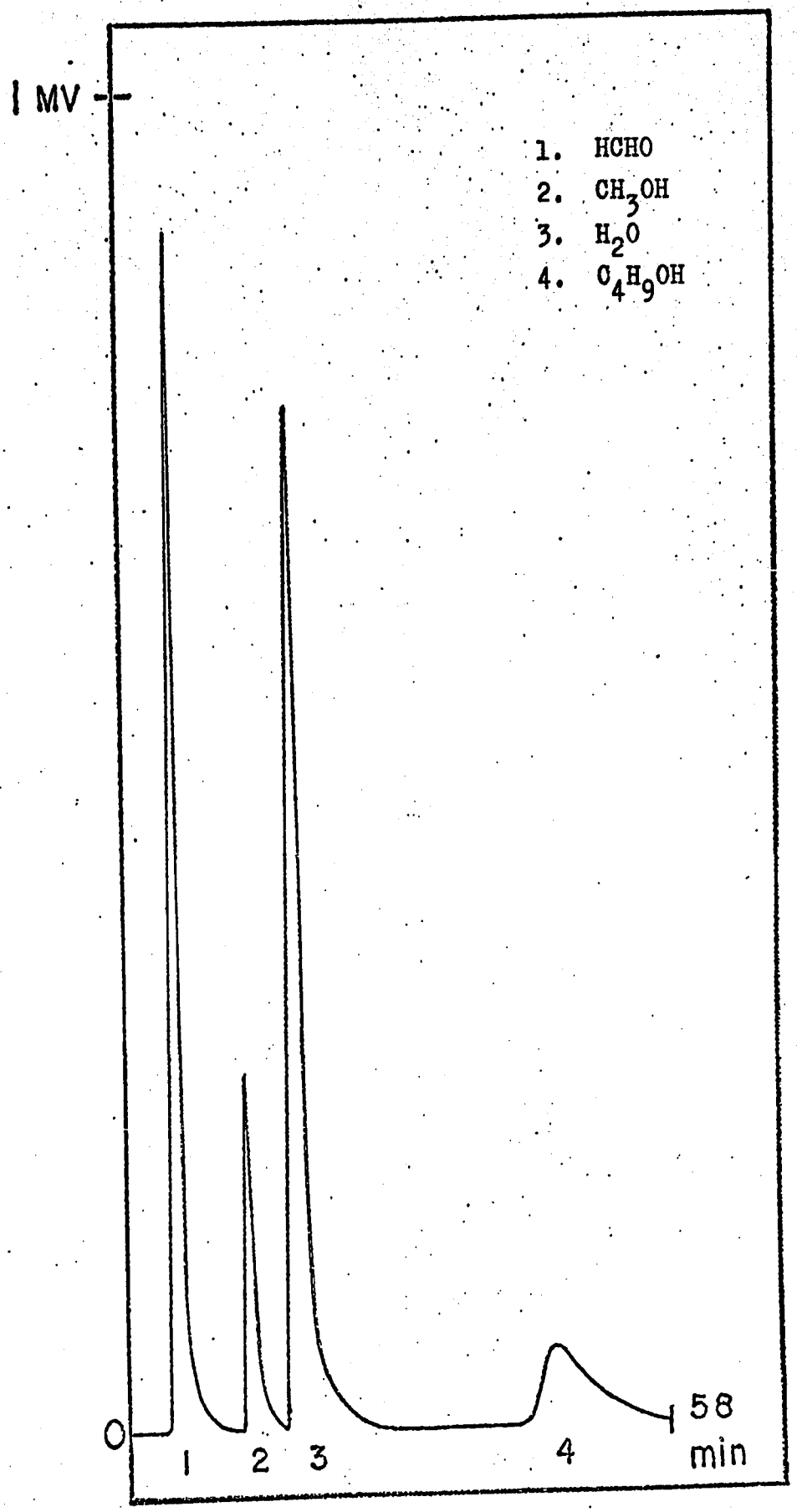

Fig. 4-1 Gas Chromatogram of HCHO, CH_3OH, H_2O, and C_4H_9OH

were 5.4, 5.7, and 14.5 respectively. Similarly, the smallest number of theoretical plates were, respectively, in that order 160, 179, and 1162. The MDQ-formaldehyde in milligrams for Ethofat 60/25 and Porapak N was 0.525 and 0.0441. Thus the column containing sucrose octa-acetate on Columpak T gave the best results and was used for all remaining analyses.

The effect of the catalysts--manganese dioxide-molybdenum trioxide, vanadium pentoxide, molybdenum trioxide, and manganese dioxide--on conversion, yield, and selectivity was determined.

Conversion may be defined as the ratio of the moles of methanol converted per hour to the moles of methanol fed per hour; the yield, the ratio of the moles of formaldehyde produced per hour to the moles of methanol fed per hour; the selectivity, the ratio of the moles of formaldehyde produced per hour to the moles of methanol converted per hour.

The highest yields obtained with manganese dioxide-molybdenum trioxide, vanadium pentoxide, molybdenum trioxide and manganese dioxide were 84, 69, 10 and 2 percent respectively. The results secured with manganese dioxide-molybdenum trioxide as catalyst are given in Table 8-B-1 and Figure 5-3, and with the others in Table 8-B-2 and Figure 4-2.

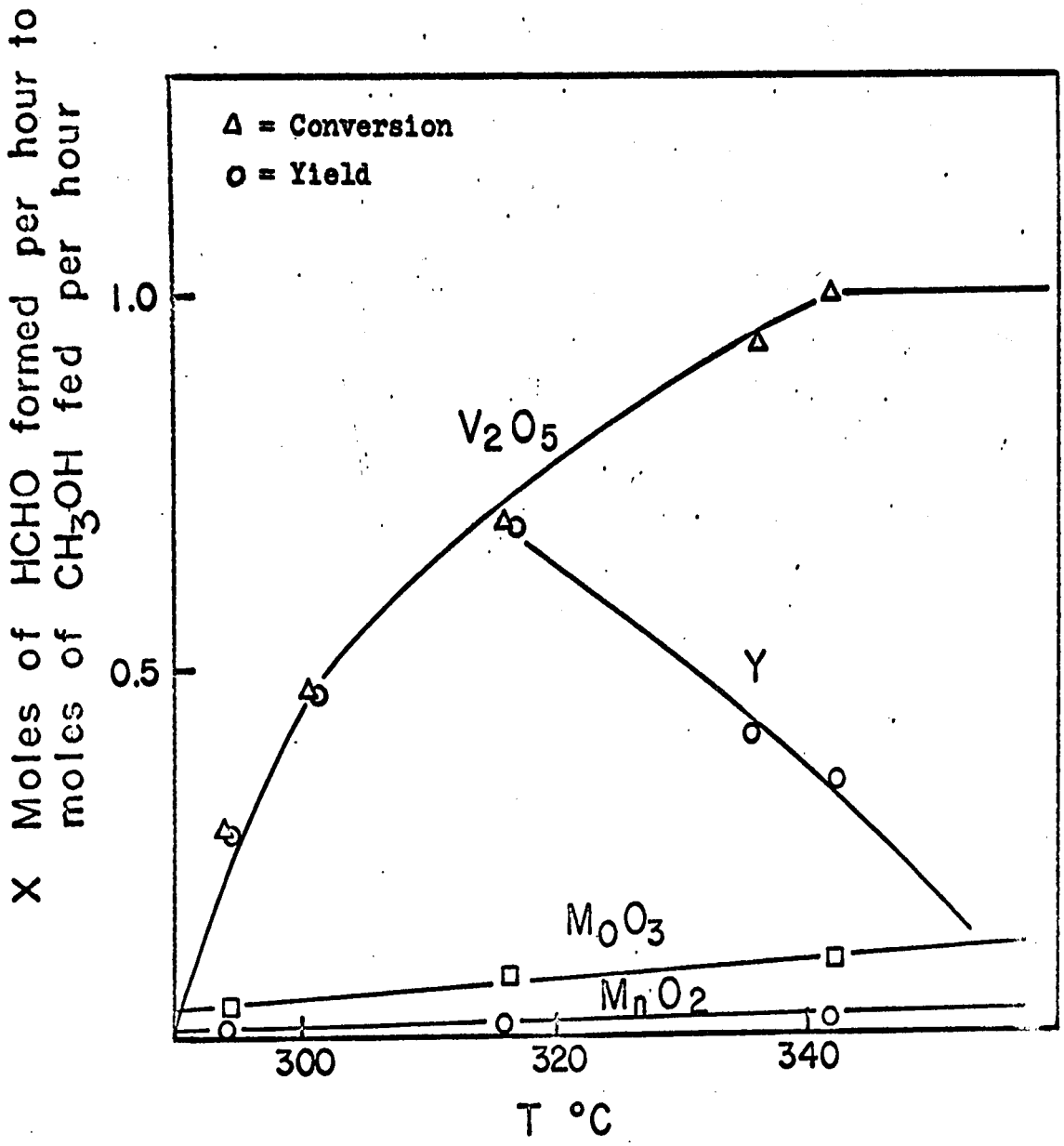

Fig. 4-2. Temperature Effect on Conversion and Yield of V_2O_5, MoO_3, and MnO_2.

V. KINETIC ANALYSIS OF DATA

The pertinent problem in the design or analysis of a catalytic flow process is the relationship between the weight of the catalyst and the reactant feed rate. In a steady state flow system, this relationship is obtained by consideration of an elementary section of the reactor containing a mass of catalyst dW in which a conversion dx is produced. Then

$$Fdx = rdW \qquad (5\text{-}1)$$

where F = feed rate, moles per unit time
W = mass of catalyst in the reactor
x = conversion, moles per unit mole of feed
r = reaction rate, moles/(mass of catalyst)(time)

Integration yields

$$\frac{W}{F} = \int_0^x \frac{dx}{r} \qquad (5\text{-}2)$$

The reaction rate, r, can be expressed as a function of conversion. It is customary to correlate and derive a rate equation in terms of partial pressures of reactants based on the well known Hougen-Watson method (45, 109). This method assumes one of the reaction steps to be the rate controlling step, and is based on the Langmuir-Hinshelwood theory of catalysis on solid surfaces(61).

A. Rate Steps in Heterogeneous Kinetics

The overall catalytic process is the result of a series of reaction steps. For non-porous catalysts these steps are:

1. Transport of the reactants from the bulk-fluid phase to the solid-fluid interface.
2. Adsorption of reactants (one or more) on the solid surface.
3. A surface reaction between the adsorbed reactants or one of the gaseous reactants and an adsorbed reactant on the catalyst surface.
4. Desorption of products (one or more) from the surface to the fluid-solid interface.
5. Transport of the products from the interface to the bulk-fluid stream.

In the case of porous catalysts, internal diffusion through the pores of the catalyst may also be involved in addition to external diffusion in the fluid phase surrounding the catalyst particle (steps 1 and 5). Some of the reactant molecules, for example, will not be adsorbed on the outer surface of the catalyst but will diffuse into the pores and be adsorbed and react on the internal pore surface. In such cases two additional steps should be added to the list: (1a) internal diffusion of reactants along the pores; (5a) internal diffusion of the products along the pores to the outer surface.

The relative importance of these steps can vary greatly, and depends on the operating conditions for the system. Processes 1 and 5 can be handled independently of the others. However, the internal-diffusion steps 1a and 5a cannot be separated from the surface reactions 2, 3 and 4. Conventionally, they have been treated by basing the rate of reaction upon the total catalytic surface (internal and external).

Each of these steps offers some resistance to the overall process. If all these resistances were considered, the resulting rate equations would be very complicated. The diffusion steps 1, 1a, 5, and 5a are physical processes which can be minimized or accounted for independently as will be described later. The chemical steps 2, 3 and 4 contribute significant resistances which cannot be reduced by altering physical conditions and hence are the most important ones to consider. Inclusion of only these three types results in equations of high complexity. Usually only one of these three offers a much higher resistance than the other two, and is therefore considered to be the rate-controlling, or rate-determining step, while the other two are considered to be at equilibrium.

B. Correlation of Rate Equations

1. Classical Langmuir-Hinshelwood Mechanism

The classical Langmuir-Hinshelwood theory of

catalysis on solid surfaces is founded primarily on the concept of monolayer chemisorption on the surface of the catalyst and assumes an equilibrium between the adsorption and desorption processes under isothermal conditions.

Three possible five-step oxidation-reduction mechanisms for the conversion of methanol to formaldehyde are described in the following pages under the headings, Groups I, II, and III. The significance of this series lies in the fact that if only one step controls the kinetics of the reaction fifteen different rate mechanisms can be postulated, based on the rate-controlling step. The general development of one rate equation, the selection of a rate controlling step, and correlation of the kinetic data taken in this study are described.

Group I: Atomic oxygen and molecular formaldehyde adsorbed on separate sites:

$$CH_3OH(g) + s \underset{k_{-1}}{\overset{k_1}{\rightleftharpoons}} CH_3OH\text{-}s \qquad (5\text{-}3)$$

$$\tfrac{1}{2}O_2(g) + s \underset{k_{-2}}{\overset{k_2}{\rightleftharpoons}} O\text{-}s \qquad (5\text{-}4)$$

$$CH_3OH\text{-}s + O\text{-}s \underset{k_{-3}}{\overset{k_3}{\rightleftharpoons}} HCHO\text{-}s + H_2O\text{-}s \qquad (5\text{-}5)$$

$$HCHO\text{-}s \underset{k_{-4}}{\overset{k_4}{\rightleftharpoons}} HCHO(g) + s \qquad (5\text{-}6)$$

$$H_2O\text{-}s \underset{k_{-5}}{\overset{k_5}{\rightleftharpoons}} H_2O(g) + s \qquad (5\text{-}7)$$

where θ_1, θ_2, θ_3, θ_4, and θ_5 are the fractions of the surface that are bare, covered with methanol, atomic oxygen, formaldehyde and water respectively.

The rate of adsorption and desorption of methanol per unit of total surface is $k_1 p_M \theta_1$, and $k_{-1}\theta_2$. At equilibrium,

$$\frac{\theta_2}{\theta_1} = \frac{k_1 p_M}{k_{-1}} = K_1 p_M \qquad (5\text{-}8)$$

p_M being the methanol gas pressure, k_1 and k_{-1} the adsorption and desorption rate constants.

Similarly, from equations 5-4 to 5-7 the following relationships can be derived:

$$\frac{\theta_3}{\theta_1} = \frac{k_2}{k_{-2}} p_{O_2}^{\frac{1}{2}} = K_2 p_{O_2}^{\frac{1}{2}} \qquad (5\text{-}9)$$

$$\frac{\theta_4\theta_5}{\theta_2\theta_3} = \frac{k_3}{k_{-3}} = K_3 = \left(\frac{p_F p_W}{K_2 K_3 K_4 K_5 p_{O_2}^{\frac{1}{2}}}\right)\theta_1 \qquad (5\text{-}10)$$

$$\frac{\theta_1}{\theta_4} = \frac{k_4}{k_{-4}} p_F = K_4/p_F \qquad (5\text{-}11)$$

$$\text{Since} \sum_{i=1}^{f} \theta_i = 1 \qquad (5\text{-}12)$$

eliminating θ_2, θ_3, θ_4, and θ_5, by combining equations 5-9 to 5-12 and solving

$$\theta_1 = \frac{1}{1 + p_f p_w / K_2 K_3 K_4 K_5 p_{O_2}^{\frac{1}{2}} + K_2 p_{O_2}^{\frac{1}{2}} + p_f / K_4 + p_w / K_5} \qquad (5\text{-}13)$$

If the adsorption of methanol controls the surface process, the net rate of the reaction would be

$$r = k_1 p_M \theta_1 - k_{-1} \theta_2 = k_1 \theta_1 (p_M - p_f p_w / K_1 K_2 K_3 K_4 K_5 p_{O_2}^{\frac{1}{2}}) \qquad (5\text{-}14)$$

Groups II: Molecular oxygen and formaldehyde adsorbed on separate sites.

$$CH_3OH(g) + s \underset{k_{-1}}{\overset{k_1}{\rightleftharpoons}} CH_3OH\text{—}s$$

$$O_2(g) + s \underset{k_{-2}}{\overset{k_2}{\rightleftharpoons}} O_2\text{—}s$$

$$2\ CH_3OH\text{—}s + O_2\text{—}s \underset{k_{-3}}{\overset{k_3}{\rightleftharpoons}} 2\ HCHO\text{—}s + (H_2O)_2\text{—}s \qquad (5\text{-}15)$$

$$HCHO\text{—}s \underset{k_{-4}}{\overset{k_4}{\rightleftharpoons}} HCHO(g) + s$$

$$(H_2O)_2\text{—}s \underset{k_{-5}}{\overset{k_5}{\rightleftharpoons}} 2\ H_2O(g) + s$$

GROUP III: One molecule of oxygen and two molecules of formaldehyde adsorbed on separate sites:

$$CH_3OH(g) + s \underset{k_{-1}}{\overset{k_1}{\rightleftharpoons}} CH_3OH\text{—}s$$

$$O_2(g) + s \underset{k_{-2}}{\overset{k_2}{\rightleftharpoons}} O_2\text{—}s$$

$$2\ CH_3OH\text{—}s + O_2\text{—}s \underset{k_{-3}}{\overset{k_3}{\rightleftharpoons}} (HCHO)_2\text{—}s + 2H_2O\text{—}s \qquad (5\text{-}16)$$

$$(HCHO)_2\text{—}s \underset{k_{-4}}{\overset{k_4}{\rightleftharpoons}} 2\ HCHO(g) + s$$

$$H_2O\text{—}s \underset{k_{-5}}{\overset{k_5}{\rightleftharpoons}} H_2O(g) + s$$

Rate equations for Groups II and III could be similarly derived following the procedure used for Group I reactions. Laidler (64) and Hougen-Watson (46) have derived rate expressions for several of the rate-controlling steps.

2. Redox Mechanism (Modified Langmuir-Hinshelwood Mechanism)

The oxidation of oxygenated hydrocarbons can be visualised as an irreversible oxidation-reduction reaction taking place in either two or three stages. The

Langmuir-Hinshelwood mechanism applied to this process is generally referred to as the "Redox Mechanism." This mechanism may be applied to the oxidation of methanol to formaldehyde, which can be treated as an irreversible two- or three-stage oxidation-reduction reaction.

a. Two-stage Redox Mechanism

Gaseous methanol reacts with either adsorbed or lattice oxygen of the catalyst to form formaldehyde, water and a reduced site. Subsequently oxygen in the air replaces the oxygen which was used in the conversion of methanol:

$$m(CH_3OH(g) + s_{ox} \xrightarrow{k_1} HCHO(g) + H_2O + s_{red}) \quad (5\text{-}17)$$

$$n(O_2(g) + s_{red} \xrightarrow{k_2} s_{ox}) \quad (5\text{-}18)$$

The equilibrium in both stages is shifted to the right side of equations 5-17 and 5-18. It is therefore possible to consider in the kinetic mechanism only the reaction rates from left to right.

The rate of the process is therefore given by equation 5-19:

$$r_1 = k_1 p_M^m \theta \quad (5\text{-}19)$$

where θ is the fraction of the catalyst surface covered by adsorbed or lattice oxygen. The rate of process 5-18

may be defined as

$$r_2 = k_2 p_{O_2}^n (1 - \theta) \qquad (5\text{-}20)$$

At steady state when the rates of both processes 5-17 and 5-18 are the same and "$\propto$", that is, the number of oxygen molecules required for converting one methanol molecule to formaldehyde, is equal to 0.5,

$$\propto r_1 = r_2 \qquad (5\text{-}21)$$

If one substitutes equations 5-19 and 5-20 in 5-21, then

$$\theta = \frac{1}{1 + \propto k_1 p_M^m / k_2 p_{O_2}^n} \qquad (5\text{-}22)$$

and the rate of oxidation of methanol (r) to formaldehyde is

$$r = r_1 = k_1 p_M^m \theta = \frac{k_1 p_M^m}{1 + k_1 p_M^m / k_2 p_{O_2}^n} \qquad (5\text{-}23)$$

The integrated forms of rate equation 5-23 with different m and n values are listed in Table 5-1, where

$$p_M = {}_o p_M (1 - x)$$

$$p_{O_2} = {}_o p_{O_2} - \tfrac{1}{2} {}_o p_M x$$

P_M = partial pressure of methanol at time t

${}_oP_M$ = partial pressure of methanol in the feed

P_{O_2} = partial pressure of oxygen at time t

${}_oP_{O_2}$ = partial pressure of oxygen in the feed

x = percentage conversion of methanol to formaldehyde

Table 5-1

Two-Stage Redox Mechanisms

No	Reaction Order m CH_3OH	Reaction Order n O_2	Integrated Rate Equation
1	1	0.5	$\frac{V}{F}\frac{{}_oP_M}{\ln(1-x)} = -\frac{1}{K_1} + \frac{4\alpha}{K_2}\frac{\left[{}_oP_{O_2}^{\frac{1}{2}} - ({}_oP_{O_2} - \frac{1}{2}x\,{}_oP_M)^{\frac{1}{2}}\right]}{\ln(1-x)}$
2	1	0	$\frac{V}{F}\frac{1}{x} = -\frac{1}{K_1}\frac{\ln(1-x)}{{}_oP_M x} + \frac{\alpha}{K_2}$
3	0.5	0	$\frac{V}{F}\frac{1}{x} = \frac{2}{K_1}\frac{\left[1-(1-x)^{\frac{1}{2}}\right]}{{}_oP_M^{\frac{1}{2}} x} + \frac{\alpha}{K_2}$
4	1	1	$\frac{V}{F}\frac{{}_oP_M}{\ln(1-x)} = -\frac{1}{K_1} + \frac{2\alpha}{K_2}\frac{\ln\left[{}_oP_{O_2}/({}_oP_{O_2} - \frac{1}{2}\,{}_oP_M x)\right]}{\ln(1-x)}$
5	0.5	0.5	$\frac{V}{F}\frac{{}_oP_M^{\frac{1}{2}}}{\left[1-(1-x)^{\frac{1}{2}}\right]} = \frac{2}{K_1} + \frac{4\alpha}{K_2}\frac{{}_oP_{O_2}^{\frac{1}{2}} - ({}_oP_{O_2} - \frac{1}{2}\,{}_oP_M x)^{\frac{1}{2}}}{{}_oP_M^{\frac{1}{2}}\left[1-(1-x)^{\frac{1}{2}}\right]}$

b. Three-Stage Redox Mechanism

The oxidation of methanol to formaldehyde according to the "three-stage redox mechanism" can be visualized to occur in the following ways:

1) Gaseous methanol is adsorbed at the oxidized site on the catalyst surface, which then decomposes to give gaseous formaldehyde, water, and a reduced site. Oxygen subsequently reacts with the reduced site to give the oxidized site.

2) Gaseous methanol reacts with the oxidized site at the catalyst surface to give water and adsorbed formaldehyde. The adsorbed formaldehyde is then desorbed to yield gaseous formaldehyde and a reduced site. The reduced site reacts with gaseous oxygen to form the oxidized site.

3) Gaseous methanol reacts with the oxidized site at the catalyst surface to give gaseous formaldehyde and adsorbed water, which subsequently desorbs to yield gaseous water and a reduced site. Gaseous oxygen then reacts with the reduced site to give back the oxidized site.

4) Gaseous methanol reacts with the oxidized site at the catalyst surface forming formaldehyde, water and a reduced site. Subsequently gaseous oxygen is

adsorbed at the reduced site, and reacts with the reduced site to form the oxidised site.

5) Gaseous methanol reacts with the oxidised site at the catalyst surface forming water and adsorbed formaldehyde. The latter enters into equilibrium with desorbed formaldehyde and the reduced site. Gaseous oxygen reacts with the reduced site to yield the oxidised site.

The three-stage redox mechanisms with their respective rate equations and m and n values are listed in Table 5-2. The rate equation for the oxidation of methanol to formaldehyde according to mechanism 1 can be derived as follows:

$$mCH_3OH(g) + s_{ox} \longrightarrow (CH_3OH)_m\text{---}s_{ox} \qquad (5\text{-}24)$$

$$(CH_3OH)_m\text{---}s_{ox} \longrightarrow mHCHO(g) + mH_2O(g) + s_{red} \qquad (5\text{-}25)$$

$$s_{red} + nO_2(g) \longrightarrow s_{ox} \qquad (5\text{-}26)$$

where θ_1, θ_2, and θ_3 represent the fractions of the surface of the catalyst that are bare, covered by methanol, and the reduced site respectively.

Hence:

Table 5-2

Three-Stage Redox Mechanisms

No	Reaction Order m CH_3OH	Reaction Order n O_2	Reaction Mechanism	Rate Equation
1	1, 2	0.5	$mCH_3OH(g) + S_{ox} \xrightarrow{k_1} (CH_3OH)_m\text{---}S_{ox}$ $(CH_3OH)_m\text{---}S_{ox} \xrightarrow{k_2} mHCHO(g) + mH_2O(g) + S_{red}$ $S_{red} + nO_2(g) \xrightarrow{k_3} S_{ox}$	$r = \frac{k_1 p_M^m}{1+(k_1/k_2)p_M^m+0.5k_1 p_M^m/k_3 p_{O_2}^n}$
2	1, 2	0.5	$mCH_3OH(g) + S_{ox} \xrightarrow{k_1} (HCHO)_m\text{---}S_{red} + mH_2O(g)$ $(HCHO)_m\text{---}S_{red} \xrightarrow{k_2} mHCHO(g) + S_{red}$ $S_{red} + nO_2(g) \xrightarrow{k_3} S_{ox}$	$r = \frac{k_1 p_M^m}{1+(k_1/k_2)p_M^m+0.5k_1 p_M^m/k_3 p_{O_2}^n}$

Table 5-2

Three-Stage Redox Mechanisms

No	Reaction Order m (CH_3OH)	Reaction Order n (O_2)	Reaction Mechanism	Rate Equation
3	1, 2	0.5	$mCH_3OH(g) + S_{ox} \xrightarrow{k_1} (H_2O)_m\text{---}S_{red} + mHCHO(g)$ $(H_2O)_m\text{---}S_{red} \xrightarrow{k_2} mH_2O(g) + S_{red}$ $S_{red} + mO_2(g) \xrightarrow{k_3} S_{ox}$	$r = \frac{k_1 p_M^m}{1+(k_1/k_2)p_M^m+0.5k_1 p_M^m/k_3 p_{O_2}^n}$
4	1, 2	0.5	$mCH_3OH(g) + S_{ox} \xrightarrow{k_1} mH_2O(g) + S_{red} + mHCHO(g)$ $S_{red} + mO_2(g) \xrightarrow{k_2} (O_2)_m\text{---}S_{red}$ $(O_2)_m\text{---}S_{red} \xrightarrow{k_3} S_{ox}$	$r = \frac{k_1 p_M^m}{1+0.5(k_1/k_3)p_M^m+0.5(k_1 p_M^m/k_2 p_{O_2}^n)}$

Table 5-2

Three-Stage Redox Mechanisms

No	Reaction Order m (CH$_3$OH)	Reaction Order n (O_2)	Reaction Mechanism	Rate Equation
5			$mCH_3OH(g) + S_{ox} \xrightarrow{k_1} (HCHO)_m\text{---}S_{red} + mH_2O(g)$ $(HCHO)_m\text{---}S_{red} \underset{}{\overset{K_2}{\rightleftharpoons}} mHCHO(g) + S_{red}$ $S_{red} + nO_2(g) \xrightarrow{k_3} S_{ox}$	$r = \dfrac{k_1 p_M^m}{1+0.5(k_1 p_M^m/k_3 p_{O_2}^n)+0.5(k_1 p_M^m p_F^m/K_2 k_3 p_{O_2}^n)}$

$$r_1 = k_1\theta_1 p_H^n \tag{5-27}$$

$$r_2 = k_2\theta_2 \tag{5-28}$$

$$r_3 = k_3\theta_3 p_{O_2}^n \tag{5-29}$$

$$r_1 = r_2 \tag{5-30}$$

$$\theta_2 = k_1\theta_1 p_H^n/k_2 \tag{5-31}$$

$$r_2 = 2r_3 \tag{5-32}$$

$$\theta_3 = k_2\theta_2/2k_3 p_{O_2}^n = k_1 p_H^n\theta_1/2k_3 p_{O_2}^n \tag{5-33}$$

$$\sum_{i=1}^{3} \theta_i = 1 \tag{5-34}$$

where θ_i is that fraction of the surface covered by the ith species.

$$\theta_1 = 1/(1 + k_1 p_H^n/k_2 + k_1 p_H^n/2k_3 p_{O_2}^n) \tag{5-35}$$

If r_1 is in control

$$\begin{aligned} r &= r_1 \\ &= k_1\theta_1 p_H^n \\ &= k_1 p_H^n/(1 + k_1 p_H^n/k_2 + k_1 p_H^n/2k_3 p_{O_2}^n) \end{aligned} \tag{5-37}$$

If r_2 is in control

$$r = r_2 = k_2\theta_2 = k_2 \cdot \frac{k_1 p_M \theta_1}{k_2}$$
$$= k_1 \theta_1 p_M^n / k_2 \qquad (5\text{-}38)$$

If r_3 is the rate-controlling step, then

$$r = r_3$$
$$= k_3 \theta_3 p_{O_2}^n = k_1 p_M^n \theta_1 / 2 = k_3 \cdot \frac{k_1 p_M \theta_1}{2 k_3 p_O} \cdot p_O \qquad (5\text{-}39)$$

C. Factors effecting the Rate Mechanism

The rate of reaction is generally a function of temperature, pressure, and composition of the reactants. The actual kinetics of the reaction may sometimes be hidden by several factors, as for example, catalytic activity of the reactor system, stability of the catalyst, diffusion, and catalyst surface temperature effects. In order to derive a true rate equation, the preceding factors which may effect the mechanism significantly should be either eliminated or minimized.

1. Activity of the System and Stability of the Catalyst

No reaction between methanol and air (0.05 moles of methanol/hr and 0.345 moles of air/hr) was observed to take place, in the absence of the catalyst even after three hours at 450°C.

The activity of the catalyst remained fairly constant during the course of the study (Figure 5-1 and Table 8-B-1). In addition, the experiments were performed at random in order to nullify any effects due to changes in catalytic activity.

2. Exterior Heat and Mass Transfer Effects

In the rate equations for reactions catalyzed by solid surfaces the partial pressures and temperature should represent values at the gas-solid interface. These values can usually be calculated from measurements of bulk-stream values. Because of resistances imposed by heat and mass transfer, the interfacial and bulk-stream quantities are different. It is desirable to eliminate these transfer resistances to simplify the correlation of experimental data on reaction rates.

The effect of heat and mass transfers can be visualised from the following:

Heat Transfer	Mass Transfer
$\Delta T = T_i - T = \frac{q_m}{h_g a_m}$	$\Delta p_A = p_{A_i} - p_A = \frac{r_A}{k_g a_m}$
where	
T_i = temperature of the gas-solid interface	p_{A_i} = partial pressure of component A at gas-solid surface

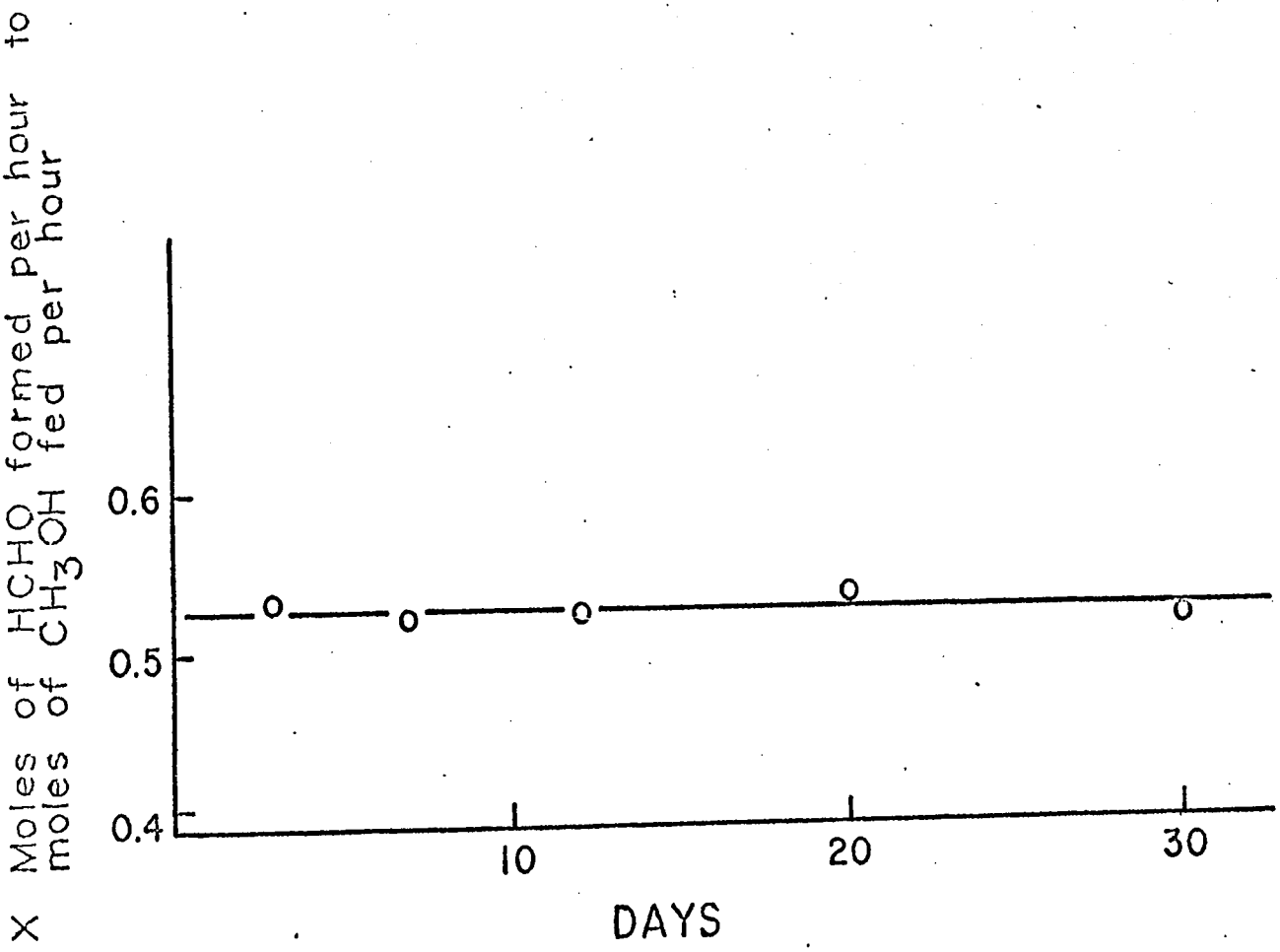

Fig. 5-1 Stability of Catalyst Activity

Heat Transfer	Mass Transfer
T = temperature of the bulk stream	p_A = partial pressure of component A in the bulk stream
ΔT = temperature drop across the film	Δp_A = partial pressure difference of component A across the gas film
q_m = heat transfer due to heat of reaction per unit mass of catalyst	r_A = rate of reaction or mass transfer of A per unit mass of catalyst
h_g = heat transfer coefficient of the gas film	k_g = mass transfer coefficient of the gas film

a_m = partial surface area per unit mass of catalyst. The transfer coefficients h_g and k_g can be calculated from the dimensionless Chilton-Colburn (18,20) j-factors.

$$j_h = \left(\frac{h_g}{C_p G}\right)\left(\frac{C_p \mu}{k}\right)_f^{2/3} \qquad j_d = \left(\frac{k_g M_m p_{f_A}}{G}\right)\left(\frac{\mu}{\rho D_{Am}}\right)_f^{2/3} \tag{5-40}$$

where c_p = specific heat of the gas

G = mass velocity of flow based on the total cross-sectional area of the bed, mass per unit time per unit area

μ = viscosity of the gas

k = thermal conductivity of the gas

$\frac{c_p \mu}{k}$ = the dimensionless Prandtl number

M_m = mean molecular weight of the gas film

P_{f_A} = film pressure factor, defined by equation (5-41).

ρ = density of gas

D_{Am} = average diffusivity of component A

$\frac{\mu}{\rho D_{Am}}$ = the dimensionless Schmidt number

Subscript f = properties at average condition of the gas film

For

$$\frac{D_p G}{\mu} > 350,$$

j_h and j_d can be obtained from Gamson, Thodos and Hougen's (32) equations:

$$j_h = 1.06 \left(\frac{D_p G}{\mu}\right)^{-0.41} \qquad j_d = 0.99 \left(\frac{D_p G}{\mu}\right)^{-0.41}$$

For

$$\frac{D_p G}{\mu} < 350,$$

j_h and j_d are obtained by Wilkie and Hougen's (108) equation:

$$j_h = 1.95 \left(\frac{D_p G}{\mu}\right)^{-0.51} \qquad j_d = 1.82 \left(\frac{D_p G}{\mu}\right)^{-0.51}$$

where $\frac{D_p G}{\mu}$ = modified Reynolds number

D_p = effective particle diameter = $\sqrt{\frac{a_p}{\pi}}$

where a_p = average surface area per particle

The film pressure factor for component A, p_{f_A}, in Equation (5-40) is defined by:

$$p_{f_A} = \frac{(\pi \pm \delta_A p_A) - (\pi \pm \delta_A p_{A_i})}{\ln\left(\frac{\pi \pm \delta_A p_A}{\pi \pm \delta_A p_{A_i}}\right)} \qquad (5\text{-}41)$$

where π = total pressure

and $\delta_A = \frac{r + s + \ldots - a - b \ldots}{a}$

where r, s, ... a, b, ... are the coefficients of components R, S, ..., A, B, ..., respectively, in the reaction equation $aA + bB + \ldots \longrightarrow rR + sS + \ldots$

It can easily be recognised that for the diffusion of component A, p_{f_A} is the log-mean value of $(\pi + \delta_A p_A)$

across the gas film. Similarly, for B, $p_{f_B} = (\pi + \delta_B p_B)_{lm}$, for S, $p_{f_S} = (\pi - \delta_S p_S)_{lm}$, etc. If the ratios $\left(\frac{\pi + \delta p_2}{\pi + \delta p_1}\right)$'s are small, for example, less than 1.2, the arithmetic means are sufficiently accurate for practical purposes.

Yoshida et al (111) recently developed a method for calculating the drop in temperature and partial pressure between the bulk gas stream and the exterior surface of the catalyst, and even within the catalyst pellet itself.

The temperature (ΔT) and pressure gradients (Δy) can be easily determined from the charts proposed by Yoshida et al (111) using calculated values of the constants and dimensionless numbers for the particular system. In essence, they can be represented by:

$$T = Q(j_h)^{-1} (Pr)^{2/3}_f \qquad y_A = \frac{\Delta p_A}{p_A} = R(j_d)^{-1} y_{f_A} (Sc)^{2/3}_f$$

Where

$$Q = \frac{r \Delta H_A}{a_w G C_p G_M} \qquad R = \frac{r_s}{a_w G G_M}$$

ΔH_A = heat of reaction per mole of A reacted

$$y_{f_A} = \frac{p_{f_A}}{\pi}$$

Pr = Prandtl number $= \frac{C_p \mu}{k}$

Sc = Schmidt number $= \mu / \rho D_{AM}$

G_M = molal mass velocity of gas based on total cross section of bed

ϕ = shape factor, defined as the ratio of actual external surface area available for mass and heat transfers to the total external surface area, assumed to be 0.90 for irregular granules.

The j-factors are related to the modified Reynolds number defined as, $Re = \frac{G}{a\phi\mu}$ by the equations:

(i) for Re = 0.01——50

$$j_d = 0.84\ Re^{-0.51}$$

(ii) for Re = 50——1000

$$j_d = 0.57\ Re^{-0.41}$$

and $j_h = 1.076\ j_d$

The data of many investigators have been correlated by this method. The gradients are found to fall in a narrow band on a Δy_A verses R or a ΔT verses Q plot, indicating that R and Q are the most significant factors in controlling the pressure and the temperature gradients respectively.

It can also be seen that both the temperature and partial pressure differences across the film are proportional to $r_A D_p^{n+1} G^{n-1}$. Since n is either 0.51 or 0.41 decreasing the particle size and increasing the flow rate are effective means of eliminating the heat and mass transfer resistances.

A sample calculation based on the method of Yoshida et al (111) for estimating the temperature

and pressure drop from the bulk gas phase to the surface of the catalyst is shown in Appendix D and C. The temperature and pressure drop ($\Delta p_g/p_g$) were found to be only 0.01°C and 0.1%. Hence, these effects could be neglected.

3. Internal Diffusion and Effectiveness Factor

Two kinds of diffusion in pores are possible. If the mean free path of the diffusing molecule is small with respect to the pore radius, the collisions between molecules control diffusion and the usual molecular diffusivity is applicable. The pore size is unimportant, but the diffusivity is inversely proportional to the pressure.

If the pore size is small in comparison with the mean freepath, collisions with the pore wall control the process. Pressure has no effect on this diffusivity.

For most conditions of operation of catalytic reactors, the pore diffusion is of the Knudsen type. Only at high pressures and large pore radii does the process occur by molecular diffusion. For example, at atmospheric pressure for nearly all porous materials useful as catalysts, Knudsen diffusion controls.

(a). Knudsen Diffusion

As most catalysts are porous, their external surface area only constitutes a small fraction of the total surface area on which the reaction takes place. The diffusion of the reactants into and of the product out of the pores could, therefore, be important factors in controlling the reaction rate. Yet, even if the exact concentrations (in this case partial pressures) of the reactants at the gas-solid interface on the outside of the catalyst particles are known, the conditions existing in the interior surface are different due to resistance offered by internal diffusion and heat transfer.

The effectiveness factor, used to evaluate the effect of Knudsen diffusion, is defined as the ratio of the actual rate of reaction per unit mass of catalyst to the rate which would exist if the concentrations at all interior interfaces were the same as those at the gross exterior interface (44, 45, 98).

The effects of diffusion in this investigation were kept to a minimum by passing the gas mixture at high velocity through the catalyst bed. The Knudsen diffusion effect itself was eliminated by decreasing the particle size of the catalyst. For

this reason, three particle sizes (1.65, 0.53, and 0.20 mm) were tested. These three sizes produced no significant change in the conversion rate. This meant that the Knudsen diffusion effect was not rate-determining and therefore could be neglected. The detailed calculation and experimental conditions used are given in Appendix C.

(b). Molecular Diffusion

The extent of molecular diffusion was evaluated by varying the feed rate from 0.37 moles/hr to 0.5 moles/hr at 326 °C. The experimental data are recorded in Table 8-C-1 and the results are shown in Figure 5-2. The constancy of conversion indicates that molecular diffusion was negligible.

C. Effect of Process Variables

The effect of temperature, weight of catalyst to methanol feed ratio (W/F), and oxygen (in the air) to methanol feed ratio (R) on the conversion of methanol (x), yield of formaldehyde (y), and selectivity (s) of the catalyst were investigated. The effect of several catalysts on conversion and yield was also studied. The results are tabulated in the Appendix (Tables B-1, B-2, and D-1).

The effect of temperature on the conversion, yield and selectivity was investigated in the temperature range 250° - 460 °C, and the results are given in

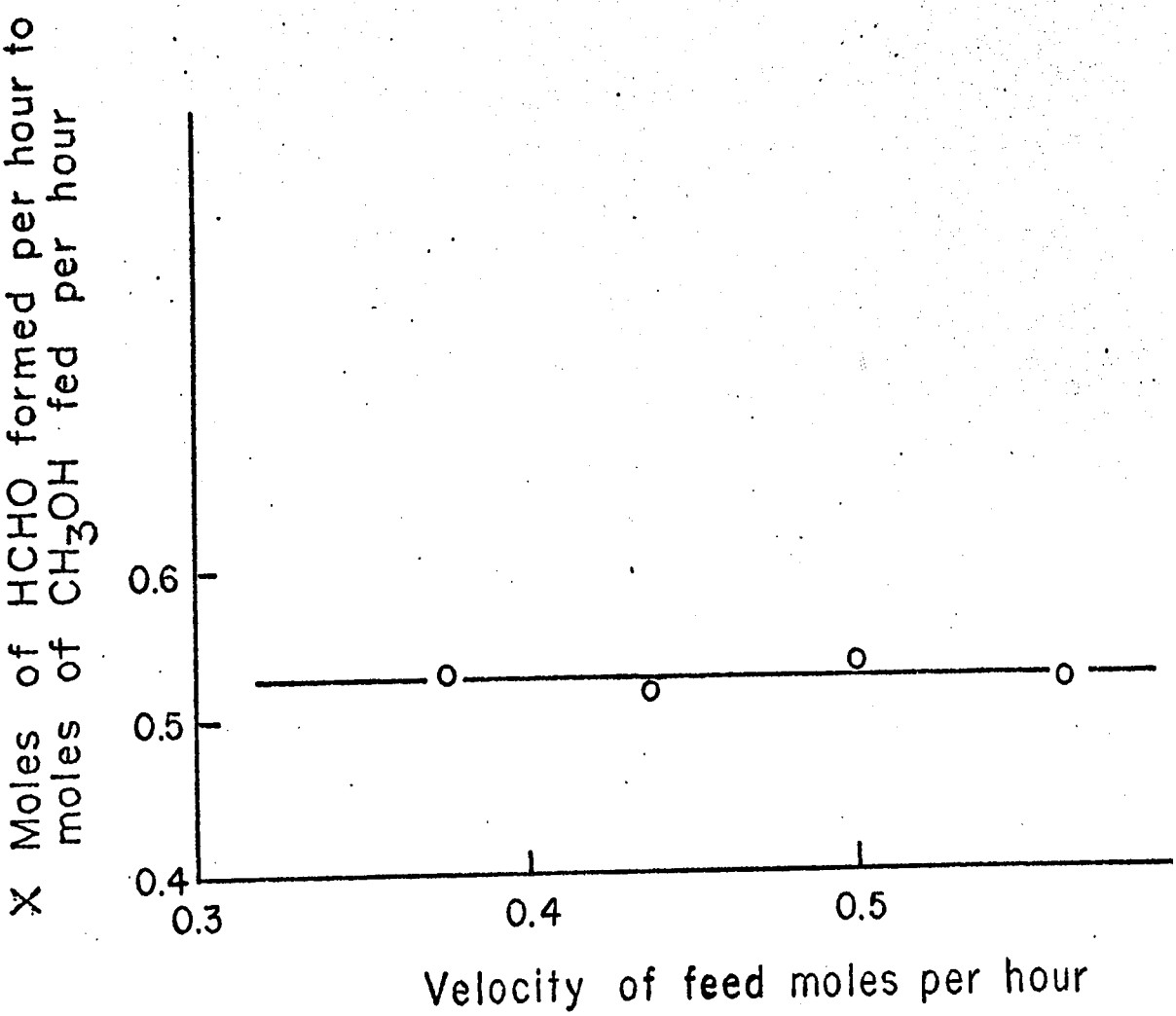

Fig. 5-2 Feed Velocity Effect on Conversion

Appendices D and E. Figure 5-3 shows the effect of temperature at a W/F ratio of 16.3, and an oxygen to methanol ratio of 2.42, over a manganese dioxide-molybdenum trioxide catalyst. With increasing temperature, both conversion and yield increased up to a temperature of 365°C, after which conversion continued to increase reaching 100% at 460°C while yield decreased. The selectivity was 100% up to 365°C, decreasing at higher temperatures.

The effect of the oxygen to methanol ratio in the feed (R) on the conversion and yield for a W/F ratio of 13.3 at 365°C over manganese dioxide-molybdenum trioxide is shown in Figure 5-4; data for this and other W/F ratios and temperatures are given in the Appendix (Tables E-1 to E-4). The ratio of oxygen to methanol in the feed varied between 2.42 and 5.04. The conversion of methanol and the yield of formaldehyde decreased rapidly with increased reactant ratio (R). The selectivity was found to be independent of the reactant ratio in these experiments.

The effect of various W/F ratios on the conversion of methanol and the yield of formaldehyde was investigated for W/F ratio's in the range 2.5 - 22.0. Figures 5-5 and 5-6 show the effect on the conversion and yield at a temperature of 365°C for various feed ratios containing 4 to 8 moles percent methanol in the air. Figures 5-7 to 5-9 show the

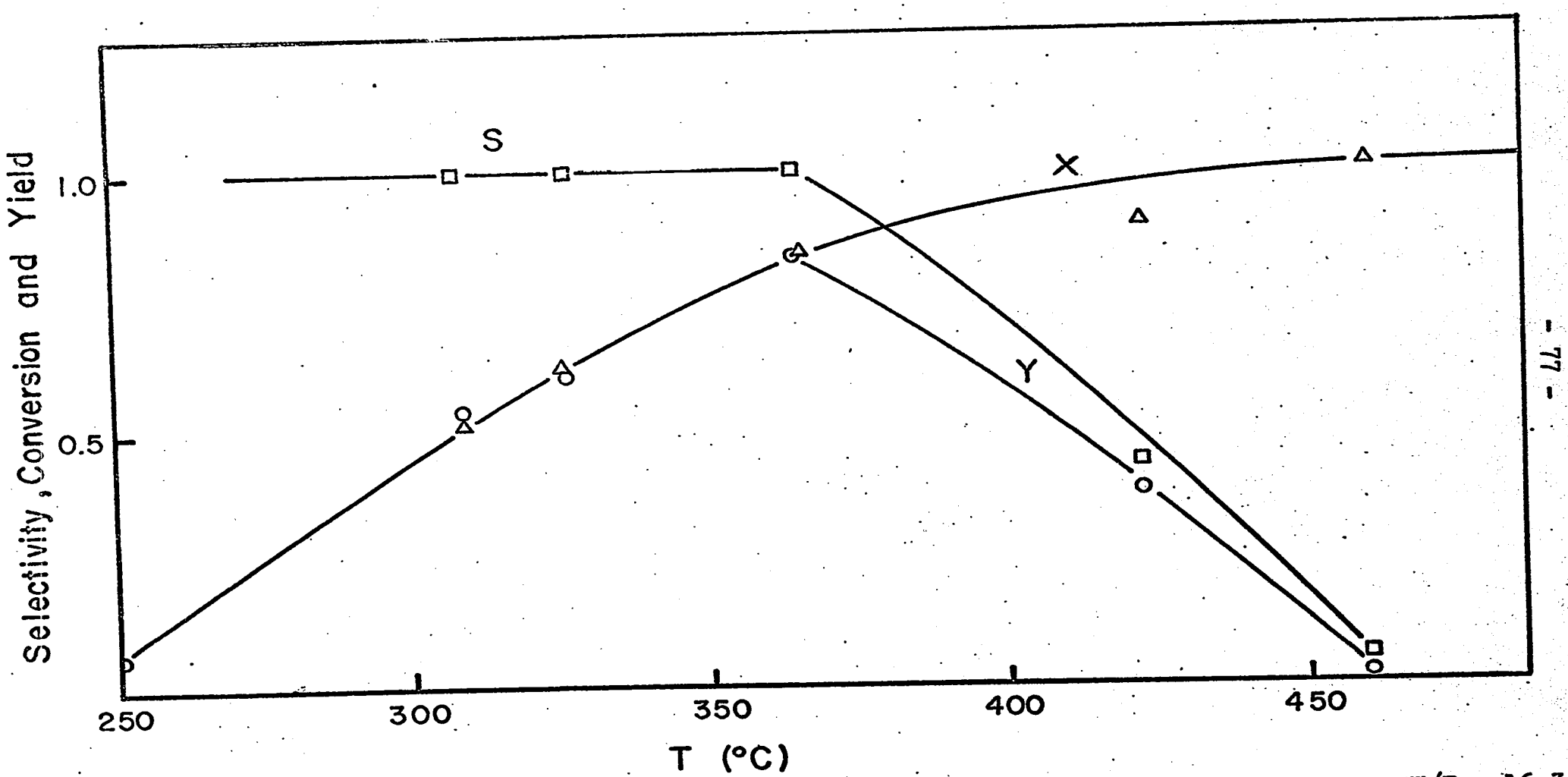

Fig. 5-3. Temperature Effect on Conversion, Yield, and Selectivity of MnO_2-MoO_3, W/F = 16.3

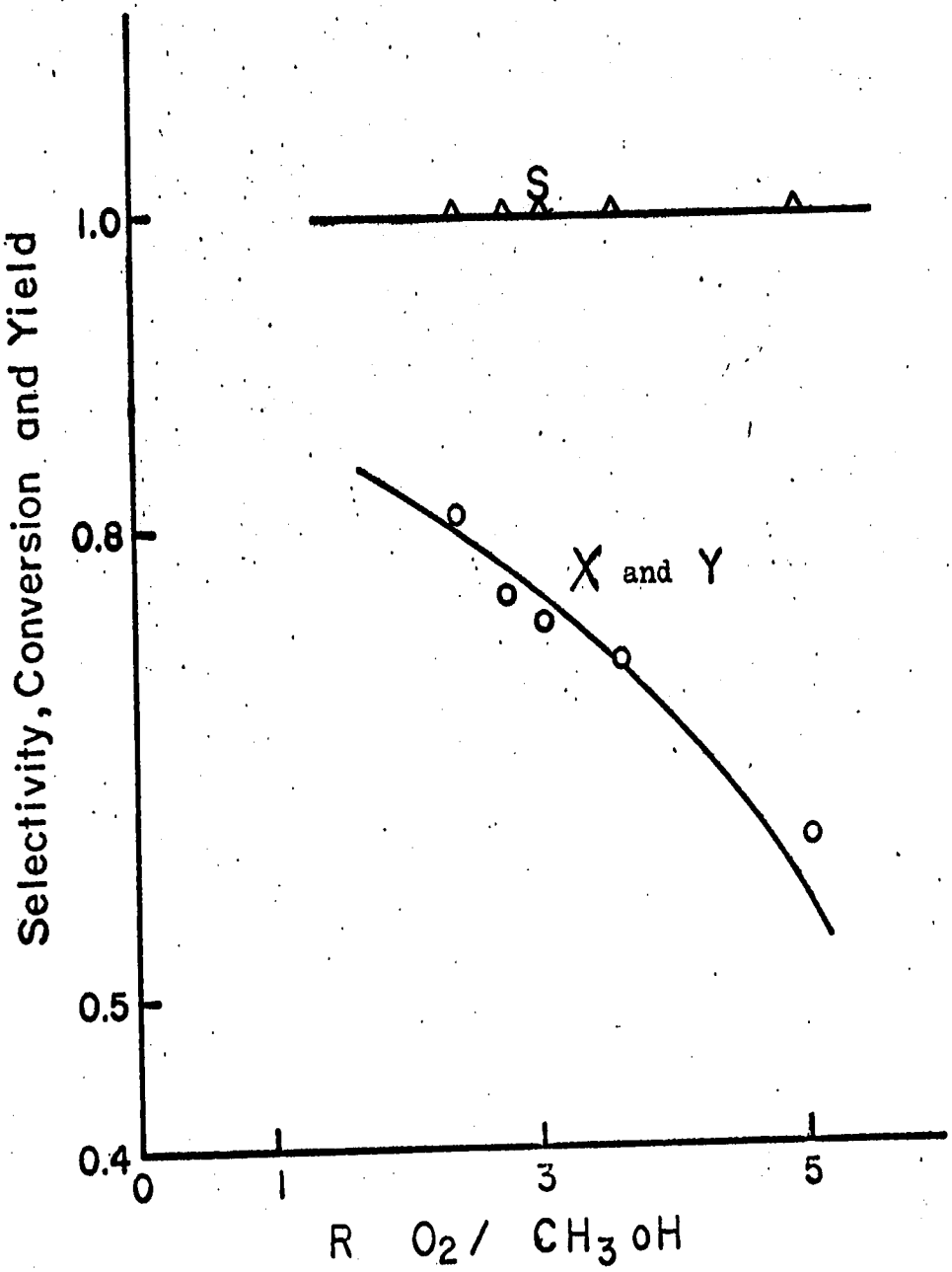

Fig. 5-4 R Effect on Conversion, Yield and Selectivity at 365°C, W/F=13.3

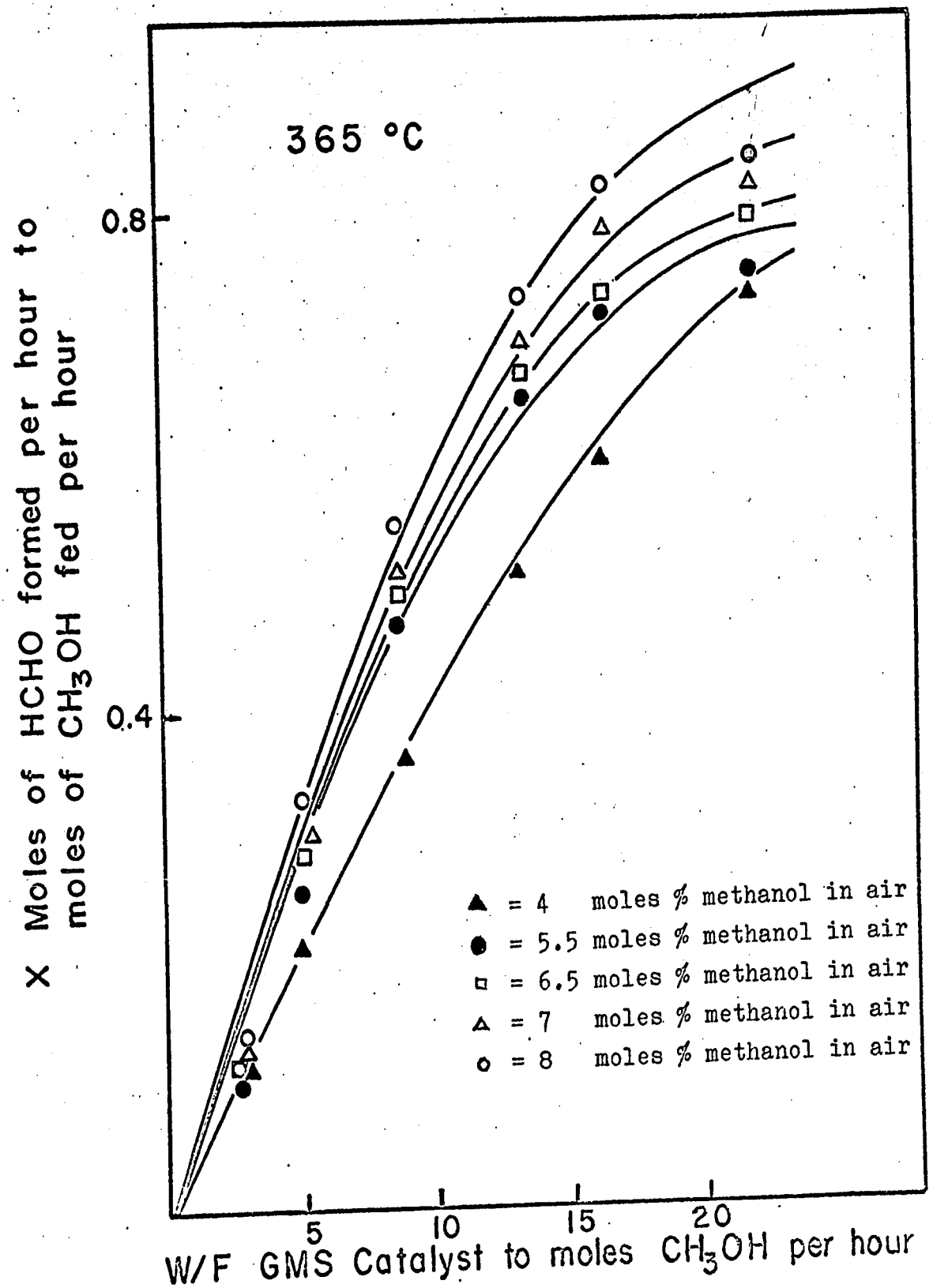

Fig.5-5 W/F Effect on Conversion and Yield of HCHO at 365°C

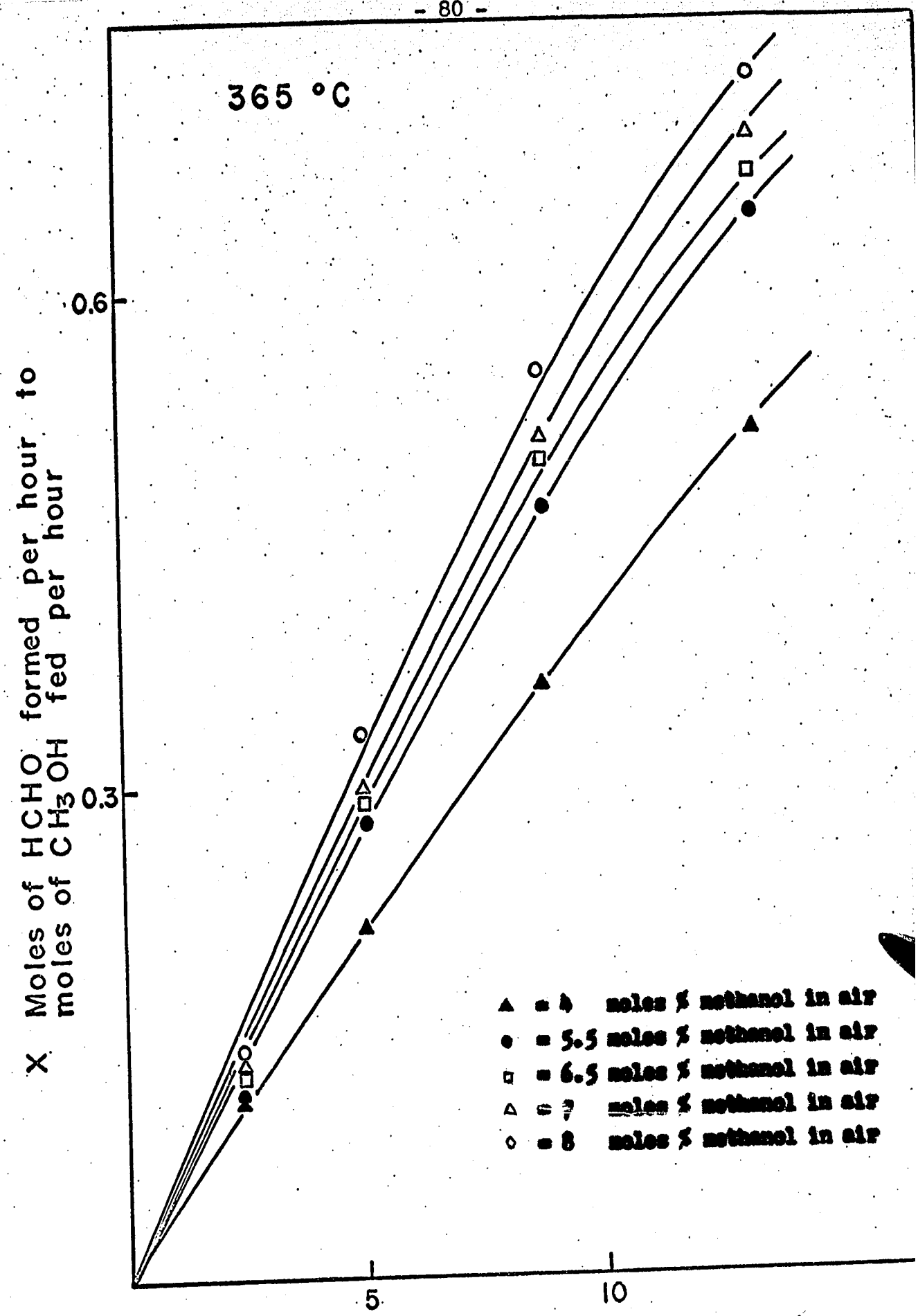

Fig. 5-6 W/F Effect (Initial Values) on Conversion and Yield of HCHO at 365°C

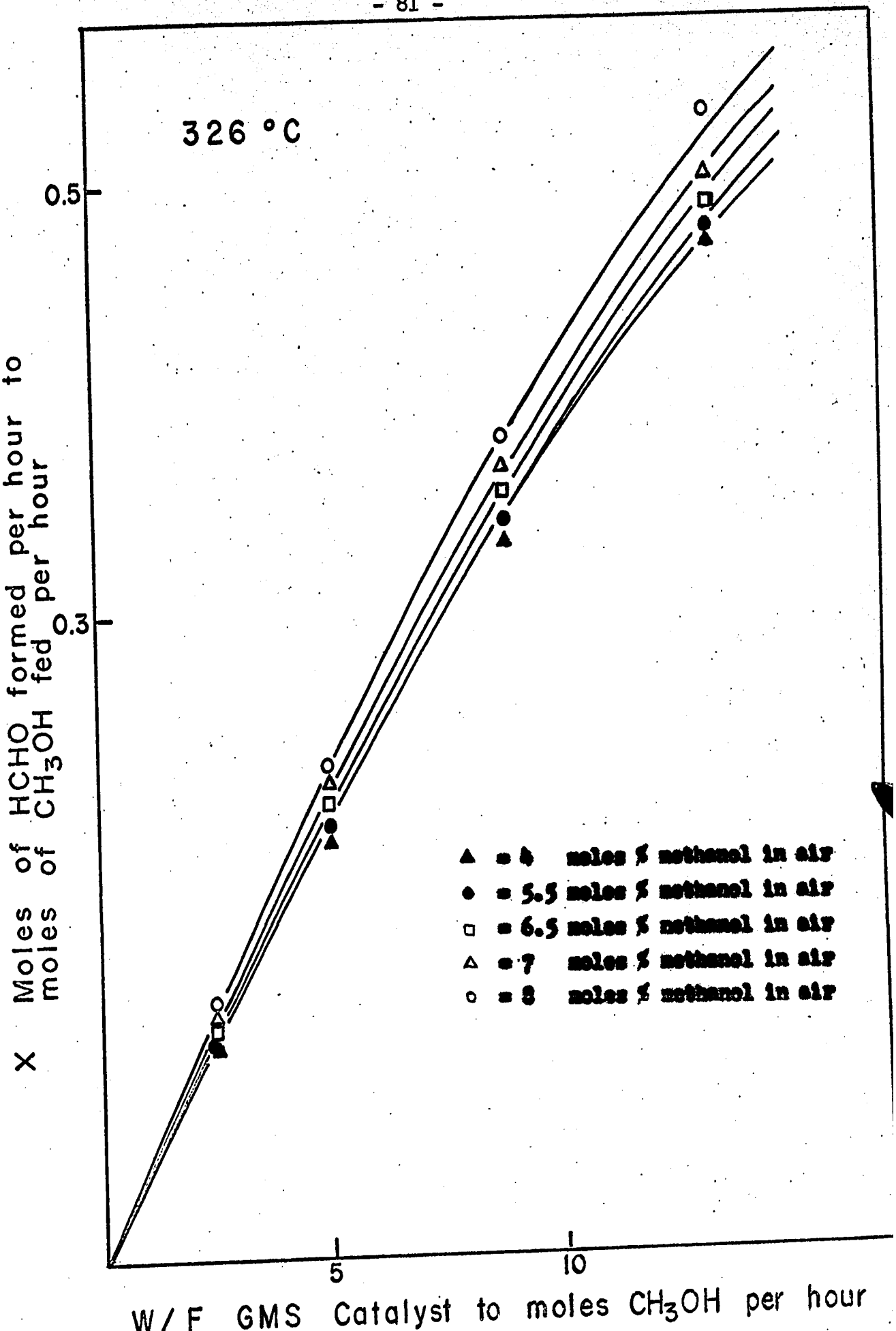

Fig. 5-7. W/F Effect on Conversion and Yield of HCHO at 326°C.

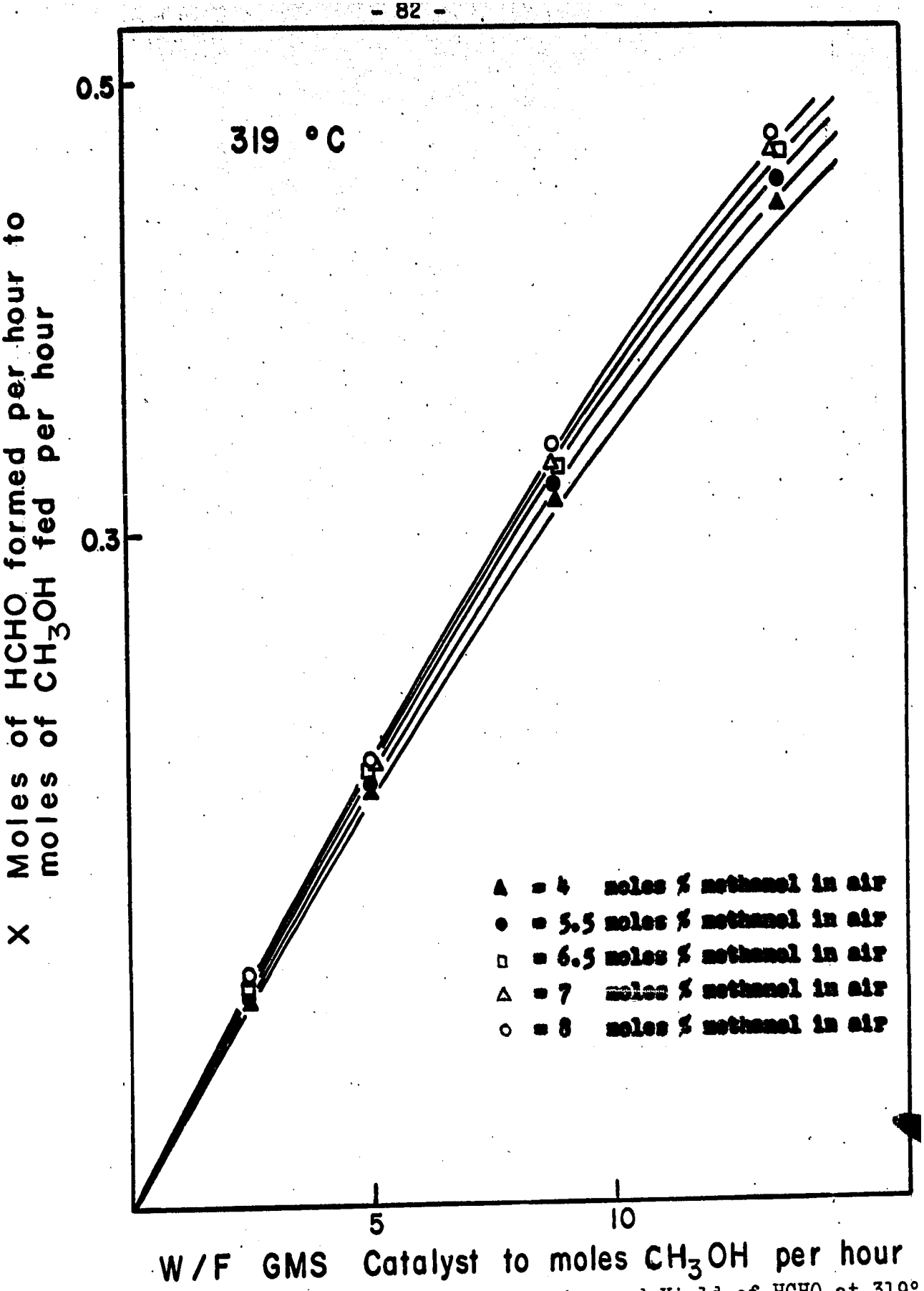

Fig. 5-8. W/F Effect on Conversion and Yield of HCHO at 319°

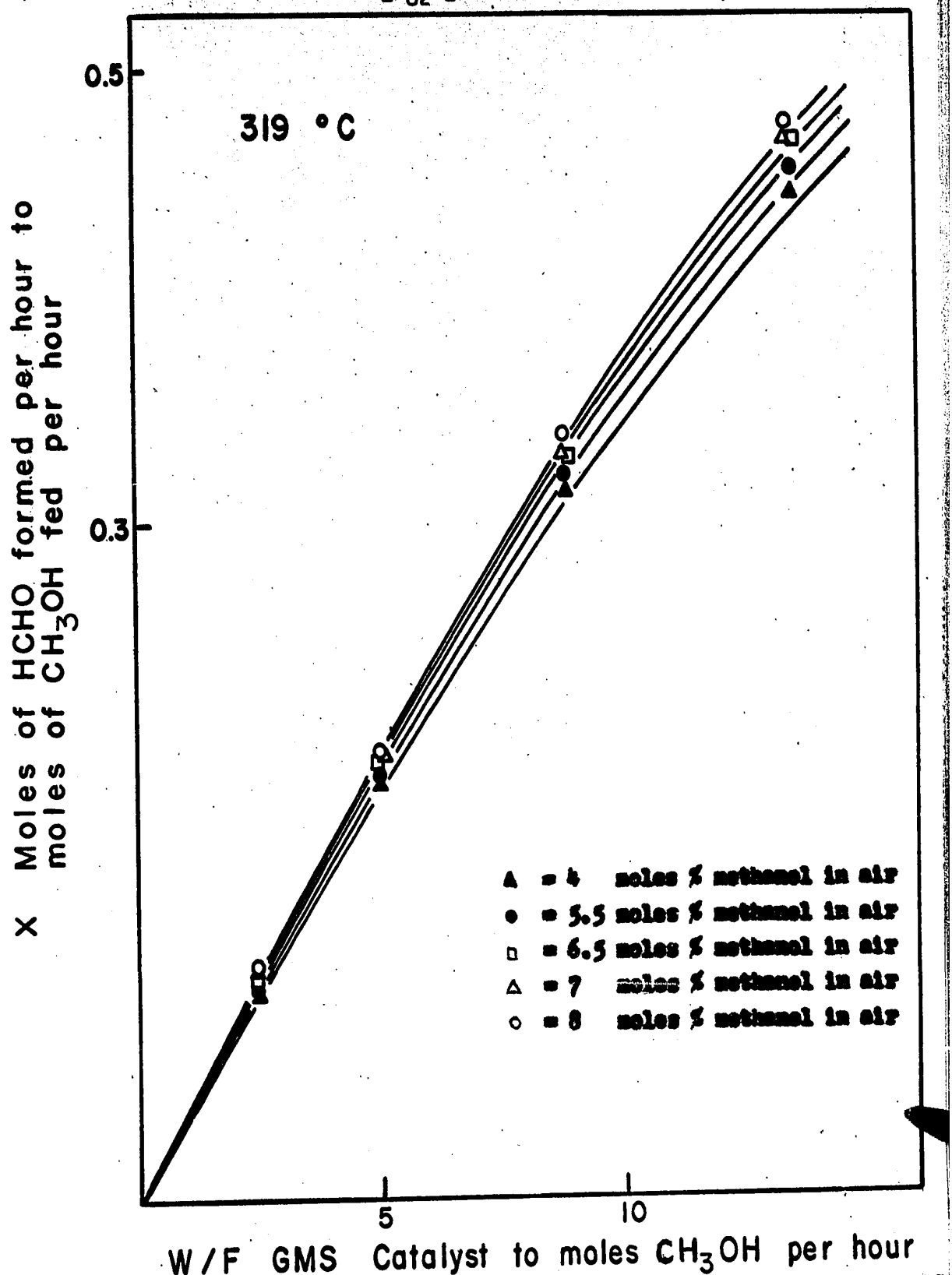

Fig. 5-8. W/F Effect on Conversion and Yield of HCHO at 319°C

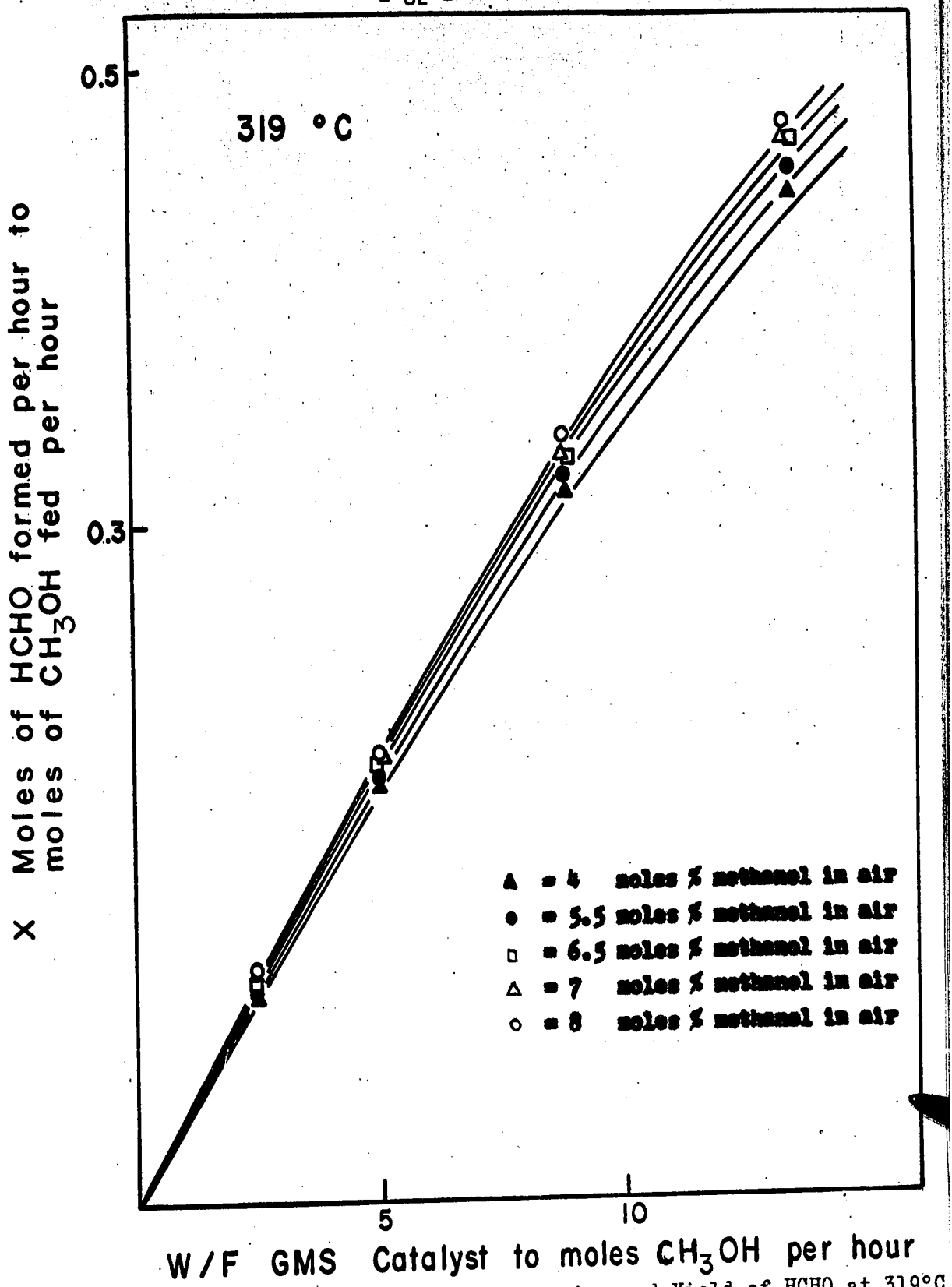

Fig. 5-8. W/F Effect on Conversion and Yield of HCHO at 319°C

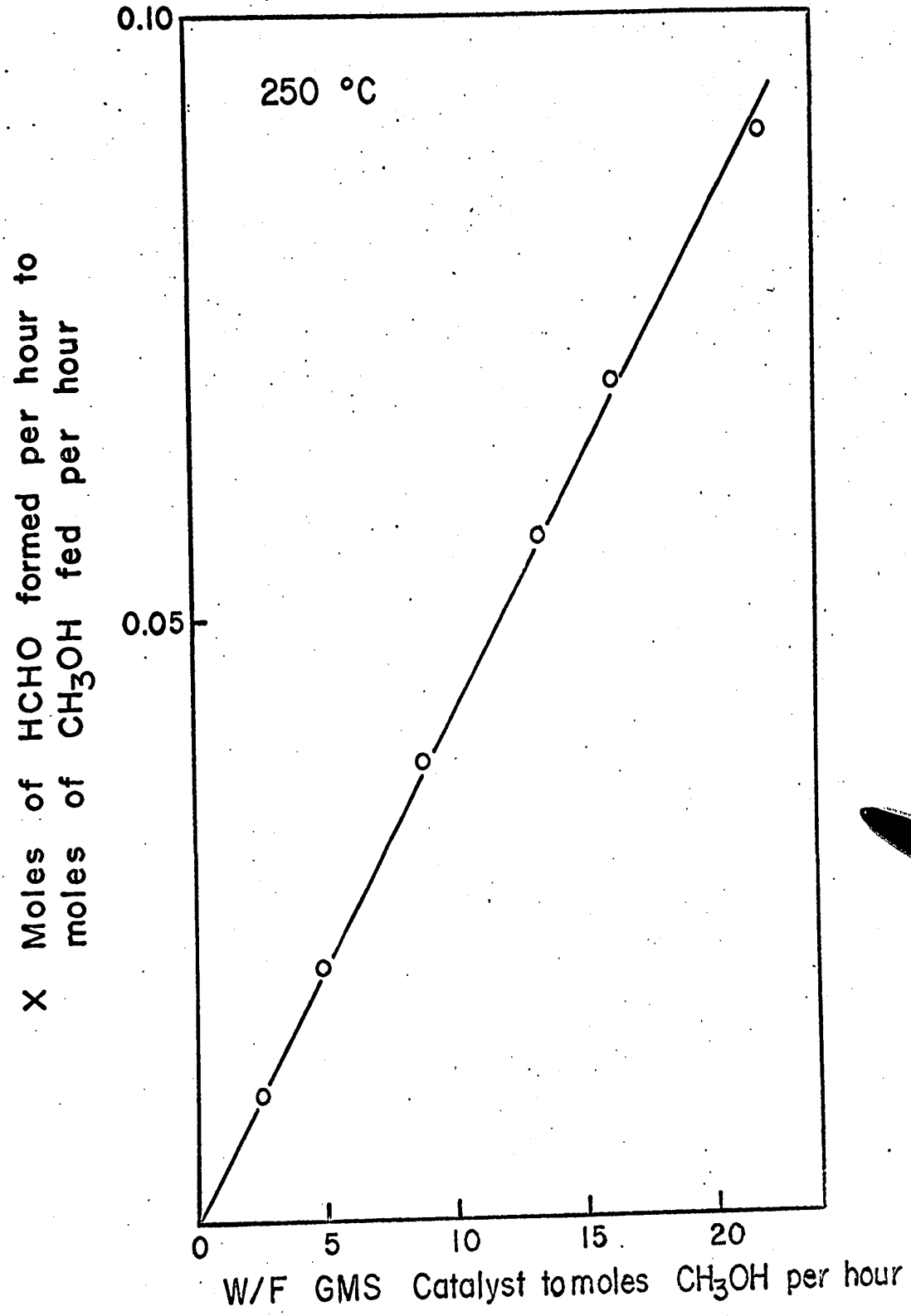

Fig. 5-9. W/F Effect on Conversion and Yield of HCHO at 250°C.

effect of W/F at other temperatures. The conversion and yield increased with increased ratios of W/F.

D. Correlation of Data

1. Initial Rate

In a steady state flow system, the relationship between conversion, flow rate and reaction rate is given by the equation

$$Fdx = rdW$$

which on integration yields

$$\int_0^W \frac{dW}{F} = \int_0^x \frac{dx}{r}$$

or

$$\frac{W}{F} = \int_0^x \frac{dx}{r}$$

Yang and Hougen (109), who considered several reactions, have shown that by considering the effect of pressure on initial rate (x=0) it is possible to reduce the number of reaction mechanisms and finally to test some of them for their suitability in representing the data.

This method briefly envisages the plotting of the experimental data (conversion versus W/F ratio), and determining the slope of the curve as W/F approaches zero. This rate of reaction at zero conversion is defined as the initial rate.

The advantage of the initial rate method is that a more simple rate equation can be obtained, since the partial pressures of the products are neglected. However, the big draw-back is the necessity to estimate the slopes at low conversions by use of extrapolation.

The initial rate equations are obtained by neglecting the partial pressures of the product. In equation (5-23) and rate equations 1 to 4 in Table 5-2, the initial rate equations are the same as the rate equations. However rate equation 5 in Table 5-2, and equation 5-30, can be reduced to

$$r_o = \frac{k_1 p_M^n}{1 + 0.5(k_1 p_M^n / k_3 p_{O_2}^n)} \qquad (5\text{-}35)$$

and

$$r_o = \frac{k_1 p_M}{1 + k_2 p_{O_2}^{\frac{1}{2}}} \qquad (5\text{-}36)$$

2. Correlation of Initial Rate Data

The initial rates were obtained by finding the slopes of the curves at x=0 (Figures 5-6 to 5-9, x vs W/F). The plots of moles percentage methanol in the feed versus the initial rates (r_o) for 365°, 326°, and 319°C are given in Figures 5-10, 5-11 and 5-12 respectively.

The advantage of the initial rate method is that a more simple rate equation can be obtained, since the partial pressures of the products are neglected. However, the big draw-back is the necessity to estimate the slopes at low conversions by use of extrapolation.

The initial rate equations are obtained by neglecting the partial pressures of the product. In equation (5-23) and rate equations 1 to 4 in Table 5-2, the initial rate equations are the same as the rate equations. However rate equation 5 in Table 5-2, and equation 5-30, can be reduced to

$$r_o = \frac{k_1 p_M^n}{1 + 0.5(k_1 p_M^n / k_3 p_{O_2}^n)} \qquad (5\text{-}35)$$

and

$$r_o = \frac{k_1 p_M}{1 + k_2 p_{O_2}^{\frac{1}{2}}} \qquad (5\text{-}36)$$

2. Correlation of Initial Rate Data

The initial rates were obtained by finding the slopes of the curves at x=0 (Figures 5-6 to 5-9, x vs W/F). The plots of moles percentage methanol in the feed versus the initial rates (r_o) for 365°, 326°, and 319°C are given in Figures 5-10, 5-11 and 5-12 respectively.

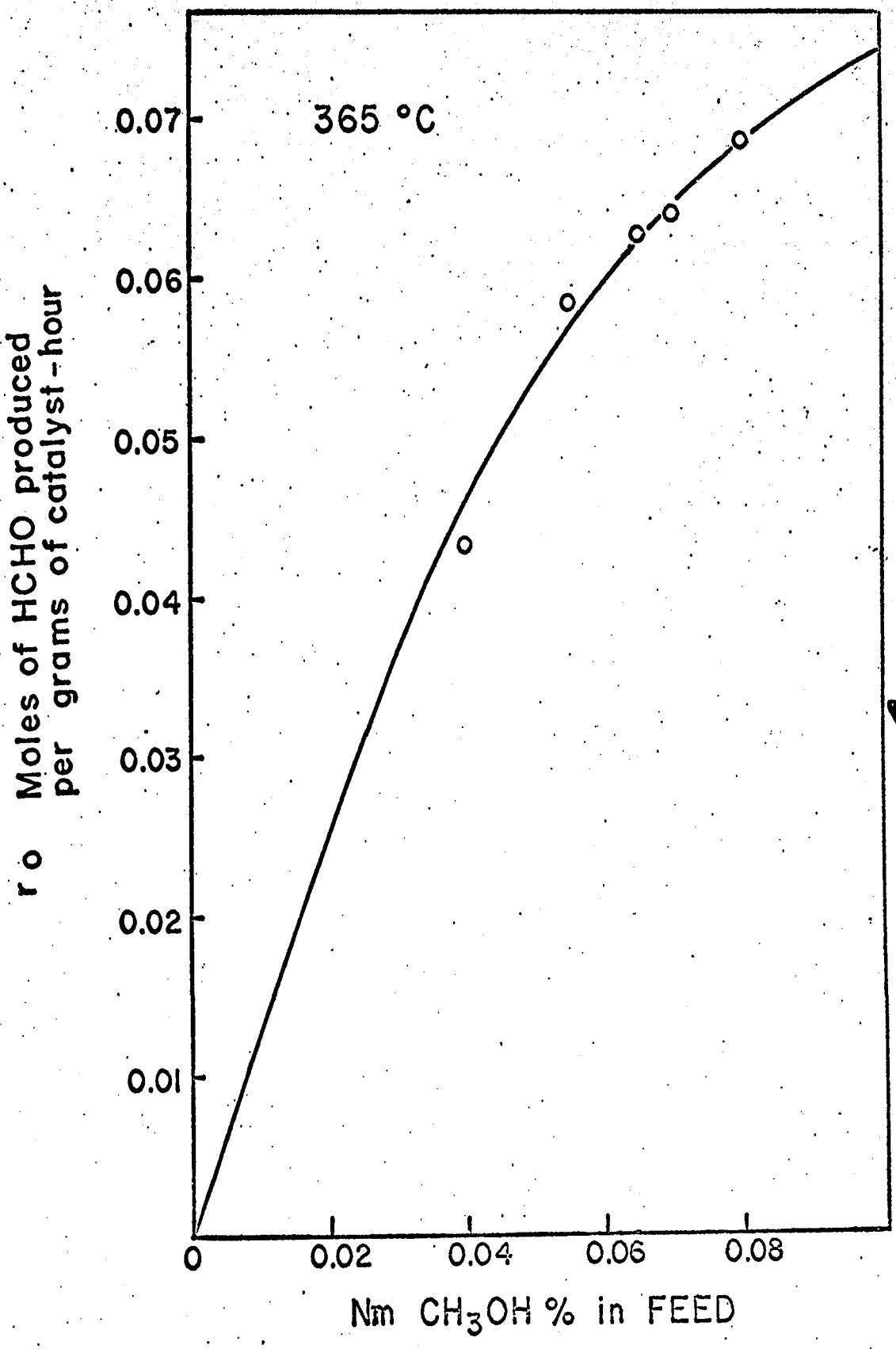

Fig. 5-10. Initial Rates (r_o) vs. moles % CH_3OH at 365°C.

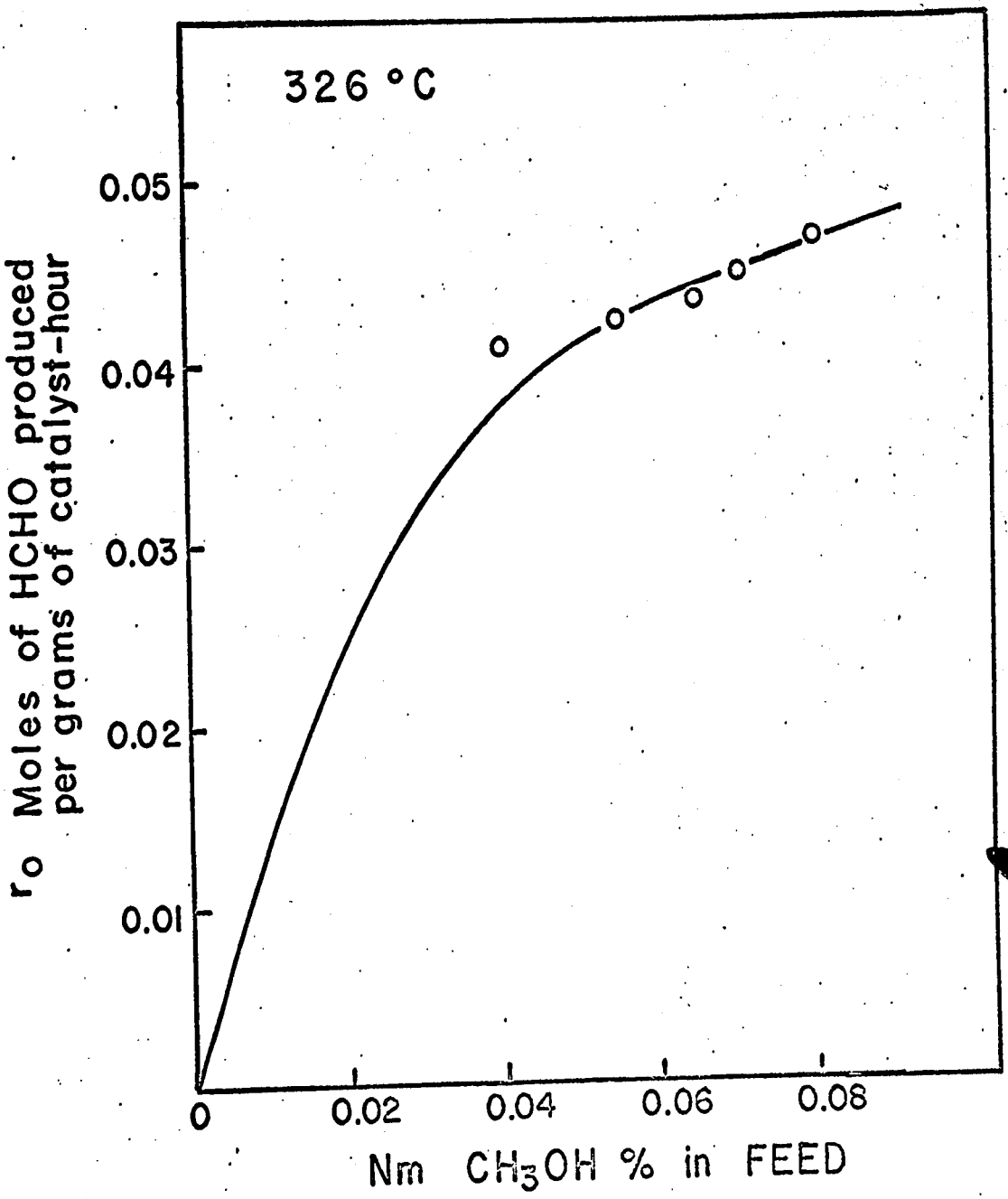

Fig. 5-11. Initial Rates (r_o) vs. moles % CH_3OH at 326°C.

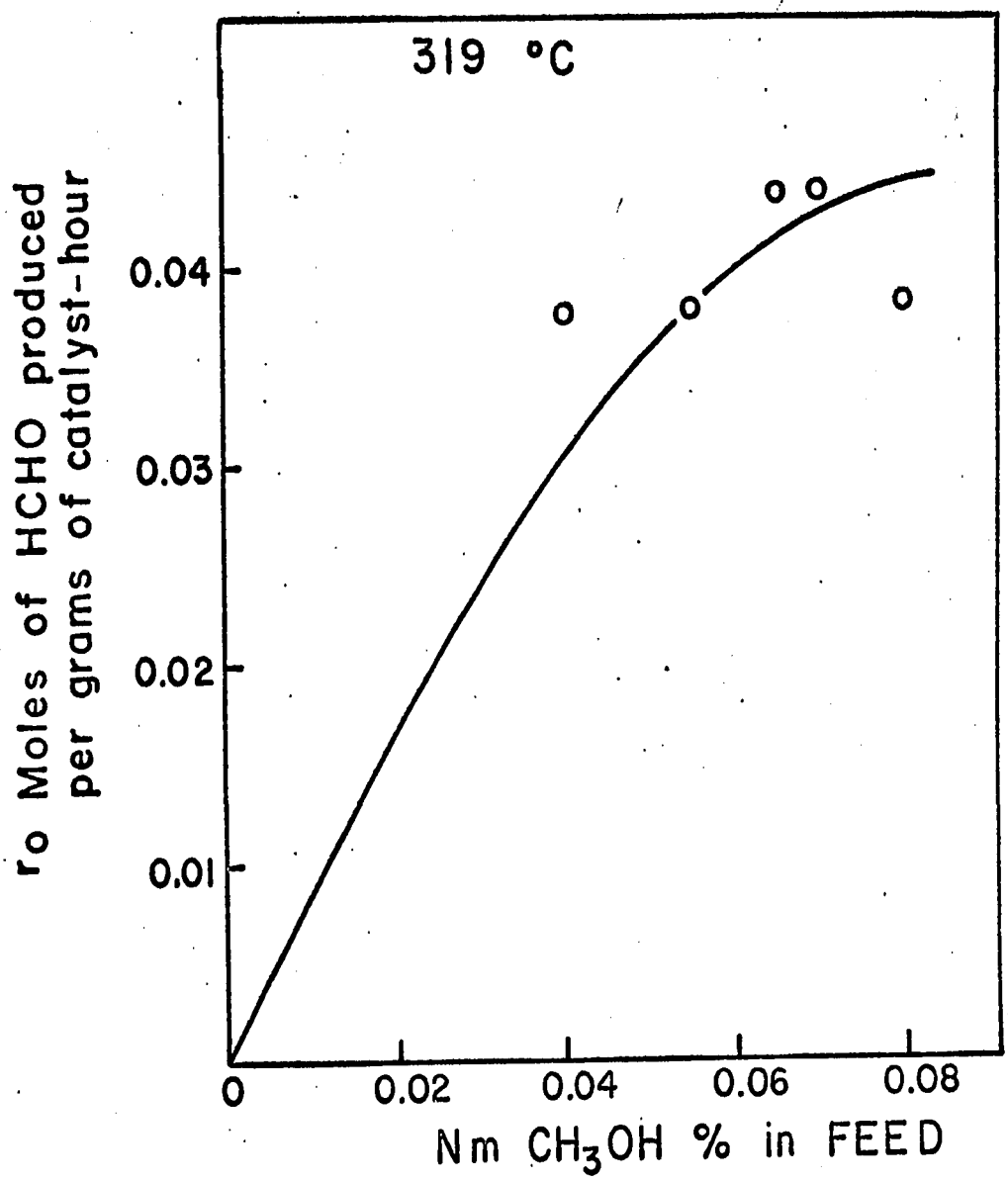

Fig. 5-12. Initial Rates (r_o) vs. moles % CH_3OH at 319°C.

A comparison of the curves in Figures 5-10 to 5-12 with the type of curve used by Yang and Hougen (109) for identifying various mechanisms, suggested that the controlling step in the reaction was either the adsorption of the reactants or a surface reaction between the reactants.

5. Correlation of Conversion Data

The integrated form of the rate equations in Table 5-1 can be rearranged into a new form as shown in Table 5-3, where $\alpha = \frac{1}{F}$ and $y = a_0 + a_1 x$. The values for y and x in columns six and seven of the table are calculated from the experimental data by substituting the values of W/F and the respective partial pressures. The values of a_0 and a_1 may be determined from the intercept and slope of the line in the y versus x plot (Figure 5-13), using the method of least-square-error (Appendix G). The values for a_0 and a_1 can be expressed by this method as

$$a_0 = \frac{\sum_{i=1}^{\ell} y_i - a_1 \sum_{i=1}^{\ell} x_i}{\ell} \qquad (5\text{-}37)$$

$$a_1 = \frac{\sum_{i=1}^{\ell} x_i y_i - \left(\sum_{i=1}^{\ell} x_i\right)\left(\sum_{i=1}^{\ell} y_i\right)/\ell}{\sum_{i=1}^{\ell} x_i^2 - \left(\sum_{i=1}^{\ell} x_i\right)^2/\ell} \qquad (5\text{-}38)$$

where ℓ is the total number set of experimental data.

Table 5-3
Correlated y and x Relations

No.	Reaction Order n_{CH_3OH}	Reaction Order n_{O_2}	a_0	a_1	y	x
1	1	0.5	$1/k_1$	$1/k_2$	$(-W/P)\left[{}_oP_M/\ln(1-x)\right]$	$\left[4\alpha/\ln(1-x)\right]$ $\left[({}_oP_{O_2} - x\,{}_oP_M/2)^{\frac{1}{2}} - {}_oP_{O_2}^{\frac{1}{2}}\right]$
2	1	0	$1/k_2$	$1/k_1$	$W/Px\alpha$	$-\ln(1-x)/{}_oP_M x\alpha$
3	0.5	0	$1/k_2$	$1/k_1$	$W/Px\alpha$	$2\left[1-(1-x)^{\frac{1}{2}}\right]/{}_oP_M^{\frac{1}{2}}x\alpha$
4	1	1	$1/k_1$	$1/k_2$	$-W\,{}_oP_M/P\ln(1-x)$	$\dfrac{-2\alpha\ln\left[{}_oP_{O_2}/({}_oP_{O_2} - \frac{1}{2}\,{}_oP_M x)\right]}{\ln(1-x)}$
5	0.5	0.5	$1/k_1$	$1/k_2$	$W\,{}_oP_M^{\frac{1}{2}}/2P\left[1-(1-x)^{\frac{1}{2}}\right]$	$2\alpha\left[{}_oP_{O_2}^{\frac{1}{2}} - ({}_oP_{O_2} - \frac{1}{2}P_M x)^{\frac{1}{2}}\right]$ $/{}_oP_M^{\frac{1}{2}}\left[1-(1-x)^{\frac{1}{2}}\right]$

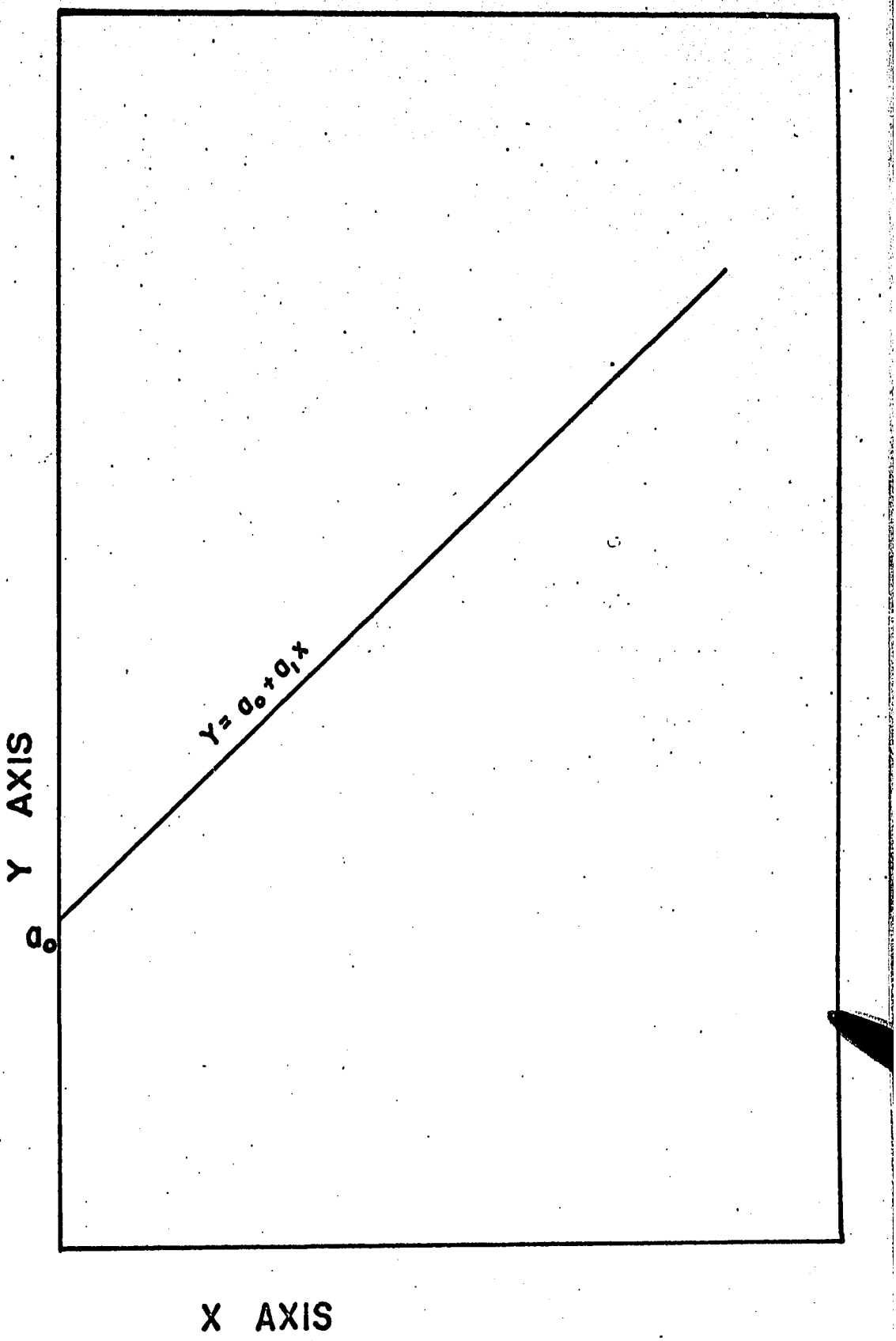

Fig. 5-13 Correlated y vs x Relations

and i, the number assigned to each set of experimental data.

Suitable correlation was obtained for the two-stage oxidation-reduction mechanism when m equalled 1 and n equalled 0.5. The rate equation is

$$r = \frac{k_1 P_M}{1 + k_1 P_M / 2k_2 P_{O_2}^{\frac{1}{2}}} \qquad (5\text{-}39)$$

The values of k_1 and k_2 between 250° and 365°C for m = 1 and n = 0.5 are listed in Table 5-4. Proper fitting was not found in the classical or modified Langmuir-Hinshelwood mechanisms with other values of m and n. The other two-stage redox mechanisms gave negative k_1 values, and there was no proper fitting for the three-stage mechanism (Appendix J).

4. Temperature Effect on Rate Constants

The temperature dependence of the rate constants k_1 and k_2 was determined for temperatures between 250° and 365°C, and an oxygen to methanol ratio (R) of 2.42 (Figure 5-14). The mathematical relations are given in equations 5-40 and 5-41:

$$\log k_1 = 3.432 - \frac{3.81 \times 10^3}{T} \qquad (5\text{-}40)$$

$$\log k_2 = -7.508 + \frac{3.23 \times 10^3}{T} \qquad (5\text{-}41)$$

Table 5-4
Temperature Effect on Rate Constants
when n = 1 and n = 0.5

Temp. °C	Temp. °K	1/Temp. 1/°K x 10^3	K_n %	k_1 moles/gm-cm Hg^{-1}-hr x 10^3	k_2 moles/gm-cm $Hg^{-\frac{1}{2}}$-hr x 10^3
365	638	1.575	8.0	3.41	3.89
			7.0	3.59	3.63
			6.5	3.31	4.08
			5.5	4.79	3.13
			4.0	3.26	3.34
326	599	1.670	8.0	1.14	8.13
			7.0	1.22	8.00
			6.5	1.29	7.39
			5.5	1.44	7.73
			4.0	2.11	6.93
319	592	1.690	8.0	0.96	7.54
			7.0	1.10	6.85
			6.5	1.05	12.50
			5.5	1.21	10.10
			4.0	1.64	8.82
250	523	1.910	8.0	0.173	0.295

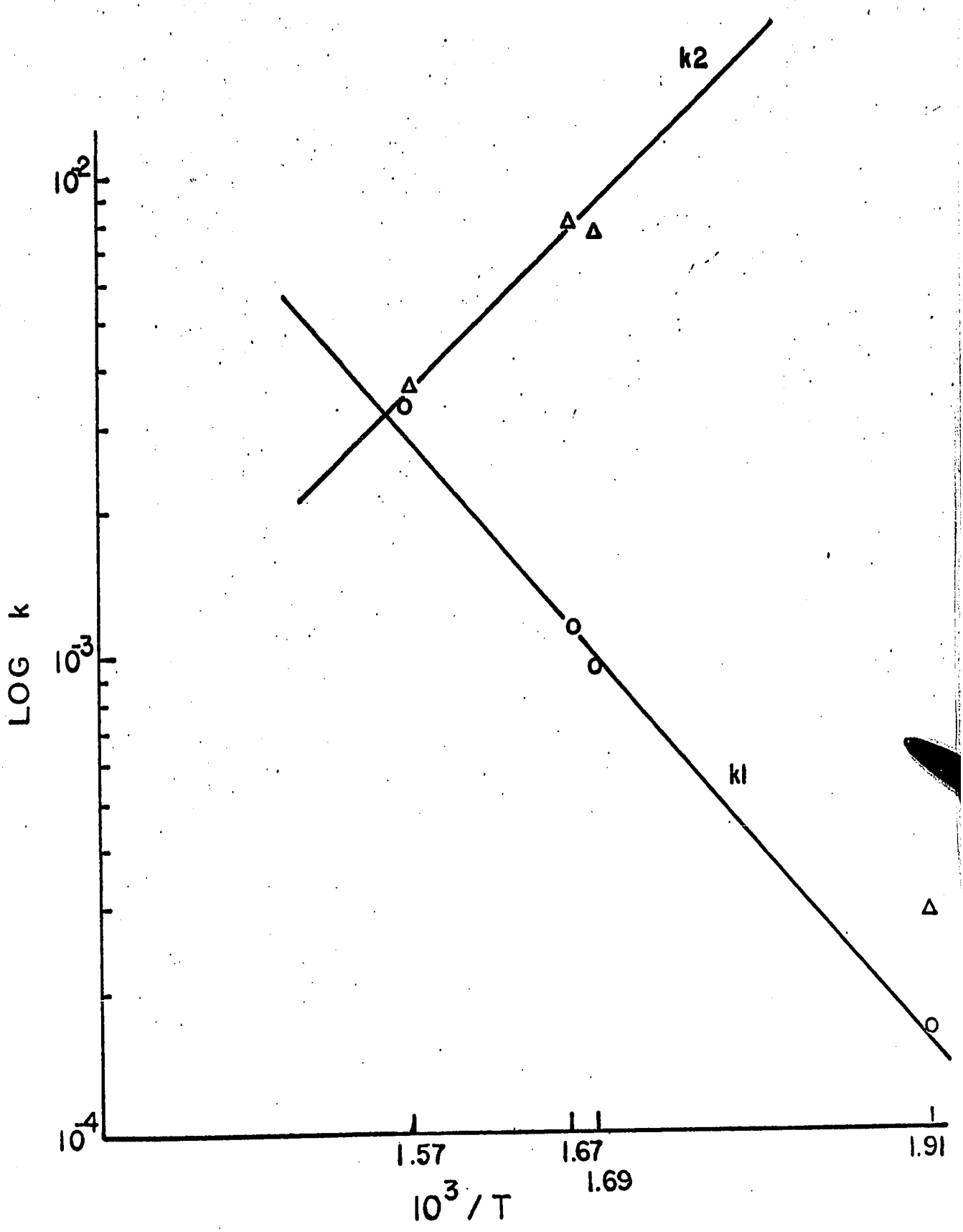

Fig. 5-14 Temperature Effect on Rate Constants, R=2.42

Similar temperature dependencies were determined for other feed ratios (R). The reaction appears to follow the Arrhenius Law in the temperature range studied.

The values of k_1 and k_2 obtained from the Arrhenius correlation were substituted into equation 1 of Table 5-1 to determine the W/F versus x relation. Figures 5-5 to 5-9 show the comparison between the experimental and predicted values of this relation for methanol to air ratios of 4 to 8% at various temperatures. The solid lines in the figures refer to the curves predicted by substituting the appropriate values of k_1 and k_2 in the relation; the circles represent the experimental data. A sample calculation is given in Appendix F.

Similar temperature dependencies were determined for other feed ratios (R). The reaction appears to follow the Arrhenius Law in the temperature range studied.

The values of k_1 and k_2 obtained from the Arrhenius correlation were substituted into equation 1 of Table 5-1 to determine the W/F versus x relation. Figures 5-5 to 5-9 show the comparison between the experimental and predicted values of this relation for methanol to air ratios of 4 to 8% at various temperatures. The solid lines in the figures refer to the curves predicted by substituting the appropriate values of k_1 and k_2 in the relation; the circles represent the experimental data. A sample calculation is given in Appendix F.

VI. DISCUSSION

The kinetics for the air oxidation of methanol to formaldehyde have been investigated between 250° and 460°C, over a manganese dioxide-molybdenum trioxide catalyst and a possible rate mechanism has been proposed. A similar catalyst was used by Kliesouraki et al (58) for methanol oxidation, but these authors did not report the kinetic details of the reaction, nor attempt to postulate a reaction mechanism. They simply compared the activity of the catalyst at several temperatures for various manganese/molybdenum ratios.

More recently, Bliznakov et al (12) have published a note regarding the rate mechanism of the oxidation, using the same manganese-molybdenum catalyst. Based on seventeen runs at 370°C in a differential reactor, they suggest the rate mechanism to be similar to the one postulated by Jiru et al (52) for the oxidation of methanol over iron oxide (Fe_2O_3)-molybdenum trioxide, and to the oxidation of benzene, naphthalene, and anthracene over vanadium pentoxide as proposed by Mars and Krevelen (74). However, Bliznakov et al could not define the exact rate mechanism, and did not study the effect of temperature on conversion, yield, and selectivity, nor provide other aspects of the system.

Jiru et al (51, 52), on the other hand, carried out an extensive study of the kinetics of methanol oxidation over the iron oxide-molybdenum trioxide catalyst. This catalyst has characteristic properties similar to the manganese dioxide-molybdenum trioxide catalyst used in the present research. The results obtained in this investigation are compared with those of Jiru and others who used similar types of oxide catalysts.

Manganese dioxide-molybdenum trioxide was chosen in this oxidation study because detailed work had already been carried out with iron oxide-molybdenum trioxide, and the manganese dioxide-molybdenum trioxide catalyst appeared to be more selective for the oxidation of methanol to formaldehyde than the ferric catalyst. The space velocities used here covered the range $9.6 \times 10^3 - 8.43 \times 10^4$ hr^{-1}.

The Hougen-Watson method based on the Langmuir-Hinshelwood isotherm, and the initial rate technique were used for the kinetic analysis of data. Since the values of equilibrium constant K_p (Table 8-H-1) for the gaseous oxidation of methanol to formaldehyde are very large, in the order of 10^{18} at 250°C, and 10^{12} at 450°C, the process can be considered highly irreversible.

The rate equation derived on the basis of a two-stage irreversible redox mechanism fitted the experimental data best in the temperature range 250°-365°C,

and one atmosphere pressure.

The mechanism and the general kinetics of the reaction over the manganese dioxide-molybdenum trioxide catalyst investigated in this study have been found to be similar to those obtained by Jiru, Wichterleva, and Tichy (52) and Mars and Krevelen (74).

Jiru et al (52) measured the rate of oxidation of methanol over iron oxide-molybdenum trioxide at 270°C for a space velocity of 1.1×10^2 and 1.8×10^2 hr^{-1}, using a microcatalytic pulse technique. They first determined the rate of interaction between oxygen and partially reduced catalyst without the participation of oxygen in the gaseous phase. They then determined the rate of interaction between oxygen and partially reduced catalyst without the participation of methanol in the gaseous phase. The mechanism postulated by Jiru envisages the same type of oxidation-reduction mechanism as given in equations 5-17 and 5-18. They specified, however, that lattice oxygen of the oxide catalyst participated in the oxidation process.

Jiru also observed a change in the color of the ferric catalyst from yellowish-green to greyish-blue during the course of the reaction, and suggested that the change in color might be due to a change in the valence caused by a loss of lattice oxygen. However, no mention was made as to whether this change in color was reversible or irreversible.

Mars and Krevelen (74) studied the mechanism of oxidation of several aromatic hydrocarbons (benzene, naphthalene, and anthracene) over a vanadium pentoxide catalyst. They obtained the same reaction mechanism as the one postulated in this research for methanol oxidation over manganese dioxide-molybdenum trioxide. They suggest, however, that since a maximum rate does not occur with changes in the partial pressures of oxygen and aromatic, a reaction must take place between the aromatic compound and oxygen present on the underlying catalyst surface.

Mars et al (74) also noted a color change in the vanadium catalyst from yellowish-brown in the oxidised state to greenish-blue in the reduced. This color change was completely reversible and on analysis of the reduced catalyst, a high concentration of tetravalent vanadium was found. Vanadium pentoxide contains two kinds of oxygen ions in its lattice—three fifths existing in about the same plane as the vanadium ions and two fifths arranged in planes parallel to and alternating with the first. Mars and Krevelen believe the alternating lattice oxygen ions to be those which interact with aromatic molecules at the surface of the catalyst.

Bhattacharyya et al (9) studied the oxidation of methanol over vanadium pentoxide, and obtained a mechanism of reaction similar to the one suggested by Mars and Krevelen (74).

Shelstad et al (29, 93) studied the kinetics of the oxidation of naphthalene and toluene. They support a two-stage redox mechanism whereby adsorbed oxygen reacts with the other reactant remaining in the gaseous phase, and the rate of removal of adsorbed oxygen by reaction equals the rate of adsorption of oxygen. Ioffe et al (49) also report in favor of this theory.

Both the mechanisms discussed above, the first in which lattice oxygen atoms react with reductant, and the second in which adsorbed oxygen molecules or atoms (not lattice oxygen) are removed, lead ultimately to the same rate expression.

It is difficult to prove the participation of lattice oxygen in the catalytic oxidation process in the manner described by Jiru using the pulse technique. It is possible, of course, that lattice oxygen does participate in the reaction, but in Jiru's experiments, oxygen could have been adsorbed by the oxide catalyst, and when methanol was injected into the reactor by the pulse technique, it reacted with the adsorbed oxygen. Huibers (52) points out that the values of k_1 and k_2, derived by Jiru, are rather small in comparison with others given for $m = 1$ and $n = 1$. This could indicate that adsorbed oxygen took part in the reaction, and that the mechanism is similar to the one obtained by Ioffe and Lyubarskii (52) for benzene oxidation, lattice oxygen being responsible for the oxidation only when adsorbed oxygen was lacking.

The color of a catalyst is one of the characteristic properties of the catalyst, and a change in color may signify a change in the structure. Several reports have appeared on the change in color of the vanadium pentoxide catalyst during oxidation-reduction reactions. Thus, if the proposed kinetic mechanism is true, and oxygen in the air can react with reduced sites in a catalyst to produce lattice oxygen, there should be a reversible color change in the ferric oxide-molybdenum trioxide from yellowish-green to greyish-blue on reduction, and vice versa on regeneration.

In the case of methanol oxidation over manganese dioxide-molybdenum trioxide, the color of the catalyst was yellowish-white in the initial stages of calcination. On successive oxidations the color changed from brown to black, depending on the degree of oxidation. Once the color of the catalyst had changed, however, it did not return to the original color upon regeneration.

From thermodynamic calculations, as developed by Jones and Fowlie (53), the optimum temperature range for the oxidation of methanol to formaldehyde is 300° - 400°C, corresponding to a working feed mixture containing 5.5 to 8% methanol in air. In the present experiments, it was found that the best temperature for maximum conversion, yield, and selectivity was around 365°C. Below this temperature the conversion of methanol and the yield

of formaldehyde increased, whereas at temperatures above 365°C, the yield decreased with temperature despite an increase in conversion.

The results obtained in this investigation have been found to agree in general with those of earlier investigators (9, 12, 51, 52, 74, 93), and with those reported in patents (22, 30).

VII. CONCLUSIONS AND RECOMMENDATIONS

The partial air oxidation of methanol was investigated over a manganese dioxide-molybdenum trioxide catalyst between 250° - 460°C, for W/F ratios of 2.5 to 22.0 gm-hr/moles, and oxygen to methanol ratios (R) of 2.42 to 5.04, in order to establish the conditions for maximum conversion and yield, to derive a suitable rate equation, and propose a possible reaction mechanism.

An experimental system and reactor, facilitating precise rate measurements, were designed in such a way that reaction conditions remained essentially uniform throughout the whole length of the catalyst bed. The drop in methanol pressure and temperature between the bulk gas and the catalyst surface was calculated to be less than 0.1% and 1°C respectively.

An analytical technique using gas chromatography was developed which could accurately measure high concentrations of formaldehyde without polymer formation, and could detect very small quantities of formaldehyde (MDQ = 0.0009 mg).

The rate of formaldehyde formation was shown to depend on the partial pressures of methanol and oxygen, and to increase with methanol partial pressures of up to 8% methanol in air.

The Hougen-Watson method based on the Langmuir-Hinshelwood isotherm was used for the kinetic analysis of data. The reaction mechanism derived from the experimental data under steady state conditions was found to be based on a two-stage irreversible oxidation-reduction process:

$$CH_3OH(g) + s_{ox} \xrightarrow{k_1} HCHO(g) + H_2O(g) + s_{red}$$

$$O_2(g) + s_{red} \xrightarrow{k_2} s_{ox}$$

where s_{ox} was an active site of lattice or adsorbed oxygen, and s_{red}, the reduced site of lattice oxygen or the empty site.

The rate equation correlating the data most satisfactorily is:

$$r = \frac{k_1 p_M}{1 + k_1 p_M / 2k_2 p_{O_2}^{\frac{1}{2}}}$$

where k_1 and k_2 are temperature-dependent constants. The values of constants k_1 and k_2 increased and decreased respectively as the temperature rose from 250° to 365°C.

It is recommended that further work on the oxidation of methanol should be at the molecular level, and include studies on (a) the adsorption of the reactants on the catalyst surface, before, during and after the reaction;

(b) conductivity changes in the catalyst; (c) low pressure studies with a mass spectrometer to obtain more information regarding reaction intermediates, and (d) a comparison of the reaction products over various metal oxides.

VIII. APPENDIX

A. Calibration of Equipment

1. Thermocouple Calibration

Errors in measurement can be introduced by lack of thermocouple calibration (10).

$$\frac{T_1 - T_a}{T_w - T_a} = \frac{1}{\cosh\sqrt{hL^2/kB}}$$

where:

T_1 = temperature indicated by thermocouple

T_w = pipe wall temperature

T_a = gas stream temperature

h = heat transfer coefficient

k = thermal conductivity

B = thickness of well wall in cm

L = length of well

L = 10 cm

$B = \frac{2.54}{32} = 0.0795$ cm

k = 0.045 gm-cal/sec-cm^2-°C/cm

h = 0.000017 gm-cal/sec-cm^2-°C

T_w = 360°C

T_1 = 361°C

$$\frac{361 - T_a}{360 - T_a} = \frac{1}{\cosh \sqrt{\frac{(1.7 \times 10^{-5})(10^2)}{(0.045)(0.0795)}}}$$

$$= \frac{1}{\cosh \sqrt{0.475}} = \frac{1}{\cosh 0.688}$$

$$= \frac{1}{1.245}$$

$$T_a = \frac{(361)(1.245) - 360}{1.245 - 1} = \frac{90}{0.245}$$

$$= 365°C$$

The thermocouples in this research were calibrated against a thermometer immersed in the same liquid bath.

2. Rotameter Calibration

Rotameter calibration (ball height in cm versus air flow rate in ml/min) is shown in Figure 8-A-1. The height of the lighter ball or float is represented in the figure by circles and the height of the heavier ball by squares.

3. Gas Chromatograph Calibration

Calibration of the Fisher Gas Partitioner for oxygen, nitrogen, carbon monoxide, and carbon dioxide is given in Figure 8-A-2, and of the departmental gas chromatograph for methanol and formaldehyde in Figure 8-A-3.

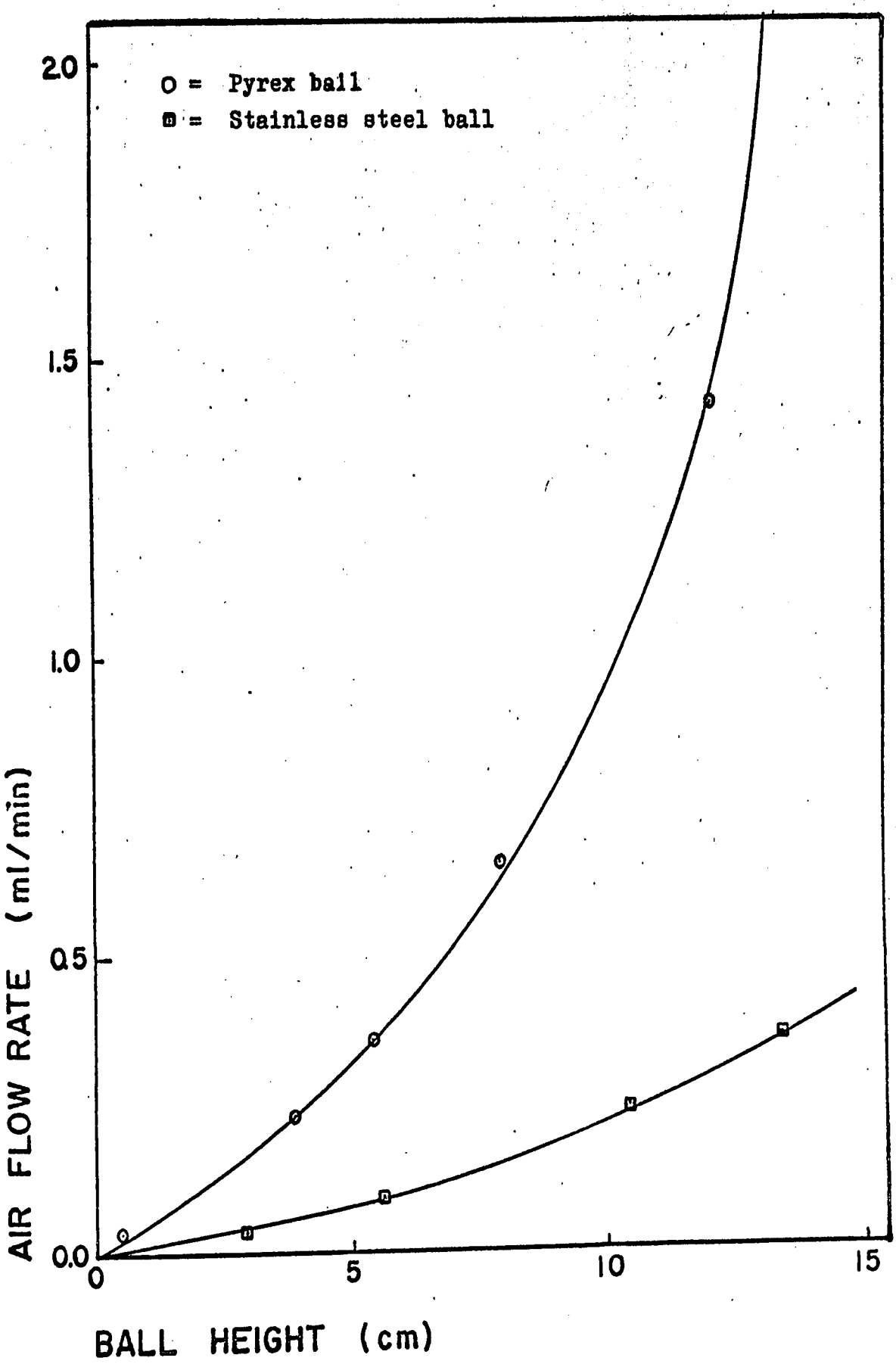

Fig. 8-A-1 Rotameter Calibration

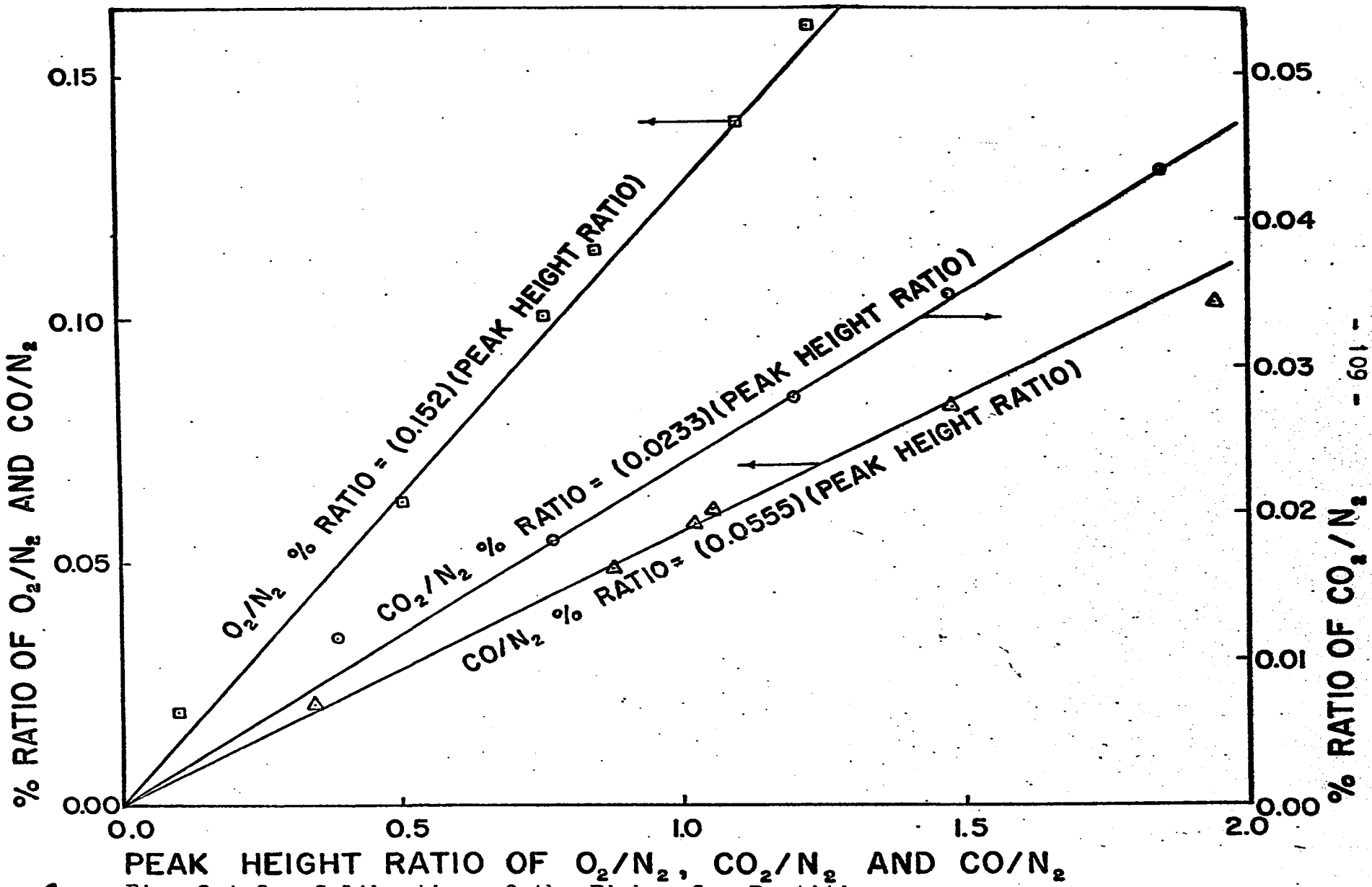

Fig. 8-A-2 Calibration of the Fisher Gas Partitioner

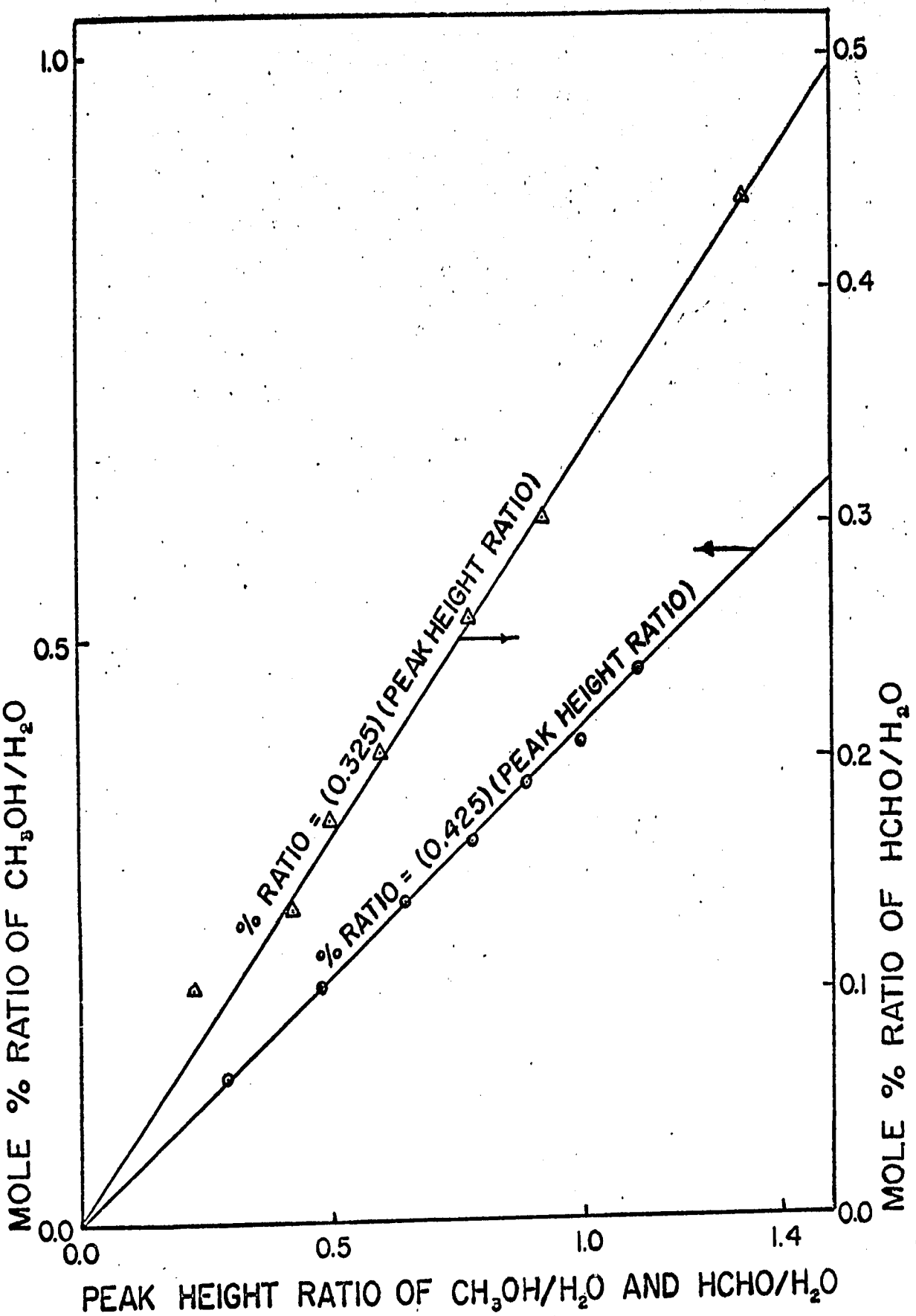

Fig. 8-A-3 Calibration of the Departmental Gas Chromatograph

The columns and detectors used in the gas chromatography analysis of formaldehyde are listed in Table 8-A-1, and a comparison of these columns in the separation of formaldehyde, methanol, water, and butanol is given in Table 8-A-2.

Table 8-A-1

Columns and Detectors Used in the Gas Chromatography Analysis of Formaldehyde

Column	Column Dimensions length diameter	Column Operating Temperature °C	Carrier gas flow rate ml/min.	Carrier gas	Detector	Detector sensing elements	Remarks
15 wt% S.O.A.* on Columpak T	200 in. ¼ in.	93	54	He	thermal conductivity	thermistors	
15 wt% S.O.A.* on Columpak T	200 in. ¼ in.	97	54	He	thermal conductivity	filaments	qualitative and quantitative determination
15 wt% S.O.A.* on Columpak T	200 in ¼ in.	93	54 83 (ref)	Ar	gas density	filaments	
10 wt% Ethofat 60/25 on Columpak T	400 in ¼ in	105	80	He	thermal conductivity	filaments	qualitative and quantitative determination

Table 8-A-1 (Continued)

10 wt% Ethofat 60/25 on Celumpak	400 in. × ¼ in	125	80	He	thermal conductivity	thermistors	qualitative and quantitative determination
Porapak N.	80 in × ¼ in.	110-125	60	He	thermal conductivity	thermistors	qualitative and quantitative determination
Porapak N.	80 in × ¼ in	110-125	60	He	thermal conductivity	filaments	qualitative and quantitative determination
28 wt% P.E.G.A. on Celite (95)	245 cm × 6 mm	90 110	55	H_2	thermal conductivity	filaments	qualitative and quantitative determination
28 wt% P.E.G.A. on Rysorb (95)	245 cm × 6 mm	90	55	H_2	thermal conductivity	filaments	qualitative and quantitative determination

Table 8-A-1 (Continued)

30 wt% Reoplex on Celite (95)	245 cm 6 mm	90	55	H_2	thermal conductivity	filaments	qualitative and quantitative determination
30% Citroflex on Embacel (95)	490 cm 4 mm	122	42.9	H_2	thermal conductivity	filaments	qualitative and quantitative determination
30% Carbowax 20 M. on Chromosorb (95)	300 cm 6.35 mm	90	32	He	thermal conductivity	-	qualitative identification
45% Octyl-decylphthalate on Firebrick C22 (79)	366 cm 6.35 mm	105	32	He	thermal conductivity	filaments	qualitative identification
23% Glycerin on Celite 545 (95)	600 cm -	78	25	He	thermal conductivity	filaments	qualitative identification
30% SAIL surfactant on C22 Firebrick (90)	450 cm 6.35 mm	95	20	N_2	thermal conductivity	filaments	qualitative identification

Table S-A-1 (Continued)

10% TIDE surfactant on Fluropak 80 (90)	120 cm 6.35 mm	145	20	N_2	thermal conductivity	filaments	quantitative determination
25% Carbowax (95) on Sterchamol	-	60	-	H_2		flame ionisation	qualitative analysis

* S.O.A. - sucrose octa-acetate

Table B-A-1 (Continued)

10% TIBK surfactant on Fluropak 80 (90)	120 cm 6.35 mm	145	20	N_2	thermal conductivity	filaments	quantitative determination
25% Carbowax (95) on Sterehamol	-	60	-	N_2		flame ionization	qualitative analysis

* S.O.A. - sucrose octa-acetate

Table 8-A-2

Comparison of Gas Chromatography Columns

Column		15 wt% Sucrose octa-acetate on Columpak T	Perapak N		10 wt% Bthofat on Columpak T (13)	20 wt% P.E.G.A. on Celite (95)	
Column temperature (°C)		93	97	110	125	115	110	90
$b_{\frac{1}{2}}$ (min.)	P	1.1	1.0	1.7	1.1	3.5	2.9	7.0
	M	1.1	1.0	1.3	1.1	0.5	1.0	1.4
	W	1.5	1.3	1.3	0.8	0.6	1.5	1.5
	B	-	5.9	-	-	1.2	-	-
$\frac{t_{dr}}{b_{\frac{1}{2}}}$	P	4.9	4.1	14.5	14.0	5.4	5.7	5.1
	M	11.8	12.5	6.2	5.3	18.1	6.2	4.4

Table 8-A-2 (Continued)

	W	12.1	12.9	10.0	11.5	18.9	5.5	7.1
	B	-	7.6	-	-	22.4	-	-
n	F	135	92	1162	1086	160	179	142
	M	771	860	213	156	1809	216	107
	W	811	925	554	732	1977	166	279
	B	-	319	-	-	2769	-	-
MDQ (mg)	F	0.0020	0.0009	0.0441	0.0189	0.0525	-	-
	M	0.0022	0.0011	0.0051	0.0026	0.1289	-	-
	W	0.0018	0.0015	0.0051	0.0042	0.0845	-	-
	B	-	0.0147	-	-	0.0039	-	-

Symbols: F = formaldehyde, M = methanol, W = water, B = butanol

B. Catalysts Tested

Stability of the manganese dioxide-molybdenum trioxide catalyst is shown in Table 8-B-1, and experimental data for the tests employing vanadium pentoxide, molybdenum trioxide, and manganese dioxide are given in Table 8-B-2.

Stability of the manganese dioxide-molybdenum trioxide catalyst was determined at 326°C, testing of the other catalysts was carried out at five temperatures between 294° and 388°C as indicated in Table 8-B-2. The conditions for conducting both series of tests are listed below:

R = 2.42

M% = 8 moles %	W/F = 13.3 gm-hr/moles		
W = 0.399 gm	$_{o}F_{M}$ = 0.03 moles/hr		
$_{o}F_{air}$ = 0.375 moles/hr	$_{o}F_{O_2}$ = 0.0788 moles/hr		
$_{o}F_{N_2}$ = 0.296 moles/hr	$_{o}P_{M}$ = 60.8 mm Hg		
$_{o}P_{O_2}$ = 146.8 mm Hg	$_{o}P_{N_2}$ = 552.4 mm Hg		

The catalyst bed heights were in the range 2 to 5 inches depending on the weight of catalyst tested.

Table 6-B-1

Experimental Data
For Manganese-dioxide-Molybdenum trioxide

Run No.	Time days	F_f moles/hr	F_N moles/hr	F_{O_2} moles/hr
200	5	0.0159	0.0141	0.06655
201	7	0.0158	0.0142	0.06660
202	12	0.0159	0.0141	0.06655
203	20	0.0160	0.0140	0.06650
204	30	0.0159	0.0141	0.06655

Run No	Conv X	F_f/T_1 $(=N/T_1)$	N/T_1	O_2/T_6	N_2/T_6
200	0.530	0.346	0.307	0.1835	0.8164
201	0.528	0.345	0.310	0.1836	0.8163
202	0.529	0.346	0.307	0.1835	0.8164
203	0.532	0.348	0.304	0.1834	0.8166
204	0.529	0.345	0.310	0.1835	0.8166

Table 8-B-2

Experimental Data for Vanadium Pentoxide

Run No.	Temp. °C	Conv. x	F_f moles/hr	F_M moles/hr	F_W moles/hr	F_{O_2} moles/hr	F_{CO} moles/hr	F_{CO_2} moles/hr
205	294	0.28	0.0084	0.0216	0.0084	0.0703	0	0
206	304	0.47	0.0141	0.0159	0.0141	0.0653	0	0
207	316	0.69	0.0207	0.0093	0.0207	0.0642	0	0
208	336	0.93	0.0123	0.0021	0.0380	0.0534	0.0058	0.0043
209	342	1.00	0.0102	0	0.0440	0.0504	0.0080	0.0060

Run No.	Yield y	F_f/T_1	W/T_1	M/T_1	O_2/T_g	N_2/T_g	CO/T_g	CO_2/T_g
205	0.28	0.219	0.219	0.563	0.200	0.800	0	0
206	0.47	0.320	0.320	0.360	0.193	0.807	0	0
207	0.69	0.408	0.408	0.183	0.190	0.810	0	0
208	0.41	0.235	0.725	0.040	0.159	0.811	0.017	0.013
209	0.34	0.187	0.813	0	0.148	0.809	0.024	0.018

Table B-B-2 (Continued)

Experimental Data for Molybdenum Trioxide

Run No.	Temp °C	F_f moles/hr	F_M moles/hr	F_W moles/hr	F_{O_2} moles/hr
208	294	0.0012	0.0288	0.0012	0.0739
209	316	0.0024	0.0276	0.0024	0.0733
210	388	0.003	0.0270	0.003	0.0730

Run No.	Conv. %	F_f/T_1 $(=W/T_1)$	M/T_1	O_2/T_g	N_2/T_g
208	0.04	0.038	0.928	0.21	0.79
209	0.08	0.074	0.852	0.21	0.79
210	0.10	0.091	0.818	0.21	0.79

Table S-B-2 (Continued)

Experimental Data for Molybdenum Trioxide

Run No.	Temp °C	F_f moles/hr	F_M moles/hr	F_W moles/hr	F_{O_2} moles/hr
208	294	0.0012	0.0288	0.0012	0.0739
209	316	0.0024	0.0276	0.0024	0.0733
210	388	0.003	0.0270	0.003	0.0730

Run No.	Conv. X	F_f/T_1 $(=W/T_1)$	M/T_1	O_2/T_g	N_2/T_g
208	0.04	0.038	0.928	0.21	0.79
209	0.08	0.074	0.852	0.21	0.79
210	0.10	0.091	0.818	0.21	0.79

Table C-B-2 (Continued)

Experimental Data for Manganese Dioxide

Run No	Temp °C	F_f moles/hr	F_H moles/hr	F_W moles/hr	F_{O_2} moles/hr
211	294	0.00045	0.02955	0.00045	0.07428
212	316	0.00054	0.02946	0.00054	0.07423
213	388	0.0006	0.02940	0.0006	0.07420

Run No.	Conv. X	F_f/F_1 $(=W/F_1)$	H/F_1	O_2/F_g	H_2/F_g
211	0.015	0.015	0.970	0.210	0.790
212	0.018	0.018	0.965	0.210	0.790
213	0.02	0.020	0.960	0.210	0.790

C. Diffusion

1. Internal Diffusion in a Porous Catalyst

a. Molecular Diffusion (Effect of Feed Velocity on Conversion)

The experimental data for molecular diffusion are given in Table 8-C-1. The conditions which apply to this table are:

Temp	= 326°C	R	= 2.42
W/F	= 13.3 gm-hr/moles	M%	= 8 moles %

b. Knudsen Diffusion

The experimental data for Knudsen diffusion is given in Table 8-C-2. The conditions which apply to Table 8-C-2 are:

Temp	= 365°C	R	= 2.79
M%	= 7 moles %	W/F	= 8.8 gm-hr/moles
W	= 0.264 gm	$_{o}F_{M}$	= 0.03 moles/hr
$_{o}F_{air}$	= 0.429 moles/hr	$_{o}F_{O_2}$	= 0.090 moles/hr
$_{o}F_{N_2}$	= 0.339 moles/hr	$_{o}P_{M}$	= 53.2 mm Hg
$_{o}P_{O_2}$	= 148.4 mm Hg	$_{o}P_{N_2}$	= 558.4 mm Hg

Table 8-C-1

Experimental Data for Molecular Diffusion

Run No.	Vel. of feed moles/hr	air moles/hr	N_o moles/hr	$_oO_2$ moles/hr	O_2 moles/hr	N_2 moles/hr	W gm
214	0.375	0.3750	0.030	0.0788	0.07085	0.2963	0.399
215	0.438	0.4375	0.035	0.0919	0.08266	0.3456	0.466
216	0.500	0.5000	0.040	0.1050	0.09436	0.3450	0.532
217	0.563	0.5625	0.045	0.1181	0.1062	0.4444	0.599

Run No.	Conv. X	F (=W) moles/hr	N moles/hr	F_1/T_1 (=W/T_1)	N/T_1	O_2/T_g	N_2/T_g
214	0.530	0.01590	0.0141	0.346	0.307	0.1930	0.8070
215	0.528	0.01848	0.0165	0.345	0.308	0.1930	0.8070
216	0.532	0.02128	0.0187	0.347	0.305	0.1928	0.8072
217	0.529	0.02381	0.0331	0.346	0.481	0.1929	0.8071

Table 6-6-2

Experimental Data for Knudsen Diffusion

Run No	Size of Catalyst mm	Q_o moles/hr	$F_{(-W)}$ moles/hr	W moles/hr
218	1.650	0.00225	0.0155	0.0146
219	0.525	0.00225	0.0155	0.0145
220	0.200	0.00230	0.0154	0.0146

Run No	Conv X	P_1/T_1 $(=W/T_1)$	M/T_1	Q_2/T_2	N_2/T_2
218	0.5150	0.340	0.320	0.195	0.805
219	0.5156	0.341	0.319	0.195	0.805
220	0.5155	0.339	0.322	0.196	0.804

2. External Diffusion (Drop in Partial Pressure)

The data for external diffusion to determine the maximum $\Delta p_j/p_j$ values are obtained from Run 331. If the $\Delta p_j/p_j$ values are small, the external diffusion can be neglected.

The calculation is based on the method of Yoshida, Ramaswami, and Hougen (111). Figure 2 of their paper is used to determine the R/y_i versus $\Delta p_j/p_j$ correlation. The results are recorded in Table 8-C-3. The conditions which apply to this table are:

Temp. = 365°C

W/F = 22.0 gm-hr/moles

M% = 8 moles %

ϕ = shape factor, or sphericity
= 0.9 for irregular granules

G_m = molal mass velocity of feed based on the total cross section of the catalyst bed in gm-moles/hr-cm^2
= $\frac{0.345 + 0.03}{\pi(1/4 \times 2.54)^2}$ = 16 gm-moles/hr-cm^2

W = weight of catalyst = 0.66 gm

A_m = surface area of the catalyst particle per unit mass
= 7.8 m^2/gm or 7.8 x 10^4 cm^2/gm

$(y_j)_{in}$ = mole fraction of component j in the feed

$(y_j)_{out}$ = mole fraction of component j in the product

y_j = mole fraction of component j at the interface

$\doteq \left[(y_j)_{in} + (y_j)_{out}\right]/2$

r_{mj} = molal reaction rate of component j per unit mass of catalyst

R_j = dimensionless term of component j

$$= \frac{r_{mj}}{(78,000)(0.9)(16)} = \frac{r_{mj}}{1.121 \times 10^6}$$

for example:

r_{mf} = molal reaction rate of formaldehyde per unit mass of catalyst

$= 0.0251/0.66 = 0.0381$ gm-moles/gm-hr

R_f = R term of formaldehyde

$$= \frac{0.0381}{1.121 \times 10^5} = 3.4 \times 10^8$$

The values shown in Table 8-C-3 can be obtained by following steps similar to those shown in the preceding calculations

where $(F_j)_{in}$ = flow rate of component j in the feed

$(F_j)_{out}$ = flow rate of component j in the product.

Since

$$\left(\frac{p_i}{p_j}\right)_{max} < 0.001$$

the external diffusion effects can be neglected.

Table 8-C-3

Experimental Data for External Diffusion

Component	$(F_j)_{in}$ moles/hr	$(F_j)_{out}$ moles/hr	$(y_j)_{in}$	$(y_j)_{out}$	y_j	r_{mj} gm-moles/hr 10^2	R_j 10^8	R_j/y_j 10^6	$\frac{P_i}{P_j}$ max
O_2	0.0745	0.0620	0.197	0.159	0.178	9.40	8.39	0.47	0.0001
N_2	0.2730	0.2730	0.724	0.700	0.712	-	-	-	0.0001
CH_3OH	0.0300	0.0049	0.079	0.013	0.046	0.74	0.66	0.14	0.0001
HCHO	0	0.0251	0	0.064	0.032	3.81	3.40	1.06	0.0001
H_2O	0	0.0251	0	0.064	0.032	3.81	3.40	1.06	0.0001

D. Temperature Effects

1. Temperature Drop from Catalyst Particle to Ambient Gas Stream

From Appendix C:

r_{mf} = 0.0381 gm-moles/gm-hr β = 0.9

e_m = 16 gm-moles/cm^2-hr A_m = 7.8 x 10^4 cm^2/gm

and

Component	C_{av} $\frac{cal}{gm\text{-}mole\text{-}^\circ C}$	C_p' $\frac{cal}{gm\text{-}mole\text{-}^\circ C}$	$C_p C_{av}$ $(\frac{cal}{gm\text{-}mole\text{-}^\circ C})^2$	H_f $\frac{kcal}{mole}$
O_2	0.178	7.80	1.388	0
N_2	0.712	7.26	5.169	0
CH_3OH	0.006	16.85	0.775	-48.08
HCHO	0.032	11.60	0.371	-28.29
H_2O	0.032	8.78	0.281	-57.80

$-(\Delta H)_f$ = molal heat of reaction of formaldehyde

$$C_p = \sum_{i=1}^{5} (C_p' C_{av})_i = 7.984 \text{ cal/gm-mole-}^\circ C$$

$$Q_f = \frac{r H_f}{A_m \rho_p G_m}$$

$$= \frac{(0.0381)(38010)}{(7.8 \times 10^4)(0.9)(7.984)(16)} = 1.615 \times 10^{-4}$$

Since from Figures 3 and 4 of Yoshida et al (111):

$\Delta T < 0.1^{\circ}C$

the catalyst surface temperature effect can be neglected.

2. Temperature Effect on Conversion, Yield, and Selectivity

The conditions used in studying the effect of temperature on conversion, yield, and selectivity are:

$R = 2.42$

M%	= 8	moles %	W/F	= 16.3	gm-hr/moles
W	= 0.489	gm	$_oF_M$	= 0.03	moles/hr
$_oF_{air}$	= 0.375	moles/hr	$_oF_{O_2}$	= 0.0788	moles/hr
$_oF_{N_2}$	= 0.296	moles/hr	$_oP_M$	= 60.8	mm Hg
$_oP_{O_2}$	= 146.8	mm Hg	$_oP_{N_2}$	= 552.4	mm Hg

The effect of temperatures between 250° and 460°C on conversion, yield, and selectivity is as follows:

Temp. °C	Yield y	Conversion x	Selectivity s	Run No.
250	0.06	0.06	1.00	396
319	0.54	0.54	1.00	390
326	0.61	0.61	1.00	360
365	0.84	0.84	1.00	330
422	0.38	0.88	0.43	300
460	0.05	1.00	0.05	301

The experimental data for run no.'s 396, 390, 360, and 330 are recorded in Appendix E. The data for 300 and 301 are shown in Table 8-D-1.

Table 8-D-1

Experimental Data for Run No. 300 and No. 301

Temperature vs Yield and Conversion

Run No.	Temp. °C	Yield y	Conv. x	F_f/T_1	W/T_1	M/T_1	O_2/T_g	N_2/T_g
300	422	0.38	0.88	0.202	0.736	0.062	0.157	0.799
301	460	0.05	1.00	0.025	0.975	0	0.131	0.787

Run No.	CO/T_g	CO_2/T_g	F_f moles/hr	F_W moles/hr	F_M moles/hr	F_{O_2} moles/hr	F_{CO} moles/hr	F_{CO_2} moles/hr
300	0.009	0.010	0.0114	0.0416	0.00352	0.0537	0.00302	0.01208
301	0.004	0.078	0.0015	0.0585	0	0.0453	0.00142	0.02708

3. Axial Temperature Gradient

The axial temperature gradient calculation was measured by adjusting the thermocouple position in the reactor. It was found the difference could be neglected. For comparison, and as a supplement to Cotter's work on this problem (21), the following approximated calculation was made using the method of J. M. Smith (Chemical Engineering Kinetics, page 300, Wiley, New York, 1956):

$$t = t_{1,1} - t_{2,1}$$

$$= t_{1,1} - t_{1,2}/\left(\frac{\Delta z}{(\Delta r)^2}\right)\left(\frac{k}{GC}\right)(3)$$

$$= 365 - 364/(192)(0.0025)(3) \neq 0.7°C.$$

where $n = 1$

$\ell = 1$

$t_{1,1} = 365°C$

$t_{1,2} = 364°C$

$\Delta z = 1" = 0.0834$ ft

$\Delta r = 0.25" = 0.0208$ ft

$C = 0.252$

$G = 16700$ lb/hr-ft^2

$k_e = 10.5$ Btu/(hr)(ft)(°C).

B. Effect of W/F

The effect of W/F on conversion (x) was studied in the experimental range 365° - 250°C. In this range, the selectivity was one, conversion equalled yield, and the flow rate of water was approximately equal to the flow rate of formaldehyde. The running conditions used for the five values of the oxygen to methanol ratio (R) were:

(1). R = 5.04

M% = 4 moles % $_oF_M$ = 0.03 moles/hr

$_oF_{air}$ = 0.750 moles/hr $_oF_{O_2}$ = 0.158 moles/hr

$_oF_{N_2}$ = 0.593 moles/hr $_oP_M$ = 30.4 mm Hg

$_oP_{O_2}$ = 153.2 mm Hg $_oP_{N_2}$ = 576.4 mm Hg

(2). R = 3.61

M% = 5.5 moles % $_oF_M$ = 0.03 moles/hr

$_oF_{air}$ = 0.546 moles/hr $_oF_{O_2}$ = 0.115 moles/hr

$_oF_{N_2}$ = 0.431 moles/hr $_oP_M$ = 41.8 mm Hg

$_oP_{O_2}$ = 150.8 mm Hg $_oP_{O_2}$ = 567.4 mm Hg

(3). R = 3.02

M% = 6.5 moles % $_oF_M$ = 0.03 moles/hr

$_oF_{air}$ = 0.462 moles/hr $_oF_{O_2}$ = 0.097 moles/hr

$_oF_{N_2}$ = 0.365 moles/hr $_oP_M$ = 49.4 mm Hg

$_oP_{O_2}$ = 149.2 mm Hg $_oP_{N_2}$ = 561.4 mm Hg

(4). R = 2.79

M% = 7 moles % $_oF_M$ = 0.03 moles/hr

$_oF_{air}$ = 0.429 moles/hr $_oF_{O_2}$ = 0.090 moles/hr

$_oF_{N_2}$ = 0.339 moles/hr $_oP_M$ = 53.2 mm Hg

$_oP_{O_2}$ = 148.4 mm Hg $_oP_{N_2}$ = 558.4 mm Hg

(5). R = 2.42

M% = 8 moles % $_oF_M$ = 0.03 moles/hr

$_oF_{air}$ = 0.375 moles/hr $_oF_{O_2}$ = 0.0788 moles/hr

$_oF_{N_2}$ = 0.296 moles/hr $_oP_M$ = 60.8 mm Hg

$_oP_{O_2}$ = 146.8 mm Hg $_oP_{N_2}$ = 552.4 mm Hg

The experimental data recorded at 365°, 326°, 319°, and 250°C, for the various values of R employed, are summarized in Tables 8-E-1, 8-E-2, 8-E-3, and 8-E-4 respectively.

Table 8-E-1

Effect of W/F on Conversion at 365°C for R = 5.04

Run No.	W/F gm-hr/moles	F_f/T_1 $(=W/T_1)$	M/T_1	O_2/T_E	N_2/T_E
302.	2.5	0.095	0.810	0.208	0.792
303	5.0	0.174	0.653	0.207	0.793
304	8.8	0.265	0.471	0.204	0.796
305	13.3	0.339	0.323	0.202	0.798
306	16.3	0.375	0.250	0.200	0.800
307	22.0	0.422	0.156	0.198	0.802

Run No.	Conv. x	F_f moles/hr	F_M moles/hr	F_{O_2} moles/hr	W gm
302	0.105	0.0032	0.0269	0.156	0.075
303	0.210	0.0063	0.0237	0.154	0.150
304	0.360	0.0108	0.0192	0.152	0.264
305	0.513	0.0154	0.0146	0.150	0.399
306	0.600	0.0180	0.0120	0.149	0.489
307	0.730	0.0219	0.0081	0.147	0.660

Table 8-E-1 (Continued)

Effect of W/F on Conversion at 365°C for R = 3.61

Run No.	W/F gm-hr/moles	F_f/T_1 $(-W/T_1)$	M/T_1	O_2/T_g	N_2/T_g
308	2.5	0.099	0.802	0.207	0.793
309	5.0	0.218	0.563	0.204	0.796
310	8.8	0.321	0.357	0.199	0.801
311	13.3	0.394	0.212	0.194	0.806
312	16.3	0.417	0.165	0.193	0.807
313	22.0	0.429	0.143	0.192	0.808

Run No.	Conv. x	F_f moles/hr	F_M moles/hr	F_{O_2} moles/hr	W gm
308	0.110	0.0033	0.0267	0.1060	0.075
309	0.280	0.0084	0.0216	0.1040	0.150
310	0.473	0.0142	0.0158	0.1010	0.264
311	0.650	0.0195	0.0105	0.0980	0.399
312	0.717	0.0215	0.0085	0.0973	0.489
313	0.749	0.0225	0.0075	0.0968	0.660

Table 8-E-1 (Continued)

Effect of W/F on Conversion at 365°C for R = 3.02

Run No.	W/F gm-hr/moles	F_f/T_1 ($=W/T_1$)	M/T_1	O_2/T_g	N_2/T_g
314	2.5	0.111	0.778	0.207	0.793
315	5.0	0.231	0.538	0.202	0.798
316	8.8	0.333	0.333	0.197	0.803
317	13.3	0.404	0.193	0.192	0.808
318	16.3	0.425	0.149	0.190	0.810
319	22.0	0.441	0.117	0.188	0.812

Run No.	Conv. x	F_f moles/hr	F_M moles/hr	F_{O_2} moles/hr	W gm
314	0.125	0.00375	0.0263	0.0091	0.075
315	0.300	0.00900	0.0210	0.0065	0.150
316	0.500	0.01500	0.0150	0.0035	0.264
317	0.677	0.02030	0.0097	0.0809	0.399
318	0.740	0.02220	0.0078	0.0799	0.489
319	0.790	0.02370	0.0063	0.0792	0.660

Table 8-B-1 (Continued)

Effect of W/F on Conversion at 365°C for R = 2.79

Run No.	W/F gm-hr/moles	F_f/T_1 $(=W/T_1)$	M/T_1	O_2/T_g	N_2/T_g
320	2.5	0.120	0.760	0.206	0.794
321	5.0	0.225	0.550	0.201	0.799
322	8.8	0.340	0.515	0.194	0.806
323	13.3	0.410	0.180	0.189	0.811
324	16.3	0.440	0.120	0.186	0.814
325	22.0	0.450	0.100	0.185	0.815

Run No.	Conv. x	F_f moles/hr	F_M moles/hr	F_{O_2} moles/hr	W gm
320	0.136	0.00408	0.0259	0.0817	0.075
321	0.290	0.00870	0.0212	0.0793	0.150
322	0.517	0.01550	0.0146	0.0760	0.264
323	0.697	0.02090	0.0092	0.0733	0.399
324	0.787	0.02360	0.0064	0.0719	0.489
325	0.817	0.02450	0.0055	0.0715	0.660

Table 8-B-1 (Continued)

Effect of W/F on Conversion at 365°C for R = 2.42

Run No.	W/F gm-hr/moles	F_f/T_1 $(=W/T_1)$	M/T_1	O_2/T_6	N_2/T_6
326	2.5	0.123	0.754	0.206	0.795
327	5.0	0.248	0.504	0.199	0.801
328	8.8	0.355	0.290	0.192	0.808
329	13.3	0.422	0.156	0.186	0.814
330	16.3	0.451	0.099	0.183	0.817
331	22.0	0.456	0.089	0.183	0.817

Run No.	Conv. x	F_f moles/hr	F_M moles/hr	F_{O_2} moles/hr	W gm
			$M_0 = 0.0390$?		
326	0.140	0.0042	0.0258	0.0767	0.075
327	0.330	0.0099	0.0201	0.0738	0.150
328	0.500	0.0165	0.0135	0.0705	0.264
329	0.730	0.0219	0.0081	0.0678	0.399
330	0.820	0.0246	0.0054	0.0665	0.489
331	0.837	0.0251	0.0049	0.0662	0.660

Table S-E-2

Effect of W/F on Conversion at 326°C for R = 5.04

Run No.	W/F gm-hr/moles	F_f/T_1 $(-W/T_1)$	H/T_1	O_2/T_g	H_2/T_g
332	2.5	0.091	0.818	0.208	0.792
333	5.0	0.166	0.668	0.207	0.793
334	8.8	0.251	0.498	0.205	0.795
335	13.3	0.323	0.355	0.202	0.798
336	16.3	0.358	0.284	0.201	0.799
337	22.0	0.398	0.205	0.199	0.801

Run No.	Conv. x	F_f moles/hr	F_H moles/hr	F_{O_2} moles/hr	W gm
332	0.100	0.0030	0.0270	0.156	0.075
333	0.199	0.0060	0.0240	0.155	0.150
334	0.333	0.0100	0.0200	0.153	0.264
335	0.477	0.0143	0.0157	0.150	0.399
336	0.557	0.0167	0.0133	0.149	0.489
337	0.660	0.0198	0.0102	0.148	0.660

Table 8-E-2 (Continued)

Effect of W/F on Conversion at 326°C for R = 3.61

Run No.	W/F gm-hr/moles	F_f/T_1 $(=W/T_1)$	N/T_1	O_2/T_t	N_2/T_t
338	2.5	0.099	0.802	0.208	0.792
339	5.0	0.174	0.655	0.205	0.795
340	8.8	0.254	0.493	0.203	0.797
341	13.3	0.321	0.358	0.200	0.800
342	16.3	0.357	0.286	0.198	0.802
343	22.0	0.402	0.196	0.195	0.805

Run No.	Conv. x	F_f moles/hr	F_N moles/hr	F_{O_2} moles/hr	W gm
338	0.110	0.0033	0.0267	0.113	0.075
339	0.210	0.0063	0.0237	0.111	0.150
340	0.340	0.0102	0.0198	0.110	0.264
341	0.473	0.0142	0.0158	0.108	0.399
342	0.557	0.0167	0.0134	0.106	0.489
343	0.673	0.0202	0.0098	0.105	0.660

Table B-B-2 (Continued)

Effect of W/F on Conversion at 326°C for R = 3.02

Run No.	W/F gm-hr/moles	F_f/T_1 $(=W/T_1)$	M/T_1	O_2/T_g	N_2/T_g
344	2.5	0.099	0.802	0.207	0.795
345	5.0	0.179	0.642	0.204	0.796
346	8.8	0.262	0.476	0.201	0.799
347	13.3	0.328	0.344	0.197	0.803
348	16.3	0.361	0.278	0.195	0.805
349	22.0	0.405	0.191	0.192	0.808

Run No.	Conv. x	F_f moles/hr	F_M moles/hr	F_{O_2} moles/hr	W gm
344	0.110	0.0033	0.0267	0.0953	0.975
345	0.217	0.0065	0.0235	0.0937	0.150
346	0.357	0.0107	0.0194	0.0916	0.264
347	0.487	0.0146	0.0154	0.0896	0.399
348	0.567	0.0170	0.0131	0.0885	0.489
349	0.680	0.0204	0.0096	0.0867	0.660

Table 8-E-2 (Continued)

Effect of W/F on Conversion at 326°C for R = 2.79

Run No.	W/F gm-hr/moles	F_f/T_1 (=W/T_1)	N/T_1	O_2/T_g	N_2/T_g
350	2.5	0.103	0.794	0.207	0.793
351	5.0	0.180	0.639	0.204	0.796
352	8.8	0.267	0.465	0.200	0.800
353	13.3	0.333	0.333	0.196	0.804
354	16.3	0.366	0.267	0.194	0.806
355	22.0	0.408	0.183	0.191	0.810

Run No.	Conv. x	F_f moles/hr	F_N moles/hr	F_{O_2} moles/hr	W gm
350	0.115	0.0035	0.0266	0.0880	0.075
351	0.220	0.0066	0.0234	0.0867	0.150
352	0.367	0.0110	0.0191	0.0845	0.264
353	0.500	0.0150	0.0150	0.0825	0.399
354	0.577	0.0173	0.0127	0.0813	0.489
355	0.690	0.0207	0.0093	0.0797	0.660

Table 8-K-2 (Continued)

Effect of W/F on Conversion at 326°C for R = 2.42

Run No.	W/F gm-hr/moles	F_f/T_1 (=W/T_1)	M/T_1	O_2/T_g	N_2/T_g
356	2.5	0.107	0.786	0.206	0.794
357	5.0	0.187	0.626	0.203	0.797
358	8.8	0.275	0.449	0.198	0.802
359	13.3	0.346	0.307	0.193	0.807
360	16.3	0.377	0.245	0.190	0.810
361	22.0	0.412	0.176	0.187	0.813

Run No.	Conv. x	F_f moles/hr	F_M moles/hr	F_{O_2} moles/hr	W gm
356	0.120	0.0036	0.0264	0.0770	0.075
357	0.230	0.0069	0.0231	0.0753	0.150
358	0.380	0.0114	0.0186	0.0731	0.264
359	0.530	0.0159	0.0141	0.0708	0.399
360	0.607	0.0182	0.0118	0.0697	0.489
361	0.700	0.0210	0.0090	0.0683	0.660

Table 8-B-3

Effect of W/F on Conversion at 319°C for R = 5.04

Run No.	W/F gm-hr/moles	F_f/T_1 $(=W/T_1)$	M/T_1	O_2/T_6	N_2/T_6
362	2.5	0.087	0.826	0.209	0.791
363	5.0	0.156	0.688	0.207	0.793
364	8.8	0.239	0.522	0.205	0.795
365	13.3	0.308	0.394	0.203	0.797
366	16.3	0.340	0.320	0.202	0.798
367	22.0	0.371	0.258	0.200	0.800

Run No.	Conv. x	F_f moles/hr	F_M moles/hr	F_{O_2} moles/hr	W gm
362	0.095	0.0029	0.0272	0.1560	0.075
363	0.187	0.0056	0.0245	0.1550	0.150
364	0.314	0.0094	0.0206	0.1530	0.264
365	0.447	0.0134	0.0167	0.1510	0.399
366	0.517	0.0155	0.0146	0.1500	0.489
367	0.590	0.0177	0.0123	0.1490	0.660

Table B-E-3 (Continued)
Effect of W/F on Conversion at 319°C for R = 3.61

Run No.	W/F gm-hr/moles	F_f/T_1 $(=W/T_1)$	H/T_1	O_2/T_E	N_2/T_E
368	2.5	0.089	0.822	0.208	0.792
369	5.0	0.160	0.681	0.206	0.794
370	8.8	0.242	0.515	0.203	0.797
371	13.5	0.312	0.376	0.200	0.800
372	16.3	0.344	0.311	0.198	0.802
373	22.0	0.375	0.250	0.197	0.803

Run No.	Conv. x	F_f moles/hr	F_H moles/hr	F_{O_2} moles/hr	W gm
368	0.098	0.0029	0.0271	0.1130	0.075
369	0.190	0.0057	0.0243	0.1121	0.150
370	0.320	0.0096	0.0204	0.1101	0.264
371	0.453	0.0136	0.0164	0.1080	0.399
372	0.527	0.0158	0.0143	0.1071	0.489
373	0.600	0.0180	0.0120	0.1062	0.660

Table 8-B-3 (Continued)

Effect of W/F on Conversion at 319°C for R = 3.02

Run No.	W/F gm-hr/moles	F_f/T_1 $(-W/T_1)$	N/T_1	O_2/T_6	N_2/T_6
374	2.5	0.093	0.813	0.207	0.793
375	5.0	0.167	0.667	0.205	0.795
376	8.8	0.251	0.498	0.201	0.799
377	13.3	0.320	0.361	0.198	0.802
378	16.3	0.351	0.299	0.196	0.804
379	22.0	0.383	0.235	0.194	0.806

Run No.	Conv. x	F_f moles/hr	F_N moles/hr	F_{O_2} moles/hr	W gm
374	0.103	0.0031	0.0269	0.0954	0.075
375	0.200	0.0060	0.0240	0.0959	0.150
376	0.333	0.0100	0.0200	0.0919	0.264
377	0.470	0.0141	0.0159	0.0899	0.399
378	0.540	0.0162	0.0138	0.0888	0.489
379	0.620	0.0186	0.0114	0.0876	0.660

Table B-3 (Continued)

Effect of W/F on Conversion at 319°C for R = 2.79

Run No.	W/F gm-hr/mole	F_f/F_1 ($=W/F_1$)	N/F_1	O_2/F_g	N_2/F_g
380	2.5	0.091	0.818	0.207	0.793
381	5.0	0.167	0.667	0.204	0.796
382	8.8	0.250	0.500	0.200	0.800
383	13.3	0.320	0.360	0.197	0.803
384	16.3	0.353	0.295	0.195	0.805
385	22.0	0.385	0.231	0.192	0.808

Run No.	Conv. x	F_f moles/hr	F_N moles/hr	F_{O_2} moles/hr	W gm
380	0.100	0.0030	0.0270	0.0085	0.075
381	0.200	0.0060	0.0240	0.0070	0.150
382	0.333	0.0100	0.0200	0.0050	0.264
383	0.470	0.0141	0.0159	0.0030	0.399
384	0.547	0.0164	0.0137	0.0018	0.489
385	0.627	0.0188	0.0113	0.0006	0.660

Table S-E-3 (Continued)

Effect of W/F on Conversion at 319°C for R = 2.42

Run No.	W/F gm-hr/moles	F_f/T_1 $(=W/T_1)$	N/T_1	O_2/T_g	N_2/T_g
386	2.5	0.095	0.810	0.207	0.793
387	5.0	0.167	0.667	0.204	0.796
388	8.8	0.254	0.493	0.199	0.801
389	13.3	0.322	0.356	0.195	0.805
390	16.3	0.355	0.290	0.192	0.808
391	22.0	0.390	0.220	0.189	0.811

Run No.	Conv. x	F_f moles/hr	F_N moles/hr	F_{O_2} moles/hr	W gm
386	0.105	0.0032	0.0269	0.0772	0.075
387	0.200	0.0060	0.0240	0.0758	0.150
388	0.340	0.0102	0.0198	0.0737	0.264
389	0.475	0.0143	0.0158	0.0716	0.399
390	0.550	0.0165	0.0135	0.0705	0.489
391	0.640	0.0192	0.0108	0.0692	0.660

Table B-E-4

Effect of W/F on Conversion at 250°C for R = 2.42

Run No.	W/F gm-hr/moles	F_f/T_1 $(=W/T_1)$	M/T_1	O_2/T_g	N_2/T_g
392	2.5	0.0104	0.9792	0.2097	0.7903
393	5.0	0.0206	0.9589	0.2093	0.7907
394	8.8	0.0366	0.9268	0.2088	0.7912
395	13.3	0.0535	0.8930	0.2082	0.7918
396	16.3	0.0646	0.8709	0.2078	0.7922
397	22.0	0.0826	0.8349	0.2072	0.7928

Run No.	Conv. x	F_f moles/hr	F_M moles/hr	F_{O_2} moles/hr	$\frac{W}{F}$
392	0.0105	0.0003	0.0297	0.0786	0.075
393	0.0210	0.0006	0.0294	0.0784	0.150
394	0.0380	0.0011	0.0289	0.0782	0.264
395	0.0565	0.0017	0.0283	0.0779	0.375
396	0.0690	0.0021	0.0279	0.0777	0.468
397	0.0900	0.0027	0.0273	0.0774	0.568

F. Material Balance and Sample Calculation

This calculation is based on the experimental data of Run No. 330.

1. To determine mole percentages from peak height ratios

Since:

$$\frac{(P/I_1)_M}{(W/I_1)_M} = 0.325 \frac{(P/I_1)_h}{(W/I_1)_h}$$

$$= 0.325 \ (P/W)_h$$

$$\left(\frac{P}{I_1}\right)_M = 0.325 \left(\frac{P}{W}\right)_h \left(\frac{W}{I_1}\right)_M \qquad (8\text{-}1)$$

and

$$\left(\frac{N}{I_1}\right)_M = 0.425 \left(\frac{N}{W}\right)_h \left(\frac{W}{I_1}\right)_M \qquad (8\text{-}2)$$

if the above two relations are added together

$$\left(\frac{P}{I_1}\right)_M + \left(\frac{N}{I_1}\right)_M = 0.325\left(\frac{P}{W}\right)_h\left(\frac{W}{I_1}\right)_M + 0.425\left(\frac{N}{W}\right)_h\left(\frac{W}{I_1}\right)_M$$

$$1 - \left(\frac{W}{I_1}\right)_M = \left(\frac{W}{I_1}\right)_M \ 0.325 \left(\frac{P}{W}\right)_h + 0.425 \left(\frac{N}{W}\right)_h$$

$$(w/T_1)_M = \frac{1}{1 + 0.525(F/w)_h + 0.425(M/w)_h}$$

$$= \frac{1}{1 + 0.525(5.08) + 0.425(0.516)}$$

$$= 0.4505 \doteq 0.451 \qquad (8\text{-}3)$$

Substitute equation 8-3 into equations 8-1 and 8-2 to find the mole percentages of formaldehyde and methanol.

$$(F/T_1)_M = 0.525(5.08)(0.451)$$

$$= 0.4514 \doteq 0.451 \qquad (8\text{-}4)$$

$$(M/T_1)_M = 0.425(0.516)(0.451)$$

$$= 0.0989 \doteq 0.099 \qquad (8\text{-}5)$$

2. <u>To Determine the Material Balance from Mole Percentages</u>

Since $M = M_o - F_f$

therefore $T_1 = F_f + w + M$ ($w = F_f$)

$$= 2F_f + (M_o - F_f) = F_f + M_o$$

$$F_f/T_1 = \frac{F_f}{F_f + M_o} = \%_f = \%_w$$

$$F_f = \frac{(M_o)(\%_f)}{1 - \%_f} = \frac{(0.03)(0.451)}{1 - 0.451}$$

$$= 0.0246 \text{ moles/hr}$$

$$M = M_o - F_f = 0.03 - 0.0246$$

$= 0.0054$ moles/hr

$x = F_f/F_o = 0.0246/0.03 = 0.82$

$\%_{O_2} = F_{O_2}/F_t = F_{O_2}/(F_{O_2} + F_{N_2})$ $\quad F_{O_2} = \%_{O_2}\cdot(F_{O_2} + F_{N_2})$

$F_{O_2} = (F_{N_2})(\%_{O_2})/(1 - \%_{O_2}) = 0.0665$ moles/hr $\quad F_{O_2}[1 - \%_{O_2}] = \%_{O_2}\cdot F_{N_2}$

3. **Material Balance Check Based on Atomic Oxygen**

Component	in Feed moles/hr	in Product moles/hr
CH_3OH	0.03	0.0054
HCHO	0	0.0246
H_2O	0	0.0246
O_2	0.1448	0.1330
Total	0.1748	0.1876

$$\% \text{ Deviation} = \frac{\text{Output} - \text{Input}}{\text{Output}} \times 100$$

$= 0.0128/0.1876 \times 100 \doteq 6.8\%$

4. **Deviation between Calculated and Experimental W/F vs x Relations**

The following is a sample tabulation of the deviation between the calculated and experimental W/F versus x relations. It is based on data obtained at 365°C, with an oxygen to methanol ratio (R) of 2.42

(Table 8-B-1, Run no.'s 326 - 331). The values for k_1 and k_2 were obtained from equations 5-40 and 5-41. At 365°C, k_1 was equal to 2.86×10^{-3} and k_2 was equal to 5.08×10^{-3} moles/gm-mm Hg-hr. Substituting these values for the constants in Equation 1 of Table 5-1, the following comparison was obtained:

Comparison of Deviation

x	$(W/F)_{exp}$	$(W/F)_{cal}$	% Deviation
0.126	2.5	2.474	-1.05
0.250	5.0	5.049	0.97
0.420	8.8	8.888	1.00
0.590	13.3	13.290	-0.07
0.680	16.3	16.009	-1.78
0.837	22.0	22.180	0.82

The percentage deviation may be defined as

$$\% \text{ Deviation} = \frac{(W/F) \text{ calculated} - (W/F) \text{ experimental}}{(W/F) \text{ experimental}}$$

In general, all the deviations determined were below eight percent except for the last condition in which $(W/F)_{exp}$ equalled 22.0.

6. The Least-square-error Approach

This approach assumes that $y = y(x)$ and that N discrete values of y are known along with a corresponding number of x. These may be designated as $y_1, y_2, \ldots y_N$ and $x_1, x_2, \ldots x_N$. No particular spacing of the x values is assumed, and some may even be repeated. Instead of requiring that an approximating polynomial $\phi_{N-1}(x)$ pass through the points $y_1, y_2, \ldots y_N$, a weaker approximation may be used in which a suitable approximating function is made to pass as close as possible, in some sense, to the points. The suitable approximation is herein taken as a linear combination of m + 1 linearly independent functions $U_0(x), U_1(x), U_2(x), \ldots U_m(x)$. Thus

$$\phi_m(x) = a_0U_0(x) + a_1U_1(x) + \ldots + a_mU_m(x) \qquad (8\text{-}6)$$

where the $a_0, a_1, \ldots a_m$ are constants to be determined from the fit of equation 8-6 to the specified values $y_1, y_2, \ldots y_N$.

There are a number of possible linearly independent analytical functions which can be used in (8-6). Of particular utility are the power functions of x, or

$$\phi_m(x) = a_0 + a_1x + a_2x^2 + \ldots + a_mx^m$$

$$= \sum_{j=0}^{j=m} a_jx^j \qquad (8\text{-}7)$$

where $\phi_m(x)$ is a polynomial of degree m.

The residual at any point, R_i, can be defined as

$$R_i = y_i - \phi_m(x_i)$$

and $$R_i^2 = y_i - \phi_m(x_i)^2 \qquad i = 1, 2, \ldots, N$$

The sum of the squares of the residuals is given by

$$S_m^2 = \sum_{i=1}^{N} R_i^2 \geq 0$$

and, with (8-7),

$$S_m^2 = \sum_{i=1}^{N} (y_i - \sum_{j=0}^{m} a_j x_i^j)^2 \qquad (8-8)$$

R_i^2 is a measure of how well the approximation $\phi_m(x)$ fits the set of points $y_1, y_2, \ldots, y_N$. If $R_i^2 = 0$, $\phi_m(x_i)$ coincides with y_i; if R_i^2 is large, the approximation is not close to the values of y_i.

The residual form can be written out for each point i to yield

$$R_1 = y_1 - (a_0 + a_1 x_1 + a_2 x_1^2 + \ldots + a_m x_1^m)$$

$$R_2 = y_2 - (a_0 + a_1 x_2 + a_2 x_2^2 + \ldots + a_m x_2^m)$$

$$\cdots\cdots\cdots\cdots\cdots\cdots$$

$$R_N = y_N - (a_0 + a_1 x_N + a_2 x_N^2 + \ldots + a_m x_N^m)$$

This is a set of N simultaneous algebraic equations with m + 1 unknowns, a_0, a_1, ... , a_m. If N>m + 1, there are more equations than unknowns. The unknowns may be determined uniquely by imposing the condition that s_m^2 or s_{mw}^2 be minimized. Using the latter it can be seen that it is necessary that

$$\frac{\partial s_{mw}^2}{\partial a_j} = 0 \qquad j = 0, 1, 2, \ldots , m \qquad (8-9)$$

Since there are only two unknown constants, a_0 and a_1, equation 8-9 can be reduced to

$$n a_0 + a_1 \sum_{i=1}^{n} x_i = \sum_{i=1}^{n} y_i$$

$$a_0 \sum_{i=1}^{n} x_i + a_1 \sum_{i=1}^{n} x_i^2 = \sum_{i=1}^{n} x_i y_i \qquad (8-10)$$

where n is the number of sets of experimental data.

From equation 8-10 , the two unknown constants can be derived as

$$a_1 = \frac{\sum_{i=1}^{n} x_i y_i - (\sum_{i=1}^{n} x_i)(\sum_{i=1}^{n} y_i)/n}{\sum_{i=1}^{n} x_i^2 - (\sum_{i=1}^{n} x_i)^2/n} \qquad (8-11)$$

$$a_0 = \frac{\sum_{i=1}^{n} y_i - (\sum_{i=1}^{n} x_i)(a_1)}{n}$$

The least-square-error numerical technique is well developed. Other details of this technique can be found in the literature (3, 15, 19, 33, 47, 57, 60, 70, 83).

H. Thermodynamic Aspects

The values of the change in free energy, ΔG, and the equilibrium constant, K_p, of the gaseous oxidation of methanol to formaldehyde and water are given in the following table:

Table S-H-1
The Values of ΔG and K_p
for Gaseous Formaldehyde Formation
at 1 Atmosphere and Different Temperatures

Temperature °C	$-(\Delta G)$ (kcal/gm-mole)	K_p
25	26.266	1.785×10^{19}
127	25.713	1.115×10^{14}
227	25.068	9.040×10^{10}
327	24.347	7.371×10^{8}
527	22.749	1.637×10^{6}

The values were calculated as functions of temperature, necessary data being either collected from the literature or calculated by the Group-contribution Method (48). Since the values of ΔG and K_p are very large, the process can be considered highly irreversible.

I. Correlation of Initial Rate Data

Correlation of the initial rate data from Chapter 5-E-2 is given in Table 8-I-1.

Table 8-I-1

Correlation of Initial Rate Data

Temp. °C	M_m %	r_o Moles HCHO / gm-hr	^oP_M mm Hg	$^oP_{O_2}$ mm Hg	$^oP_M / ^oP_{O_2}$
365	0.040	0.0432	30.4	156.0	0.1949
"	0.055	0.0596	41.8	150.8	0.2772
"	0.065	0.0629	49.4	149.2	0.3311
"	0.070	0.0640	53.2	148.4	0.3585
"	0.080	0.0689	60.8	146.8	0.4142
326	0.040	0.0410	30.4	156.0	0.1949
"	0.055	0.0430	41.8	150.8	0.2772
"	0.065	0.0436	49.4	149.2	0.3311
"	0.070	0.0446	53.2	148.4	0.3585
"	0.080	0.0468	60.8	146.8	0.4142
319	0.040	0.0378	30.4	156.0	0.1949
"	0.055	0.0380	41.8	150.8	0.2772
"	0.065	0.0440	49.4	149.2	0.3311
"	0.070	0.0440	53.2	148.4	0.3585
"	0.080	0.0384	60.8	146.8	0.4142

J. Constants for Various Mechanisms

The various constants for the acceptable two-stage redox mechanism where n equalled 1 and n equalled 0.5 are listed in Table 5-4. The following are the rejected constants obtained from the two-stage redox mechanisms, the reason for rejection being that the k_1 values were negative. The mechanism numbers refer to those given in Table 5-1. No proper fitting was obtained for the three-stage redox mechanisms of Table 5-2.

Table 8-J-1
Rejected Constants

Mechanism	Temperature °C	H_2 %	k_1 x10^3	k_2 x10^3
2	365	8.0	-0.15	2.59
		7.0	-0.17	2.62
		6.5	-0.19	2.74
		5.5	-0.21	2.68
		4.0	-0.27	2.54
	326	8.0	-0.14	2.69
		7.0	-0.15	2.60
		6.5	-0.16	2.54
		5.5	-0.19	2.48
		4.0	-0.26	2.50
	319	8.0	-0.13	2.50
		7.0	-0.14	2.45
		6.5	-0.15	2.45
		5.5	-0.17	2.36
		4.0	-0.23	2.29
	250	8.0	-0.01	0.32

Table 8-J-1 (Continued)

Mechanism	Temperature °C	K_m %	k_1 $\times 10^3$	k_2 $\times 10^3$
3	365	8.0	-0.64	7.92
		7.0	-0.72	7.75
		6.5	-0.76	7.65
		5.5	-0.88	7.43
		4.0	-1.15	7.04
	326	8.0	-0.46	6.18
		7.0	-0.52	6.07
		6.5	-0.55	6.01
		5.5	-0.67	6.05
		4.0	-1.05	6.56
	319	8.0	-0.40	5.53
		7.0	-0.46	5.46
		6.5	-0.51	5.64
		5.5	-0.61	5.58
		4.0	-0.90	5.79
	250	8.0	-0.04	0.63
4	365	8.0	-0.31	4.52
		7.0	-0.35	4.44
		6.5	-0.37	4.40
		5.5	-0.42	4.29
		4.0	-0.55	4.11
	326	8.0	-0.22	3.54
		7.0	-0.25	3.49
		6.5	-0.26	3.46
		5.5	-0.32	3.50
		4.0	-0.50	3.84

Table B-J-1 (Continued)

Mechanism	Temperature °C	M_n %	k_1 x10^3	k_2 x10^3
	319	8.0	-0.19	3.26
		7.0	-0.22	3.19
		6.5	-0.25	3.25
		5.5	-0.29	3.23
		4.0	-0.43	3.38
	250	8.0	-0.02	0.36
5	365	8.0	-0.31	4.46
		7.0	-0.34	4.37
		6.5	-0.36	4.32
		5.5	-0.42	4.19
		4.0	-0.53	3.98
	326	8.0	-0.22	3.48
		7.0	-0.25	3.43
		6.5	-0.26	3.39
		5.5	-0.31	3.42
		4.0	-0.49	3.72
	319	8.0	-0.19	3.12
		7.0	-0.22	3.13
		6.5	-0.24	3.19
		5.5	-0.28	3.15
		4.0	-0.42	3.28
	250	8.0	-0.02	0.36

IX. NOMENCLATURE

A_m	Catalyst surface area per unit mass, m^2/gm
a_m	External particle surface area per unit mass, m^2/gm
$b_{\frac{1}{2}}$	Peak width at half height, mm or min
C_{av}	Average specific heat, cal/gm-mole-°C
C_p	Specific heat of gas, cal/gm-mole-°C
D_{Am}	Average diffusivity of component A
D_p	Catalyst particle diameter, mm
F	Flow rate of feed, moles/hr
G	Molal velocity of flow based on the total cross-sectional area of the catalyst bed
ΔG	The change in free energy, kcal/gm-mole
H_f	Heat of formation, kcal/gm-mole
h_g	Heat transfer coefficient of the gas film
i	Component i
j	Dimensionless Chilton-Colburn factor
K_i	Equilibrium constant = k_1/k_{-1}
K_{ox}	Oxidized site on catalyst
K_{red}	Reduced site on catalyst
k	Thermal conductivity of the gas
k_g	Mass transfer coefficient of the gas film

k_i	Forward reaction rate constant i, from left to right
k_{-i}	Backward reaction rate constant i, from right to left
MDQ	Minimum detectable quantity of sample
M_m	Mean molecular weight of the gas film
n	Theoretical plate
N_m	Moles % methanol in air
p_i	Partial pressure of component i
$\%_i$	Percentage of component i
q_m	Heat transfer due to heat of reaction per unit mass of catalyst
R	Oxygen to methanol mole ratio in the feed
r	Reaction rate, moles/gm of catalyst-hr
r_o	Initial rate, moles/gm of catalyst-hr
s	Selectivity
s	Active site on catalyst
s_{ox}	Oxidized site, active site of lattice or adsorbed oxygen on catalyst
s_{red}	Reduced site of lattice oxygen or the empty site on the catalyst
t	Time
T	Temperature
T_g	Total gas flow rate

T_i Temperature of the gas-solid interface

F_l Total liquid component flow rate, methanol, formaldehyde and water

t_{dr} Uncorrected retention time, mm or min

W Weight of catalyst, gm

w Flow rate of water

x Conversion

y Yield

Greek Symbols

Δ Finite increment or change of property

δ Change in moles per mole of reactant (or product)

θ_i Fraction of the catalyst surface that is covered by adsorbed component i

μ Viscosity

π Total pressure

ρ Density

ρ_B Bulk density of catalyst, gm/ml

ϕ Shape factor, ratio of actual external surface area available for mass and heat transfer to the total external surface area, assumed to be 0.90 for irregular granules

Superscripts

a	Reaction order
n	Reaction order

Subscripts

A_i	Component A at the gas-solid surface interphase
cal	Calculated
f	Formaldehyde
f	Properties at the average condition of the gas film
exp	Experimental
g	Gaseous state
h	Height
i	Component i
in	Input
M	Methanol
M	In moles
o	Placed before a symbol means in the feed
out	Output

K. BIBLIOGRAPHY

1. Adkins, H., and Peterson, W.H., J. Am. Chem. Soc., 53, 1513 (1931).

2. Allyn, C.L., Barrentine, E.M., Hodgins, T.S., Rawson, R.L., and Shelton, E.J. (to Reichhold Chemicals Inc.), U.S. Patents 2,812,309 (1957) and 2,849,492 (1958).

3. Amara, R.C., J. Franklin Inst., 268, 1 (1959).

4. Aries, R.S., U.S. Patent 2,953,602 (1960).

5. Arnold, H.R. (to E.I. du Pont de Nemours & Co.), U.S. Patent 2,320,253 (1943) and 2,439,880 (1948).

6. Arrhenius, S., Z. Physik. Chem., 4, 226 (1889).

7. Bailey, G.C., and Graver, A.E. (to the Barrett Co.), U.S. Patent 1,383,059 (1921).

8. Barrentine, E.M., and Shelton, E.J. (to Reichhold Chemicals Inc.), U.S. Patents 2,812,308 (1957) and 2,849,493 (1958).

9. Bhattacharyya, S.K., Janakiram, K., Ganguly, N.D., J. Catalysis, 8, 128 (1967).

10. Bird, R.B., Stewart, W.E., and Lightfoot, E.N., "Transport Phenomenon," Wiley, New York, p. 290 (1960).

11. Blank, O., German Patent 228,697 (1910).

12. Blizmakov, G., Jiru, P., and Kliesenraki, D., Collection Czech. Chem. Commun., 31, 2995 (1966).

13. Bombaugh, K.J., and Bull, W.C., Anal. Chem., 34, 1237 (1962).

14. Bone, W.A., and Smith, H.L., J. Chem. Soc., 87, 910 (1905).

15. Box, G.P.P., Ann. N.Y. Acad. Sci., 86, 792 (1960).

16. Bugge, G., Chem. App., 18, 157 (1931).

17. Bystrom, A., Wilhelmi, K., and Brotzen, O., Acta Chem. Scand., 4, 1119 (1950).

18. Chilton, T.H., and Colburn, A.P., Ind. Eng. Chem., 26, 1183 (1935).

19. Chou, G., Ind. Eng. Chem., 50, 799 (1958).

20. Colburn, A.P., Trans. Am. Inst. Chem. Eng., 29, 174 (1933).

21. Cotter, J.T., Dissertation, University of Rhode Island, Kingston, Rhode Island (1966).

22. Craver, A.E. (to Weiss and Downs, Inc.), U.S. Patent 1,851,754 (1932).

23. Denbigh, K., "The Principles of Chemical Equilibrium," University Press, Cambridge (1964).

24. Deniges, G.J., Pharm. Chim., 6, 193 (1896).

25. Deniges, G.J., Compt. rend., 150, 529 (1910).

26. Dente, M., and Collina, A., Chimica e industria (Milan), 46, 752 (1964).

27. Ibid, p. 915.

28. Dente, M., Poppi, R., and Pasquon, J., Chimica e industria (Milan), 46, 1326 (1964).

29. Downie, J., Shelstad, K.A., and Graydon, W.F., Can. J. Chem. Eng., 39, 201 (1961).

30. Field, E. (to E.I. du Pont de Nemours & Co.), U.S. Patent 2,519,751 (1950).

31. Friedlander, J., and Bennett, C.O., "Symposium of Reaction Kinetics in Product and Process Design," Am. Inst. Chem. Eng. and Inst. Chem. Eng., joint

meeting in London, England, p. 34 (1965).

32. Gamson, B.W., Thodos, G., and Hougen, O.A., Trans. Am. Inst. Chem. Eng., 39, 1 (1943).

33. Goldstein, A.A., Levine, M., and Hereshoff, J.B., J. Assoc. Comput. Mach., 4, 43 (1957).

34. Green, S.J., "Industrial Catalysis," Benn, London (1928).

35. Hagen, G.L., Hodgins, T.S., and Warner, H.O. (to Reichhold Chemicals Inc.), U.S. Patent 2,852,564 (1958).

36. Hamlin, J.G., Ph.D Thesis, Oxford University, England (1960).

37. Hinshelwood, C.N., "The Kinetics of Chemical Change," Oxford University Press, London, p. 207 (1940).

38. Hodgins, T.S., and Shelton, F.J. (to Reichhold Chemicals Inc.), U.S. Patent 2,973,326 (1961).

39. Hodgins, T.S., Walker, R.B., and Warner, H.O. (to Reichhold Chemicals Inc.), U.S. Patent 2,812,310 (1957).

40. Hofmann, A.W., Ann., 145, 357 (1868); Ber., 2, 152 (1869).

41. Homer, K.W., J. Soc. Chem. Ind. (London), 60, 213 (1941).

42. Hood, J.J., Phil. Mag., 6, 371 (1878); 20, 325 (1885).

43. Hoogschagen, J., Ind. Eng. Chem., 47, 906 (1955).

44. Hougen, O.A., and Watson, K.M., Ind. Eng. Chem., 35, 529 (1943).

45. Hougen, O.A., and Watson, K.M., "Chemical Process Principles," Vol. III, McGraw-Hill, New York (1949).

46. Ibid, pp. 824-825; 834-857; 929-930.

47. Ibid, pp. 949-953.

48. Hougen, O.A., Watson, K.M., and Ragatz, R.A., "Chemical Process Principles," Part II, Wiley, New York, p. 1004 (1959).

49. Ioffe, I.I., and Lyubarskii, A.G., Kinetica i Katalis, 3, 261 (1962); Abt., J. Catalysis, 1, 397 (1962).

50. Jaeger, A.O. (to the Selden Co.), U.S. Patent 1,709,853 (1929).

51. Jiru, P., Tichy, J., and Wichterlova, B., Collection

Czech. Chem. Commun., 31, 674 (1966).

52. Jiru, P., Wichterlova, B., Tichy, J., Proc. 3rd Congr. Catalysis (Amsterdam), North-Holland Publishing Co., Amsterdam, p. 199 (1964).

53. Jones, E., and Fowlis, G.G., J. Applied Chem., 3, 206 (1953).

54. Kaiser, R., "Gas Phase Chromatography," Vol I, Butterworth, New York, p. 20 (1963).

55. Ketelaar, J.J., Nature, 139, 316 (1936).

56. Ketelaar, J.J., Chem. Weekblad, 33, 51 (1936).

57. Klar, M., and Schulze, C., German Patent 106,495 (1898).

58. Klissourski, D., and Klissnakov, G., Compt. rend. Acad. bulgare Sci., 18, 549 (1965).

59. Kushnarenko, I.P., and Atroshenko, V.I., Khim. i Khim. Tekhnol., 8, 47 (1965).

60. Kusnesow, M.J. (to Perth Amboy Chemical Works), U.S. Patent 1,067,665 (1913).

61. Laidler, K.J., "Chemical Kinetics," 2nd ed., McGraw-Hill, Toronto (1965).

62. Ibid, pp. 5-28.

63. Ibid, p. 18.

64. Ibid, pp. 256-286.

65. Ibid, p. 435.

66. Lambert, B., and Phillips, C.S.G., Trans. Roy. Soc. (London) A, 242, 415 (1950).

67. Lapidus, L., "Digital Computation for Chemical Engineers," McGraw-Hill, Toronto, pp. 323-337 (1962).

68. Lapidus, L., and Peterson, T.I., Am. Inst. Chem. Eng. J., 11, 891 (1965).

69. LeBlanc, M., and Plaschke, E., Z. Elektrochem., 17, 45 (1911).

70. Levenspiel, O., Weinstein, N.J., and Li, J.C.R., Ind. Eng. Chem., 48, 324 (1956).

71. Liberti, A., Conti, L., and Crescensi, V., Nature, 178, 1067 (1956); Atti accad. nasl. Lincei, Classe sci. fis. mat. e nat., 20, 623 (1956).

72. Mann, R.S., and Hahn, K.W., Anal. Chem., 39, 1314 (1967).

73. Marek, L.F., and Hahn, D.A., "The Catalytic Oxidation of Organic Compounds in the Vapor Phase," Chemical Catalog Co., New York (1932).

74. Mars, P., and van Krevelen, D.W., Chem. Eng. Sci. (special supplement) 3, 41 (1954).

75. Martin, A.J.P., and James, A.T., Biochem. J., 63, 138 (1956).

76. Meharg, V.E., and Adkins, H. (to Bakelite Corp.), U.S. Patent 1,913,405 (1933).

77. Mellor, J.W., "A Comprehensive Treatise on Inorganic and Theoretical Chemistry," 11, 571 (1959).

78. McReynolds, W.O., Pittsburgh Conference on Analytical Chemistry and Applied Spectroscopy (1961).

79. Menapace, H.R., Kyryacos, G., and Boord, C.E., Anal. Chem., 31, 222 (1959).

80. Montecatini Soc. Gen. (per l'Ind. Mineraria e Chimica), Australian Patent Application 54,029 (1959); Italian Patent 589,718 (1959).

81. Ostwald, W., Chem. Betrachtungen, Aula No. 1 (1895).

82. Ostwald, W., Physik. Z., 3, 313 (1902).

83. Parsons, J.S., Anal. Chem., 36, 1849 (1964).

84. Pearson, T.G., Z. physik. Chem., 156, 86 (1931).

85. Pings, C.J., Jr., and Sage, B.H., Ind. Eng. Chem., 49, 1315, 1321 (1957).

86. Punderson, J.O. (to E.I. du Pont de Nemours & Co., Inc.), U.S. Patent 2,939,833 (1960).

87. Rosenthaler, L., "Der Nachweis organischer Verbindungen: Die chemische Analyse," 2nd ed., Vol. XIX/XX, p. 128, F. Enke, Stuttgart (1923).

88. Rossini, F.D., Wagman, D.D., Evans, W.H., Levine, S., and Jaffe, I., "Selected Values of Chemical Thermodynamic Properties," U.S. Bur. Standards Circ. no. 500 (1952).

89. Sabatier, P., and Mailhe, A., Ann. chim. phys., 8, 20, 344 (1910).

90. Sandler, S., and Strom, R., Anal. Chem., 32, 1890 (1960).

91. Scheparts, A.I., and McDowell, P.E., Anal. Chem., 32, 723 (1960).

92. Scott, R.P.W., and Denty, D.H., Ed., "Vapor Phase Chromatography," Butterworth, London, p. 131 (1957).

93. Shelstad, K.A., Downie, J., and Graydon, W.F., Can. J. Chem. Eng., 35, 102 (1960).

94. Smith, J.M., Chem. Eng. Progress, 44, 521 (1948).

95. Smolkova, E., Kolenskova, V., and Feltl, L., Z. Anal. Chem., 202, 264 (1964).

96. Snowden, P.F., and Style, D.W.G., Trans. Faraday Soc., 35, 426 (1939).

97. Stadnik, P.M., and Fentsik, V.P., Dopovidi Akad. Nauk U.R.S.R., 1608 (1960).

98. Thiele, E.W., Ind. Eng. Chem., 31, 916 (1939).

99. Thomas, M.D., J. Am. Chem. Soc., 42, 867 (1920).

100. Thompson, H.W., Trans. Faraday Soc., 37, 251 (1941).

101. Vickery, B.C., Ind. Chemist, 23, 141 (1947).

102. von Kelker, H., Z. Anal. Chem., 176, 3 (1960).

103. Walker, J.F., "Formaldehyde," 3rd ed., Am. Chem. Soc. Monograph Series no. 159, Reinhold, New York (1964).

104. Ibid, pp. 6-24.

105. Ibid, p. 468.

106. Ibid, p. 478.

107. Ibid, p. 552.

108. Wilke, C.R., and Hougen, O.A., Trans. Am. Inst. Chem. Eng., 41, 445 (1945).

109. Yang, K.H., and Hougen, O.A., Chem. Eng. Progress, 46, 146 (1950).

110. Ibid, p. 154.

111. Yoshida, F., Ramaswami, D., and Hougen, O.A., Am. Inst. Chem. Eng., 8, 5 (1962).

All patents with the exception of Field's (30) were checked through Chemical Abstracts.